Universidad Autónoma de Madrid

Facultad de Biología

Departamento de Microbiología

Molecular interaction of the cell division protein ZapC, a regulator of the *Escherichia coli* FtsZ-ring assembly

TESIS DOCTORAL

Cristina Ortiz Cabello

Universidad Autónoma de Madrid

Facultad de Biología

Departamento de Microbiología

Molecular interaction of the cell division protein ZapC, a regulator of the *Escherichia coli* FtsZ-ring assembly

TESIS DOCTORAL

Memoria presentada para optar al grado de Doctor en Ciencias

Cristina Ortiz Cabello

TUTOR ACADÉMICO
Marta Martín Basanta

DIRECTOR
Miguel Vicente Muñoz

Consejo Superior de Investigaciones Científicas

Centro Nacional de Biotecnología

Madrid, 2015

Este trabajo ha sido realizado en el Centro Nacional de Biotecnología (CNB-CSIC) bajo la dirección del Profesor de Investigación Miguel Vicente Muñoz, y en el Molecular Research Council (MRC) Laboratory of Molecular Biology, Cambridge, UK durante una estancia de 12 meses en el laboratorio del Dr. Jan Löwe. Este trabajo ha sido financiado por el programa de Formación de Personal Investigador del Ministerio de Educación y Ciencia.

Agradecimientos:

Quiero agradecer a mi jefe, Miguel Vicente haberme aceptado en su laboratorio, haberme dado los medios para llevar a cabo esta Tesis, que sin ninguna duda, no habría acabado sin su apoyo y continuo empuje. Gracias jefe, por que has educado en la Microbiología a una química cabezota que, finalmente ha aprendido que no todo está hecho, que hay mucho por investigar y sobre todo, muchas preguntas que hacerse.

A los compañeros del lab. 217 por haberme acompañado todos estos años. A los que están ahora mismo, Anabel, Merce, Pili, Susanne, Ali y Laura. Por todo vuestro apoyo, ayuda y comprensión. De verdad que he aprendido muchas cosas de todas vosotras, y que espero poder usar en mi vida tanto científica como social. Gracias a todas.

Quiero agradecer especialmente a Merce y Pili por su apoyo en estos momentos finales de la Tesis, pero sobre todo cómo habéis trabajado en este proyecto, no os podéis imaginar lo orgullosa que me siento de haber estado a vuestro lado y, todo lo que he aprendido de Microbiología. De verdad, gracias.

A Laurix, que sólo llevamos juntas un año, el final de esta Tesis y el principio de la suya. Todo mi cariño y apoyo para ti Laurix, siempre vas a poder contar conmigo. Es lo que tiene hacerse amiga mía.

A los que ya no están, Marcin, Moira, Manu y Paolo. Por que en algún momento de este trabajo me habéis acompañado, con risas, bromas y muchos cafés. Quiero dar mi más sincero agradecimiento a Paolo, por que aunque no estás todos los días en el lab, siempre has estado a mi lado. Tengo la sensación de que siempre va ser así, siempre voy a tenerte a mi lado. Gracias por todo, de verdad.

I am very grateful to Jan Löwe for all good advices and help since I arrived to his lab. I am lucky to have met two great scientists as Linda and Fusinita. To his entire lab for helping and making me feel like at home and have a lot of fun in Cambridge. Specially Matt, Thierry, Deb, Mek, Gero, BG, and Sole all of you is amazing people and I feel really lucky to meet all of you. Thanks guys, I will always remember Cambridge with a smile. To Stephen and Chris, the biophysical department at the MRC. To Fabrice for all his help with crystals and robots.

A mi amiga Bea que llevamos juntas toda la vida, que no tengo palabras de agradecimiento por todo lo que no abarca esta Tesis. Por que sigamos bebiendo vinos mil años más. Gracias Bea.

Mi familia, mis padres y mi hermano. Por que no hubiera ni empezado ni acabado nada de todo lo que he hecho hasta ahora y, mucho menos esta Tesis, por que nunca jamás se han cansado de empujarme, de apoyarme, de quererme. Os dedico con todo mi cariño esta Tesis, que ni la milésima parte del esfuerzo que me ha llevado acabar esto es comparable con todo lo que me habéis dado vosotros.

GENERAL INDEX

GENERAL INDEX

Figure Index 4

Abbreviations 7

Resumen 11

Summary 15

Introduction 19

1. **FtsZ: the master of the ring** 22
2. **FtsA and ZipA: the proto-ring anchors** 25
3. **Min proteins: the ring scouts** 28
4. **Nucleoid occlusion: obstruction of the ring** 29
5. **ClpXP: ring degradation** 31
6. **The SOS response: an emergency division block** 32
7. **FtsZ associated Zap proteins: supporters of the ring** 33

Objectives 37

Materials & Methods 41

1. **Materials** 43
   - 1.1 *Escherichia coli* strains 43
   - 1.2 Plasmids 43
   - 1.3 Antisera 45
   - 1.4 Primers 46
   - 1.5 Chemical and reagents 47
2. **Methods** 49
   - 2.1 Bacterial growth conditions 49
   - 2.2 Cell parameter measurements 50
   - 2.3 Phase-contrast and fluorescence microscopy 50
   - 2.4 SDS-PAGE and immunoblot 50
   - 2.5 Production of anti ZapC-histidine antibody 51
   - 2.6 Protein expression and purification 51
   - 2.7 90º Light Scattering assay 54

2.8 Negative stain electron microscopy 54
2.9 GTPase assay 55
2.10 Analitical Ultracentrifugation 55
2.11 Isothermal titration calorimetry 56
2.12 ZapC crystallization 56
2.13 Structure determination of ZapC 56
Results **59**
1. Replacement of the divalent magnesium in FtsZ assembly **61**
1.1 Requirement of magnesium for *Mycobacterial* FtsZ oligomerization 62
1.2 Polymerization of FtsZ in the presence of manganese 64
1.3 The hydrolytic activity of the *Ec*FtsZ polymers with manganese 68
2. Crystallization of *Escherichia coli* FtsZ **69**
2.1 Bioinformatic analysis of *E. coli* FtsZ 70
2.2 Screening of *E. coli* FtsZ variants 72
2.3 *Ec*FtsZ$_{10}$ crystals 74
2.4 Crystals of the MinC-FtsZ complex 76
3. Molecular interaction between the cell division protein ZapC and FtsZ in *E. coli* **78**
3.1 *In vitro* interaction between ZapC and FtsZ 80
3.2 Thermodynamics parameters of the FtsZ-ZapC interaction 81
3.3 Crystal structure of the cell division protein ZapC 83
3.4 ZapC structure and its homology to the Royal superfamily 84
3.5 ZapC oligomerization 87
3.6 Effects of high ZapC levels on growth and division 88
3.7 Effect of high levels of ZapC variants on the localization of the FtsZ-ring 91
3.8 Effect on growth and division of FtsA overproduction in *E. coli* cells overproducing ZapC 93
3.9 Effect of the FtsA* gain-of-function 95
3.10 Effect of FtsA and FtsA* induction on the localization of the FtsZ-ring in cells overexpressing *zapC* 96

Discussion

1. **Manganese as a substitute of magnesium in FtsZ assembly** **103**
2. **Crystallization of *E. coli* FtsZ** **106**
3. **Crystal structure of the FtsZ associated cell division protein ZapC** **109**
4. **Molecular interaction between ZapC and FtsZ in *E. coli*** **111**

Conclusions **113**

Conclusiones **117**

References **123**

Figure Index

Figure 1. FtsZ dimer modelled from the *Methanococcus jannaschii* crystal structure.

Figure 2. Crystal structures from the *T. maritima* FtsA and the *E. coli* ZipA.

Figure 3. Mechanisms used by the negative modulators involved in the assembly of the FtsZ-ring.

Figure 4. Bundling of the FtsZ protofilaments assisted by the Zap proteins.

Figure 5. Polymerization dynamics of *Mycobacterial* FtsZ.

Figure 6. Electron micrographs of *Mycobacterial* FtsZ polymers.

Figure 7. FtsZ polymerization levels in the presence of different divalent cations.

Figure 8. Electron microscopy of FtsZ filaments formed in the presence of different divalent cations.

Figure 9. Bacterial FtsZ proteins alignments showing the identity against *E. coli* FtsZ.

Figure 10. Bioinformatic prediction of the secondary structure and disordered domains in *E. coli* and *P. aeruginosa* FtsZ.

Figure 11. Amino acid sequence identity of the different constructed *E. coli* FtsZ variants.

Figure 12. Purification of $FtsZ_{10}$ variant and its *in vitro* analysis.

Figure 13. Crystallization conditions used for $FtsZ_{10}$ variant.

Figure 14. Crystallization conditions used to crystallize the protein complex $MinC^{N}$-$FtsZ_{10}$.

Figure 15. ZapC effect on polymers formed by different carboxy terminal end FtsZ truncations.

Figure 16. Binding of FtsZ peptide to ZapC.

Figure 17. Purificatio, crystal and structure of ZapC

Figure 18. *E. coli* ZapC crystal structure and its domain homology to a superfamily domains methylation.

Figure 19. Oligomeric state of ZapC.

Figure 20. ZapC point mutations based on crystal contacts.

Figure 21. Levels of intracellular FtsZ and ZapC following induction of different *zapC* variants.

Figure 22. Effect of *zapC* overexpression on growth and division.

Figure 23. Immunolocalisation of FtsZ in *E. coli* cells transformed with the empty expression vector pBAD22.
Figure 24. Effect of high levels of ZapC variants on the FtsZ-ring.
Figure 25. Effect of *ftsA* and *zapC* overexpression on growth and division and levels of FtsZ, FtsA and ZapC following induction of different plasmids.
Figure 26. Effect of *ftsA** and *zapC* overexpression on growth and division and levels of FtsZ, FtsA* and ZapC following induction of different plasmids.
Figure 27. Effect of induced levels of ZapC, FtsA and FtsA* on the FtsZ-ring.
Figure 28. Crystal structure of FtsZ dimer from *M. jannaschii*.
Figure29. Aminoacid sequence homology between *Ec*FtsZ and *Pa*FtsZ.
Figure 30. The central hub of FtsZ.

ABBREVIATIONS

Abbreviations

Amp	Ampicillin
BSA	Bovine serum albumin
Cam	Chloramphenicol
Da	Dalton
EDTA	Ethylenediaminetertriacetic acid
GTP	Guanosine triphosphate
GTPγS	Guanosine triphosphate gamma sulphate
His	Polyhistidine tag
Kan	Kanamycin
LB	Luria Bertani
OD	Optical density at 600 nm
PCR	Polymerase chain reaction
PDB	Protein Data Bank
PMSF	Phenylmethylsulfonyl fluoride
Rpm	revolutions per minute
SDS	Sodium dodecyl sulphate
SDS-PAGE	SDS-polyacrilamide gel electrophoresis
TEMED	Tetramethylethylenediamine
Tris	Tris(hydroxymethyl)aminomethane

RESUMEN

Resumen

El divisoma, la maquinaria molecular usada por las bacterias para llevar a cabo la constricción de la membrana durante el proceso de división celular, está basado principalmente en una proteína citoplásmica, FtsZ. FtsZ se ensambla desde el proncipio de dicha constricción en forma de anillo (el anillo FtsZ) que es posicionado en el centro de la célula durante la mayor parte del proceso de septación. Sin embargo, FtsZ no se ancla a la membrana citoplásmica por sí misma. En el modelo de bacteria Gram-negativa *Escherichia coli*, FtsZ necesita de otras proteínas como FtsA y ZipA para su anclaje (Natale, *et al*., 2013), (Rico, *et al*., 2013). Además, como FtsZ se encuentra distribuida a lo largo de toda la longitud celular, el ensamblaje del anillo FtsZ requiere de precisos mecanismos de posicionamiento, como son el sistema Min (de Boer, *et al*., 1989) y el sistema de oclusión por nucleoide (Woldringh, *et al*., 1991), ambos presentes en *E. coli*, previenen el ensamblaje del anillo en cualquier sitio que no sea el centro de la célula. Durante el ensamblaje del anillo FtsZ, los polímeros de FtsZ son mantenidos por sus interacciones laterales y estabilizados por un set de proteínas asociadas a FtsZ (Zap) (Huang, *et al*., 2013).

El trabajo presentado en esta Tesis está enfocado en el estudio de FtsZ y de su interacción molecular con la proteína asociada ZapC. En la *Sección 1* se estudia el ensamblaje *in vitro* de FtsZ en presencia de cationes divalentes. Los resultados obtenidos nos han permitido intentar llevar a cabo los ensayos de cristalización de FtsZ de *E. coli*, los cuales se encuentran descritos en la *Sección 2*. Durante el proceso de cristalización, se hicieron hasta 16 construcciones diferentes de FtsZ. También FtsZ se intentó cristalizar en complejo con otras proteínas que han sido descritas por interaccionar directamente con FtsZ, el inhibidor MinC y el estabilizador ZapC. En la *Sección 3* se describe el estudio de la interacción molecular entre FtsZ y ZapC. Los datos *in vitro* mostraron que probablemente el C-terminal de FtsZ esté implicado en la interacción con ZapC. La resolución de la estructura cristalina de ZapC revelará que la proteína cristalizó como un dímero. Análisis *in vivo* mostrarán que aunque ZapC no es una proteína esencial para la división, su sobreexpresión es altamente tóxico para la división. Estudiaremos el rescate de este fenotipo con la inducción de otras proteínas esenciales de división como FtsA y su variante FtsA*, mutante puntual de FtsA.

SUMMARY

Summary

The divisome, the molecular machinery used by bacteria to effect the membrane constriction during cell division, is most often based on a cytoplasmic protein, FtsZ. FtsZ is assembled from the start of constriction as a ring (the FtsZ-ring) that is positioned at midcell during most of the septation process. However, FtsZ does not attach by itself to the cytoplasmic membrane. In the model Gram-negative *Escherichia coli* it needs other cell division proteins as FtsA and ZipA for attachment (Natale, *et al*., 2013, Rico, *et al*., 2013). Furthermore, as FtsZ is distributed along the bacterial length the assembly of the FtsZ-ring requires dedicated positioning mechanisms, as the Min system (de Boer, *et al*., 1989) and nucleoid occlusion (Woldringh, *et al*., 1991), both present in *E. coli*, to prevent assembly at sites different from the midcell. During FtsZ-ring assembly, FtsZ polymers are maintained by their lateral interactions and stabilize by a set of FtsZ associated proteins (Zap) (Huang, *et al*., 2013).

The work presented in this thesis is focused on the study of FtsZ and its molecular interaction with the associated protein ZapC. In the *Section 1*, we study the *in vitro* assembly of FtsZ in the presence of divalent cations. The results led us to attempt the crystallization of the FtsZ protein from *E. coli*, as we describe in *Section 2*. During the crystallization process, up to 16 different FtsZ variants were constructed. FtsZ was also assayed in complex with another division proteins that interact directly with FtsZ, namely MinC (inhibitor) and ZapC (stabilizer). *Section 3* describes the study of the molecular interaction between FtsZ and ZapC. *In vitro* data shows that the C-terminal of FtsZ may be involve in the interaction with ZapC. The resolution of the crystal structure of *E. coli* ZapC shows that the protein crystallized as a dimer. Further *in vivo* analysis shows that *E. coli* cells expressing *zapC* produces aberrant FtsZ-rings and leds to a filamentation phenotype. We have also investigated the rescue of excess ZapC by other cell division protein, FtsA and the gain-of-function mutant FtsA*.

INTRODUCTION

It is surprising that the divisome, the molecular machinery used by bacteria to effect the membrane constriction during cell division, is most often based on a cytoplasmic protein, FtsZ. FtsZ is assembled from the start of constriction as a ring (the FtsZ-ring) that is positioned at midcell during most of the septation process. However, FtsZ does not attach by itself to the cytoplasmic membrane. In the model Gram-negative *Escherichia coli* it needs other cell division proteins as FtsA and ZipA for attachment (Natale, *et al*., 2013, Rico, *et al*., 2013). Furthermore, as FtsZ is distributed along the bacterial length the assembly of the FtsZ-ring requires dedicated positioning mechanisms, as the Min system (de Boer, *et al*., 1989) and nucleoid occlusion (Woldringh, *et al*., 1991), both present in *E. coli*, to prevent assembly at sites different from the midcell. Although the fine structural image of the FtsZ-ring is not well resolved, most data are compatible with FtsZ polymers forming a ring in which the filaments are discontinuous and their distribution along the full equatorial circle is maintained by their lateral interactions and by a set of FtsZ associated proteins (Zap) (Huang, *et al*., 2013). In addition, the Zap proteins may also participate in mechanisms to actively remove FtsZ from the septum at the final stages of constriction (Pazos, *et al*., 2013), (Soderstrom, *et al*., 2014).

FtsZ is a GTPase and its polymerization is closely related to the binding and hydrolysis of GTP (Mukherjee & Lutkenhaus, 1994). The amount of FtsZ in the cell needs to be tightly regulated as amounts either above or below a threshold lead to the production of nucleoid-free minicells or to bacterial filamentation (Dai & Lutkenhaus, 1992). This need has left a signature in the bacterial genome, both in the chromosomal localization of *ftsZ* within the *dcw* cluster in which *ftsZ* and other division genes are located in rod-shaped bacteria together with genes coding for cell wall synthetizing enzymes (Mingorance, *et al*., 2004). A second trait is found in the complex regulation of gene expression operating in *E. coli* to transcribe the cluster (Vicente, *et al*., 1998).

The complex mechanisms driving cell division in *E. coli* may provide a wealth of regulatory alternatives to adapt division to the many circumstances faced by bacteria, and provide sufficient plasticity to allow their survival. Other bacteria, adapted to grow in different habitats possess mechanisms to divide that may have dispensed with several of the complexities that characterize the division process in *E. coli*. Among them, a reduction in the number of divisome elements in pathogens or symbionts or the

replacement of some of the FtsZ interacting proteins in Gram positives are the most frequent (Vicente, *et al*., 2004), (Massidda, *et al*., 2013). A rather extreme case is represented by the absence of FtsZ itself in the obligate intracellular parasites *Chlamydiales* where its absence was initially proposed to be linked to the lack of a peptidoglycan wall (McCoy & Maurelli, 2006). More recent evidence showing the existence of a wall in these organisms do not support this postulate (Pilhofer, *et al*., 2013). MreB and RodZ have been proposed to take over the essential role of FtsZ in *Waddlia chondrophila*, a member of the *Chlamydiales* (Jacquier, *et al*., 2014).

1. FtsZ: the master of the ring

FtsZ is the first division protein to localize at midcell, where it forms the FtsZ-ring serving as the molecular scaffold for the localization of at least ten additional essential cell division proteins that together form the divisome, a protein complex that drives the constriction during cell division (Erickson, *et al*., 2010), (Mingorance, *et al*., 2010). Even using high-resolution techniques (Fu, *et al*., 2010), it has been difficult to discern how FtsZ filaments are arranged within the FtsZ-ring. Moreover how this arrangement exerts the constriction force is a matter of debate (Li, *et al*., 2007). The FtsZ crystal structure shows that FtsZ is the structural homologue of the eukaryotic tubulin (Löwe & Amos, 1998). It comprises two domains connected by a central core helix, the H7 helix (Löwe & Amos, 1998) (**Figure 1**). The N-terminal globular domain of FtsZ (amino acids 1-220) includes the synergy T7 loop in which specific residues needed for GTP binding and hydrolysis are contained. The carboxy terminal domain (221-383 amino acids) includes a structured folded part (residues 221 to 314), followed by a flexible unstructured part of a variable length in the FtsZ from different bacteria (the C-terminal linker, CTL; residues 315 to 368 in *E. coli*) (Vaughan, *et al*., 2004), (Buske & Levin, 2013) and a short alpha helix C-terminal end (the central hub, residues 369 to 383 in *E. coli*). The unstructured part participates in lateral interactions between FtsZ protofilaments whereas the central hub is involved in the interaction with other cell division proteins. The length of the CTL part is particularly long (172 residues) in some bacteria as *Caulobacter crescentus* in which an intact CTL ensures the correct synthesis of peptidoglycan, whereas different deletions affecting it produce a defective peptidoglycan eventually leading to cell lysis when it is completely absent

(Sundararajan, *et al*., 2015).

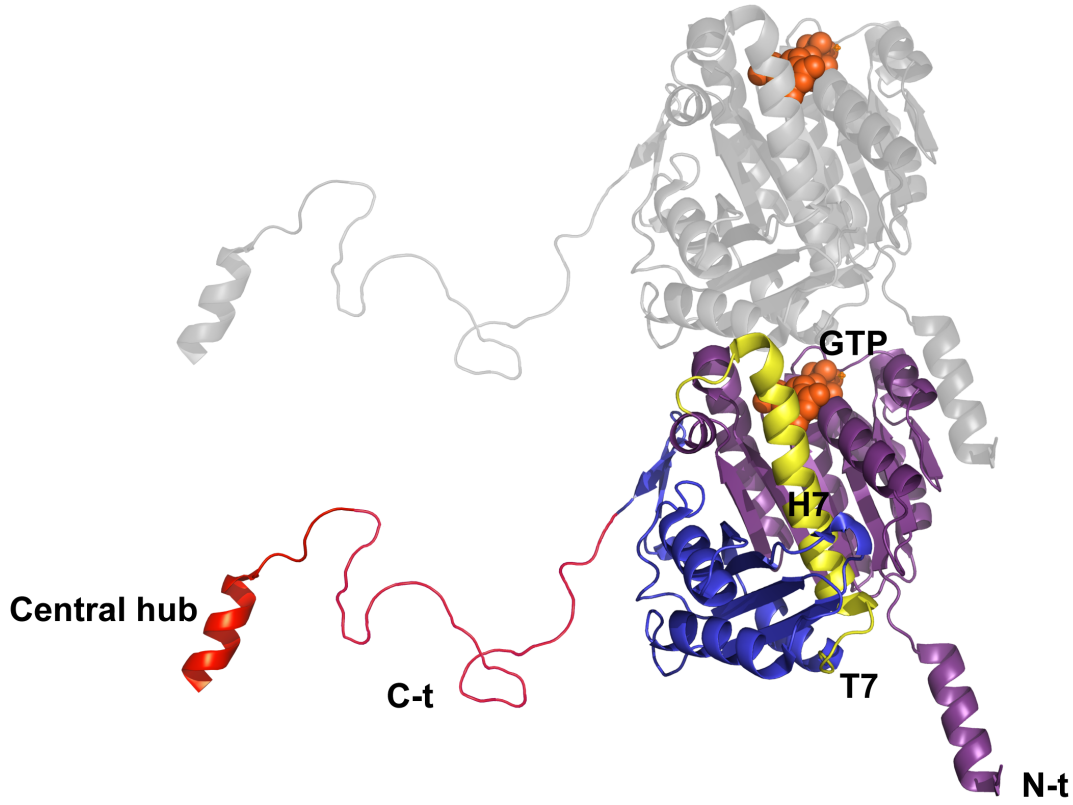

Figure 1. FtsZ dimer modelled from the *Methanococcus jannaschii* crystal structure. The bottom monomer (adapted from the Protein Data Bank (PDB) entry 1W5A) shows the N-terminal domain (purple) and the Carboxy-terminal domain (blue). Both folded domains are connected by the catalytic H7 helix followed by the T7 loop (both in yellow). A partial GTP-binding site is formed by residues belonging to the top surface of the N-terminal domain of the bottom monomer. The full structure of the GTP-binding site is formed by the overlay of the top monomer (in grey) in which the bottom surface of its Carboxy terminal domain provides the top surface of the complete active site. Once formed, the T7 loop achieves the correct positioning of the phosphate in the gamma position of the nuclotide (GTP colored in orange) activating the hydrolytic activity. The highly variable C-terminal linker (red) is depicted here as a free-drawn unstructured peptide since is not fixed in the crystal. The structure of the central hub at the C-terminal end (also colored in red), is based on the structure of the interacting region of the *E. coli* FtsZ protein with the globular domain of ZipA (adapted from the PDB entry 1F47) (see Figure 2).

The complete active site for GTP binding and hydrolysis is formed upon polymerization (Scheffers & Driessen, 2002). It involves the synergy T7 loop at the lower surface of one monomer and a section of the folded part in the C-terminal domain located at the upper surface of the next one. Both parts of the nucleotide binding site are brought into close contact by the head-to-tail assembly of monomers in the polymer (Scheffers, *et al*., 2002). The basic FtsZ polymer is a single-stranded filament, in which GTP hydrolysis activity is dependent on the binding of GTP and Mg^{2+} and is stimulated

by the presence of K^+ (Mendieta, *et al*., 2009). Under these conditions, the dynamics of FtsZ polymerization-depolymerization *in vitro* is very fast and FtsZ monomers are continuously incorporated and removed within the polymer with a turnover of approximately 10 seconds (Mingorance, *et al*., 2001), (Stricker, *et al*., 2002), (Anderson, *et al*., 2004). However, lateral associations between FtsZ polymers can achieve a variety of conformations depending on the reaction conditions including filament bundles, ribbons, tubes, sheets or spirals (Yu & Margolin, 1997), (Popp, *et al*., 2009). *In vivo* these lateral associations of FtsZ filaments are favoured by the presence of other cell division proteins.

The last residues of the carboxy terminal domain, comprising 15-amino acid residues in *E. coli* and 17-amino acid residues in *B. subtilis*, have been assigned a role as a central hub serving to integrate a variety of functions related to the stability of the protein, its polymerization and its anchoring to the cytoplasmic membrane (Buske & Levin, 2012), (Pazos, *et al*., 2013). The FtsZ loop at residue R174 is protected by the membrane from trypsin degradation. This result suggests that the N-terminal domain of FtsZ localises in close proximity to the membrane, although no direct evidence for the attachment of FtsZ to the membrane through this residue can be strictly inferred (Koppelman, *et al*., 2004).

In *E. coli* there are at least six partners that interact with the central hub: the membrane anchors FtsA (Szwedziak, *et al*., 2012) and ZipA (Mosyak, *et al*., 2000), the FtsZ polymerization inhibitors MinC (Hu, *et al*., 1999) and SlmA (Du, *et al*., 2015), the FtsZ stabilizing protein ZapD (Durand-Heredia, *et al*., 2012), and the ClpX moiety of the ClpXP protease involved in FtsZ degradation (Camberg, *et al*., 2009). In *B. subtilis* and *Mycobacteria* the central hub of FtsZ also interacts with SepF, a protein needed for anchoring FtsZ to the membrane, which in *Mycobacteria* is essential (Hamoen, *et al*., 2006), (Singh, *et al*., 2008), (Krol, *et al*., 2012), (Gola, *et al*., 2015). An additional *B. subtilis* membrane protein, EzrA, blocks FtsZ assembly by its interaction with the FtsZ central hub (Singh, *et al*., 2007). The existence of so many partners interacting with a single region of FtsZ suggest that the assembly of the divisome, the constriction of the FtsZ-ring and the disposal of spent components respond to a complex set of competing regulatory signals still to be described in detail.

2. FtsA and ZipA: the proto-ring anchors

In Enterobacteria, FtsZ is tethered to the cytoplasmic membrane by two proteins, ZipA and FtsA, both of them essential in *E. coli* (Addinall, *et al*., 1996), (Hale & de Boer, 1997). Furthermore, the midcell localization of FtsA and ZipA depends on the presence and localization of FtsZ (Hale & de Boer, 1999). The complete assembly of these three proteins forms the proto-ring structure (Vicente & Rico, 2006). In *E. coli* there are approximately 3000 to 5000 molecules of FtsZ, 50 to 200 molecules of FtsA and 1500 molecules of ZipA per cell (Pla, *et al*., 1991), (Rueda, *et al*., 2003). An equilibrium between the amounts of the proto-ring components is important for cell division since either the overproduction or depletion of these proteins results in a defective FtsZ-ring and blocks septation. The balance of FtsA relative to FtsZ is particularly important as deviations in their ratio are detrimental (Dai & Lutkenhaus, 1992).

The cytoplasmic protein FtsA is a widely conserved membrane binding protein among bacteria (Rothfield, *et al*., 1999) that attaches to the cytoplasmic membrane through its C-terminal amphipathic helix. This interaction with the membrane is essential for its function in cell division and for tethering the FtsZ-ring (Pichoff & Lutkenhaus, 2005).

The FtsA crystal structure from *Thermotoga maritima* (van den Ent & Löwe, 2000) confirmed a previously predicted *in silico* model (Sanchez, *et al*., 1994) that classified FtsA as an ATP binding protein belonging to the actin family. FtsA comprises two domains, each of them can be divided into two subdomains (1A, 1C, 2A and 2B) where the subdomains 1A, 2B and 2A together participate in the ATP binding site (van den Ent & Löwe, 2000). The FtsA 2B subdomain interacts with the central hub of FtsZ (Szwedziak, *et al*., 2012) **(Figure 2)**. However, FtsA differs from the actin family in the orientation of the 1C subdomain, which is specific to the FtsA protein whereas other members of the family contain a 1B subdomain adjacent to the 2B subdomain (van den Ent & Löwe, 2000). This FtsA-specific subdomain plays a critical role recruiting other divisome proteins as the equally essential FtsN (Rico, *et al*., 2004), (Busiek, *et al*., 2012) or in FtsA self-assembly (Krupka, *et al*., 2012), (Szwedziak, *et al*., 2012). Polymerization and attachment of FtsA to the membrane is favoured by ATP binding through a molecular mechanism in which this binding triggers a conformational switch of the amphipathic helix located at the C-terminus of FtsA. This conformational change accompanies the attachment of the protein to the membrane and facilitates its

polymerization (Krupka, *et al*., 2014). FtsA binds ATP (Sanchez, *et al*., 1994) promoting the *in vitro* self-assembly into actin-like protofilaments (Lara, *et al*., 2005), (Szwedziak, *et al*., 2012), but a clear ATPase activity has not been proven for the *E. coli* protein. Encapsulation of FtsA and FtsZ inside giant unilamelar vesicles results in the appearance of FtsZ rings attached by FtsA to the inner surface of the vesicle at sites where curvature discontinuities are present (Szwedziak, *et al*., 2014). In addition the interaction of FtsA with FtsZ detected by total internal reflection microscopy (TIRFM) suggests a role for FtsA in the dynamics of FtsZ filament reorganization (Loose & Mitchison, 2014). This reorganization of the FtsZ filaments may result from the dual function that FtsA exerts on FtsZ, first favouring the anchoring of FtsZ to the membrane, and exerting then a negative effect to destabilize the FtsZ polymers. These results are compatible with a model in which the interaction with FtsA on the membrane is essential for the rearrangements of the network of FtsZ filaments allowing the FtsZ-ring to adapt its diameter during constriction (Loose & Mitchison, 2014).

The ZipA protein is only found in gamma-proteobacteria (RayChaudhuri, 1999). It is a bitopic cytoplasmic membrane protein with a short periplasmic N-terminal end, a single transmembrane domain and a large cytoplasmic part. The cytoplasmic part contains a Map-Tau repeat, a charged domain, a proline-glutamine enriched region (P/Q) and the C-terminal globular domain (Hale & de Boer, 1997), (RayChaudhuri, 1999). While all the other parts may serve a structural role, the C-terminal globular domain contains the FtsZ binding site (FZB) that is sufficient to interact with the central hub of FtsZ (Mosyak, *et al*., 2000), (Moy, *et al*., 2000) **(Figure 2)**. This interaction protects FtsZ from degradation by the housekeeping protease complex ClpXP (Pazos, *et al*., 2013). This role is specific for ZipA and cannot be replaced by either FtsA or by FtsA* (Pazos, *et al*., 2013). FtsA* is a gain-of-function FtsA mutant (R268W) (Geissler, *et al*., 2007) able to bypass *in vivo* the requirement for ZipA during cell division. ZipA, together with FtsZ, is required for FtsI-independent preseptal peptidoglycan synthesis, which mediates the transition between cell elongation and constriction. The FtsA* protein is equally able to bypass this role of ZipA (Potluri, *et al*., 2012). Recently, it has been shown that an FtsZ mutant (L169R) is, as FtsA*, a gain-of-function mutant (FtsZ*) that not only is able to bypass the *in vivo* requirement for ZipA in the assembly of the divisome, but also enhances FtsZ polymer bundling (Haeusser, *et al*., 2015).

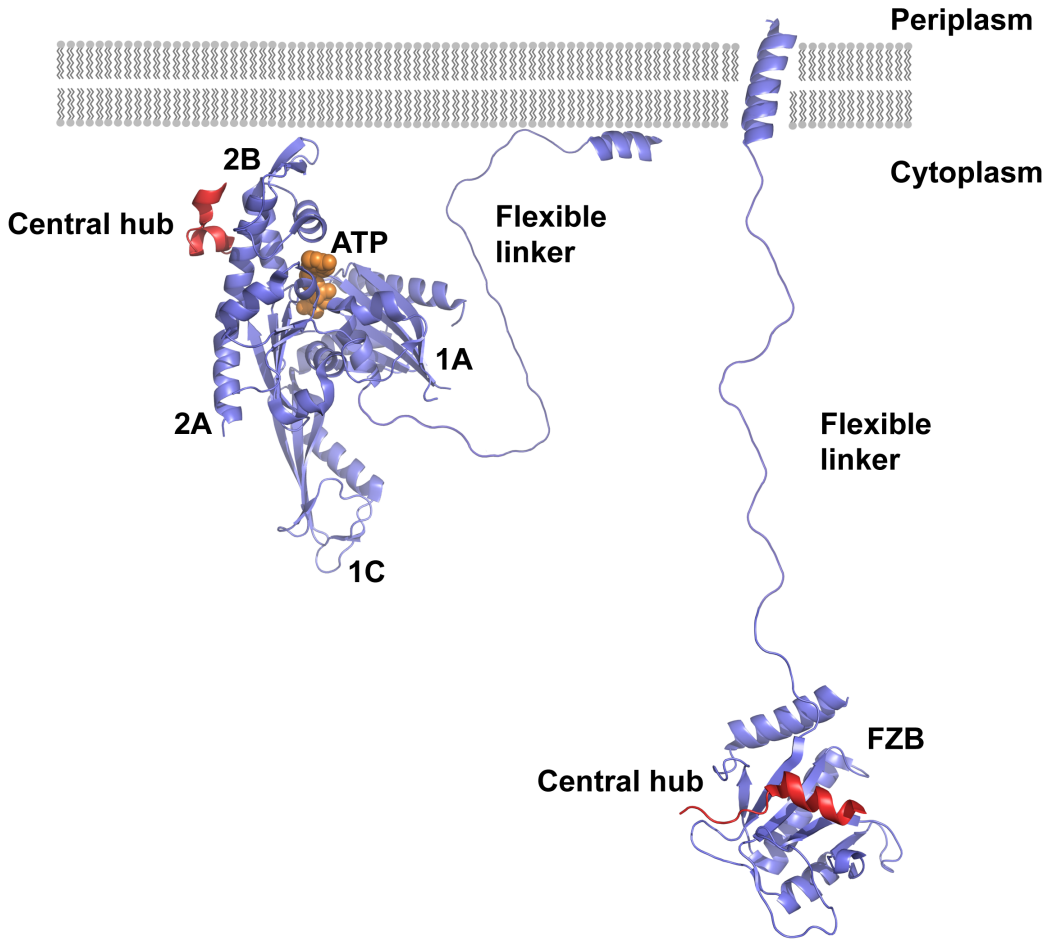

Figure 2. Crystal structures from the *Thermotoga maritima* FtsA and the *E. coli* ZipA. The FtsA molecule is depicted at left showing subdomains 1A, 2A, 2B and the FtsA specific 1C subdomain (adapted from PDB 4A2A). The ATP binding site formed by the interaction of the subdomains 1A, 2A and 2B shows ATP (orange) bound inside it. The central hub of FtsZ (red) is shown bound to the 2B FtsA subdomain. The flexible linker of FtsA is depicted here as a free-drawn unstructured peptide. The amphipathic helix (blue) attaches FtsA to the cytoplasmic membrane. ZipA is shown at right with its C-terminal globular domain, the FtsZ binding site (FZB), bound to the FtsZ central hub (red) (adapted from PDB 1F47). The flexible linker of ZipA is depicted here as a free-drawn unstructured peptide. The transmembrane segment (blue) is an alpha helix, which anchors ZipA to the membrane.

Regarding the structure of ZipA, no clear function is attributed to the P/Q domain. Electron microscopy images identified it as an unfolded flexible polypeptide (Ohashi, *et al.*, 2002) suggesting that it may play a role in the orientation of the bound FtsZ polymers on the membrane surface (Erickson, 2001). Recently this domain was found to undergo conformational changes depending on the lateral protein density packing changing from a condensed coiled state at low densities to a more extended brush-like conformation when the density is higher (López-Montero, *et al.*, 2013). Although the lipid composition of the membrane may modulate the shape and the oligomeric state of

the FtsZ polymers on the surface (Mateos-Gil, *et al*., 2012) a role of the ZipA anchoring region in this effect has not been proven (Hale & de Boer, 1999).

Studies using *E. coli* maxicells as well as *in vitro* FtsZ assembly experiments show that ZipA stabilizes FtsZ and induces the formation of higher order structures or bundles (Hale, *et al*., 2000), (Pazos, *et al*., 2013). Furthermore interaction between ZipA and FtsZ is sufficient to promote membrane constriction when both proteins are encapsulated together with GTP in giant unilamelar vesicles. *In vivo*, an excess of ZipA modifies the cytoplasmic membrane where it produces invaginations and disrupts membrane potential (Cabre, *et al*., 2013).

In contrast to FtsA that only recruits FtsZ polymers, ZipA can recruit FtsZ monomers to the membrane (Loose & Mitchison, 2014). This may be due to the higher binding affinity that ZipA has for FtsZ. FtsZ monomers are recruited to the membrane by ZipA where they polymerize, whereas the FtsA binding is too weak to allow FtsZ binding of monomers needing the multiple interaction sites provided by the FtsZ polymers to establish a more stable interaction (Loose & Mitchison, 2014).

3. Min proteins: the ring scouts

The Min system comprises the MinC, MinD and MinE proteins that spatially regulate FtsZ-ring positioning by inhibiting FtsZ polymerization near the cell poles. Upon ATP binding, MinD forms a dimer that associates via its C-terminal amphipathic helix (Szeto, *et al*., 2003) to the cytoplasmic membrane. MinC is the FtsZ-interacting protein and has itself a very low FtsZ inhibitory activity (Zhou & Lutkenhaus, 2005) that needs to be activated upon binding to membrane-bound MinD (de Boer, *et al*., 1992), (Hu & Lutkenhaus, 2003). MinC has two functional domains (Cordell, *et al*., 2001): the N-terminal domain blocks FtsZ-ring assembly by interacting with the FtsZ central hub and the C-terminal domain interacts with MinD (Hu, *et al*., 1999). The binding of MinD to ATP causes the MinCD complex to attach to the cytoplasmic membrane where it blocks the polymerization of FtsZ in its vicinity **(Figure 3)**. To specifically prevent FtsZ assembly at the cell poles a third element, the MinE protein is needed (Lutkenhaus, *et al*., 2012). It binds to the MinCD complex and stimulates the ATPase activity of MinD. As a consequence MinE dissociates the MinCD complex from the membrane (Loose, *et al*., 2008). The combined effect of the three proteins causes the soluble MinC and MinD

complex to move along the cell to occupy positions where no MinE is present. The movement of MinD and MinC results in a pole-to-pole oscillation of the Min system governed by MinE (Raskin & de Boer, 1999). The available MinDE co-crystal structure suggests an oscillating mechanism based on the conformational changes of the Min proteins where MinE senses a MinD dimer at the membrane (Park, *et al*., 2011). MinE switches between a latent state that activates the MinD ATPase activity and releases it from the membrane, and an active state, that allows MinD binding to the membrane (Park, *et al*., 2011). The co-crystal structure of the MinCD complex suggests that it polymerizes when bound to the membrane, these polymers would be the active structure to inhibit FtsZ-ring formation (Ghosal, *et al*., 2014).

In contrast to *E. coli*, where due to the action of MinE, the MinCD proteins oscillate and block septation at the poles, the Gram-positive model bacterium *B. subtilis* lacks MinE and its Min system is therefore static. In addition while the Min function in *E. coli* requires ATP the *B. subtilis* mechanism does not. In this case MinD is recruited by MinJ to the septum during the assembly of the divisome and by recruiting MinC renders the nascent poles inactive for further divisions (Marston, *et al*., 1998). In its turn, MinJ is recruited to the septum by DivIVA, a protein that localizes at sites where the membrane curvature is higher (Bramkamp, *et al*., 2008). The majority of the MinC and MinD proteins in *B. subtilis* subsequently remain at the cell poles.

4. Nucleoid occlusion: obstruction of the ring

Nucleoid occlusion prevents the FtsZ-ring from assembling at the positions occupied by the nucleoid (Jaffe, *et al*., 1990), (Woldringh, *et al*., 1991). It is only when the two nucleoids segregate to each opposite site of the dividing cell when the midcell position becomes available to place the FtsZ-ring (Jaffe, *et al*., 1990), (Woldringh, *et al*., 1991). The *E. coli* nucleoid occlusion system effector is SlmA, a DNA binding protein that when bound as a dimer of dimers (Tonthat, *et al*., 2013) to a specific DNA sequence (SBS; SlmA binding sequences) blocks the FtsZ-ring formation in the cell regions occupied by the nucleoid (Bernhardt & de Boer, 2005) **(Figure 3)**. In *E. coli* the two septum placement systems, Min and NO, contribute to the precise localization of the FtsZ-ring (Pazos, *et al*., 2014). *In vitro* studies show that SlmA needs to be bound to the SBSs to increase its affinity for the FtsZ filament and disrupt it (Cho, *et al*., 2011), (Du

& Lutkenhaus, 2014). Similarly to MinC, SlmA interferes with the FtsZ self-assembly without affecting its GTPase activity (Cabre, *et al*., 2015). However, some discrepancies regarding the molecular mechanism used by SlmA to inhibit FtsZ-ring assembly remain unsolved. A model based on the SlmA-SBS structure proposes that the complex generates a pocket, which sequesters FtsZ filaments preventing them to grow and to establish lateral interactions (Tonthat, *et al*., 2013). A different model, based on the behaviour of SlmA variants that failed to regulate FtsZ assembly, proposes that dissasembly of FtsZ from the FtsZ-ring needs only the presence of one SlmA functional FtsZ interaction interface, provided that the monomer forms part of a dimer (Cho & Bernhardt, 2013). More recently, it has been shown that the FtsZ central hub, is also involved in the interactions between SlmA and FtsZ (Du & Lutkenhaus, 2014). These results support a different model in which the SlmA/SBS complex would contact the FtsZ filaments through the central hub of FtsZ but an additional interaction with another part of FtsZ would be needed to disrupt the filament (Du & Lutkenhaus, 2014).

Noc is the effector of the nucleoid occlusion system in *B. subtilis* (Wu & Errington, 2004). As SlmA in *E. coli*, the Noc protein in *B. subtilis* inhibits cell division when it is bound to specific DNA sequences (Wu, *et al*., 2009), (Tonthat, *et al*., 2013). However, the mode of action of Noc differs from its *E. coli* equivalent (Adams, *et al*., 2015). Noc binds through its N-terminus to the cell membrane where it recruits the DNA sequences and prevents division (Adams, *et al*., 2015). On the other hand, no evidence has been found to show that Noc interacts with FtsZ (Adams, *et al*., 2015) as SlmA does (Du & Lutkenhaus, 2014).

Whereas the septum positioning mechanisms present in the rod-shaped *E. coli* and *B. subtilis* are based on the inhibition of the assembly of the FtsZ-ring, the selection of the septation site in *Streptococcus pneumoniae*, a coccal bacterium, is determined by a positive mechanism in which the FtsZ protein seems to be attracted towards the septation site. In this case a membrane protein, MapZ (Fleurie, *et al*., 2014) also known as LocZ (Holeckova, *et al*., 2015), forms a ring at midcell. MapZ guides FtsZ to the division site by a simple mechanism in which the extracelullar domain of MapZ recognizes and interacts with the nascent peptidoglycan synthetized at midcell whereas its intracellular domains provides a physical anchor for FtsZ, positioning it at the

division site. The phosphorylation state of MapZ is also involved in the stabilization of the FtsZ-ring and may participate in constriction (Fleurie, *et al*., 2014).

Positive mechanisms to control FtsZ-ring localization are also present in *Streptomyces*, the filamentous soil bacterium (Willemse, *et al*., 2011) and *Myxococcus*, a rod-shape δ-proteobacterium (Treuner-Lange, *et al*., 2013). During sporulation, the SsgAB proteins localize at the future division sites in the *Streptomyces* aerial mycellium where SsgB tethers FtsZ to the cytoplasmic membrane positioning the FtsZ-ring at the multiple septation sites required for spore formation (Willemse, *et al*., 2011). In *Myxococcus* the PomZ protein, perhaps in combination with other divisome elements, is a positive mechanism to recruit FtsZ to division site (Treuner-Lange, *et al*., 2013).

5. ClpXP: ring degradation

FtsZ is among the many substrates degraded by the two-component ClpXP protease complex. In this regard ClpXP is considered as a negative regulator of the FtsZ-ring assembly in *E. coli* (Camberg, *et al*., 2009) and *B. subtilis* (Weart, *et al*., 2005). The assembly of ClpX into an hexamer produces a cavity in which each monomer exhibits ATPase activity. A stacked double ring of ClpP heptamers, in which the degradation chamber is located, is sandwiched between two hexamers (Sauer, *et al*., 2004). In *E. coli* ClpX binds FtsZ through its central hub and uses the energy of ATP hydrolysis to unfold and translocate FtsZ through its central pore into the ClpP degradation chamber (Sauer, *et al*., 2004). *In vitro* experiments have shown that the ClpXP complex recognizes FtsZ either as monomers or polymers. When acting on polymers, the ClpXP activity may result in the depolymerization of the FtsZ-ring (**Figure 3)** (Camberg, *et al*., 2009).

Whereas in *E. coli* the ATP hydrolysis of the ClpXP complex is required for FtsZ degradation, the homologous ClpXP complex in *B. subtilis* is independent of the ATP hydrolysis activity (Haeusser, *et al*., 2009). Biochemical results suggest that the ClpX from *B. subtilis* inhibits FtsZ assembly through a ClpP-independent mechanism that does not require ATP hydrolysis to unfold the protein (Haeusser, *et al*., 2009).

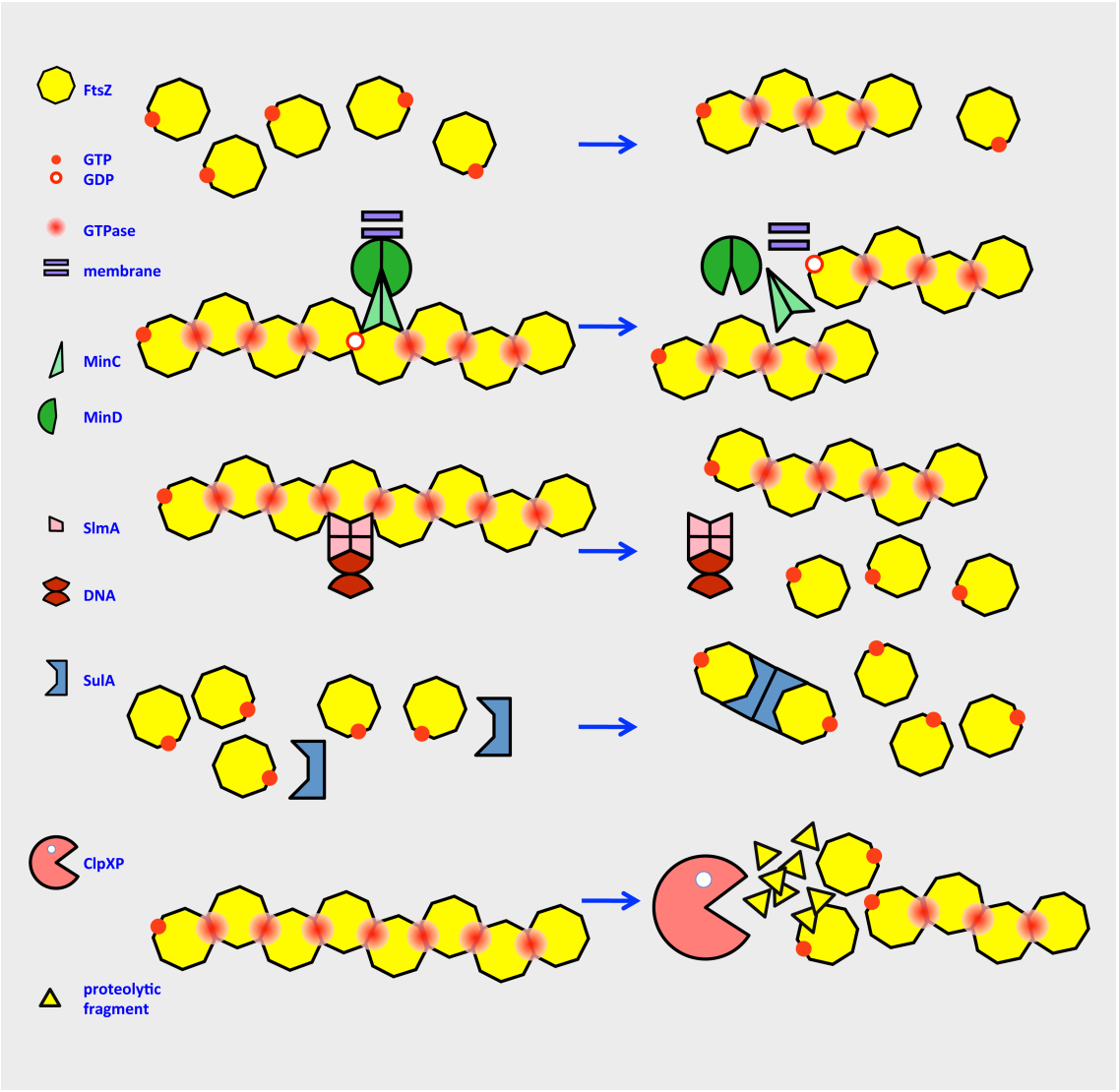

Figure 3. Mechanisms used by the negative modulators involved in the assembly of the FtsZ-ring. FtsZ monomers are represented with either one bound GDP or GTP molecule. Polymers are formed once the concentration of the charged FtsZ monomers reaches the critical concentration (arbitrarily fixed as four monomers in a field) (top row). MinC dimers in the MinCD complex (second row) interfere with already formed FtsZ filaments dissociating them into shorter polymers of narrowly distributed size. SlmA (third row) forms dimers of dimers and associate to specific DNA sequences (SBS) in the nucleoid. The SlmA SBS complex dissociates the FtsZ polymers, producing shorter polymers of assorted sizes. SulA dimers (fourth row) bind to two FtsZ monomers sequestering them from the available pool and precluding the assembly of the GTPase binding site. SulA favours the FtsZ monomer state by lowering the concentration of FtsZ below the critical value needed to polymerize. The action of the ClpXP protease complex in depolymerizing and cleaving FtsZ is depicted in the bottom row. Image modified from Cabré *et al.*, 2015.

6. The SOS response: an emergency division block

In *E. coli* septation is delayed by the induction of the SOS response in response to DNA damage, presumably to allow repair of otherwise lethal lesions (Huisman, *et al.*, 1984). The SulA protein is a division inhibitor produced as part of the SOS response (Walker,

1995). Elevated levels of SulA are sufficient to cause division inhibition (Huisman, *et al*., 1984). *In vitro* results demonstrated that SulA interacts with FtsZ and inhibits its GTPase activity and polymerization thus preventing the assembly of the FtsZ-ring (Trusca, *et al*., 1998).

The crystal structure of the *Pseudomonas aeruginosa* SulA together with *P. aeruginosa* FtsZ shows SulA as a dimer. Each monomer in the dimer retains one free region at the site opposite the dimerization surface which is available for engaging in the interaction with one FtsZ molecule **(Figure 3)** (Cordell, *et al*., 2003). The SulA interaction exclusively involves 5-amino acid residues of the catalytic T7 loop of FtsZ needed for GTP hydrolysis (Cordell, *et al*., 2003). This interaction prevents altogether the interaction between FtsZ monomers required for generating the nucleotide binding site (Cordell, *et al*., 2003). As a result, SulA binding removes the FtsZ monomers from the intracellular pool and therefore decreases the amount of FtsZ available to assemble the FtsZ-ring (Dajkovic, *et al*., 2008), (Cheng, *et al*., 2012). Once the DNA damage is repaired, the levels of SulA are rapidly decreased by the proteolytical action of the Lon protease and division is resumed (Mizusawa & Gottesman, 1983).

7. FtsZ associated Zap proteins: supporters of the ring

The FtsZ-associated proteins ZapA, ZapB, ZapC, ZapD and ZapE interact at an early stage of FtsZ-ring assembly and co-localize with it. All are dependent on the presence of FtsZ for their localization. There is no amino acid sequence homology among the different Zap proteins and deletions of individual *zap* genes do not affect cell viability (Durand-Heredia, *et al*., 2012). Only the deletion of more than one *zap* gene produces moderate filamentation phenotypes (Durand-Heredia, *et al*., 2012).

ZapA is highly conserved among bacteria, whereas ZapB, ZapC, ZapD and ZapE are restricted to gamma-proteobacteria (Ebersbach, *et al*., 2008), (Hale, *et al*., 2011), (Marteyn, *et al*., 2014). It was first discovered in *B. subtilis* as a factor that antagonizes the effect of MinCD (Gueiros-Filho & Losick, 2002). The *P. aeruginosa* ZapA monomer consists of an N-terminal globular domain and a long C-terminal coiled-coil domain (Low, *et al*., 2004) and can dimerize through the N-terminal domain. The oligomeric state of ZapA depends on its concentration, being dimeric at low concentrations and tetrameric at high protein concentrations. The tetramer is formed by

an anti-parallel association of two ZapA dimers by their long C-terminal coiled-coil domains (Low, *et al*., 2004). Considering that there are approximately 7000 ZapA molecules per *E. coli* cell (Mohammadi, *et al*., 2009), the protein may adopt *in vivo* any of the possible oligomeric states (Low, *et al*., 2004). *In vitro* FtsZ polymerization assays show that ZapA hinders the GTPase activity of the FtsZ polymers and organizes them into bundles (Gueiros-Filho & Losick, 2002), (Low, *et al*., 2004), (Small, *et al*., 2007). Although no structural data of the ZapA-FtsZ complex are available, predictions from the surface electrostatic potential suggest that the ZapA N-terminal globular domain may be involved in the interaction with FtsZ (Low, *et al*., 2004).

The ZapB protein may be involved in FtsZ-ring assembly as its overproduction results in nucleoid condensation and formation of ectopic cell division septa (Ebersbach, *et al*., 2008). In *E. coli* ZapB is an abundant protein with approximately 13000 molecules per cell. Structural studies show that ZapB is a coiled-coil protein and its oligomers assemble spontaneously into long filaments through their termini (Ebersbach, *et al*., 2008). Once ZapB is self-assembled, it interacts with ZapA and with FtsZ **(Figure 4)** (Galli & Gerdes, 2012). ZapB and ZapA interact through the N-terminal region of ZapB and the C-terminal coiled-coil domain of ZapA (Galli & Gerdes, 2012). The interaction of ZapB with FtsZ is proposed to be mediated by ZapA (Galli & Gerdes, 2012) but it may also be direct as was found in a *zapA* deletion strain (Pazos, *et al*., 2013). Furthermore it has been proposed that ZapB participates in the withdrawal of FtsZ from midcell preceding the closure of the septum (Pazos, *et al*., 2013). ZapB also interacts with MatP, a DNA-binding protein involved in the condensation and segregation of the chromosome (Espeli, *et al*., 2012), (Buss, *et al*., 2015). These data could explain why nucleoid condensation occurs when ZapB is overproduced.

The *zapC* gene was identified under conditions of Min system depletion as its deletion causes severe cell division defects (Hale, *et al*., 2011). The ZapC protein binds to FtsZ polymers and inhibits the FtsZ GTPase activity **(Figure 4)**. ZapA, ZapB, FtsA or ZipA are not needed *in vivo* for ZapC localization that only depends on FtsZ (Hale, *et al*., 2011). Overproduction of ZapC causes a severe stop in cell division and, as a consequence, aberrant FtsZ structures have been visualized (Hale *et al*., 2011). Details on the ZapC interaction with FtsZ are not available.

ZapD is a low abundance protein with approximately 500 molecules per cell (Durand-Heredia, *et al*., 2012). The potential role of *E. coli* ZapD as a stabilizer of the FtsZ-ring has been proposed given its inability to localize in a *ftsZ84*(Ts) strain when FtsZ is inactivated at the restrictive temperature. Cells carrying *ftsZ84* form filaments with no visible FtsZ-rings when they are shifted to the restrictive temperature (42ºC) (RayChaudhuri & Park, 1994). These results indicate that FtsZ is required for the localization of ZapD at midcell. *In vitro* ZapD interacts with the central hub of FtsZ promoting the assembly of FtsZ polymers into bundles (Durand-Heredia, *et al*., 2012) **(Figure 4)**. This suggests that ZapD could also enhance the lateral interactions between FtsZ polymers (Durand-Heredia, *et al*., 2012).

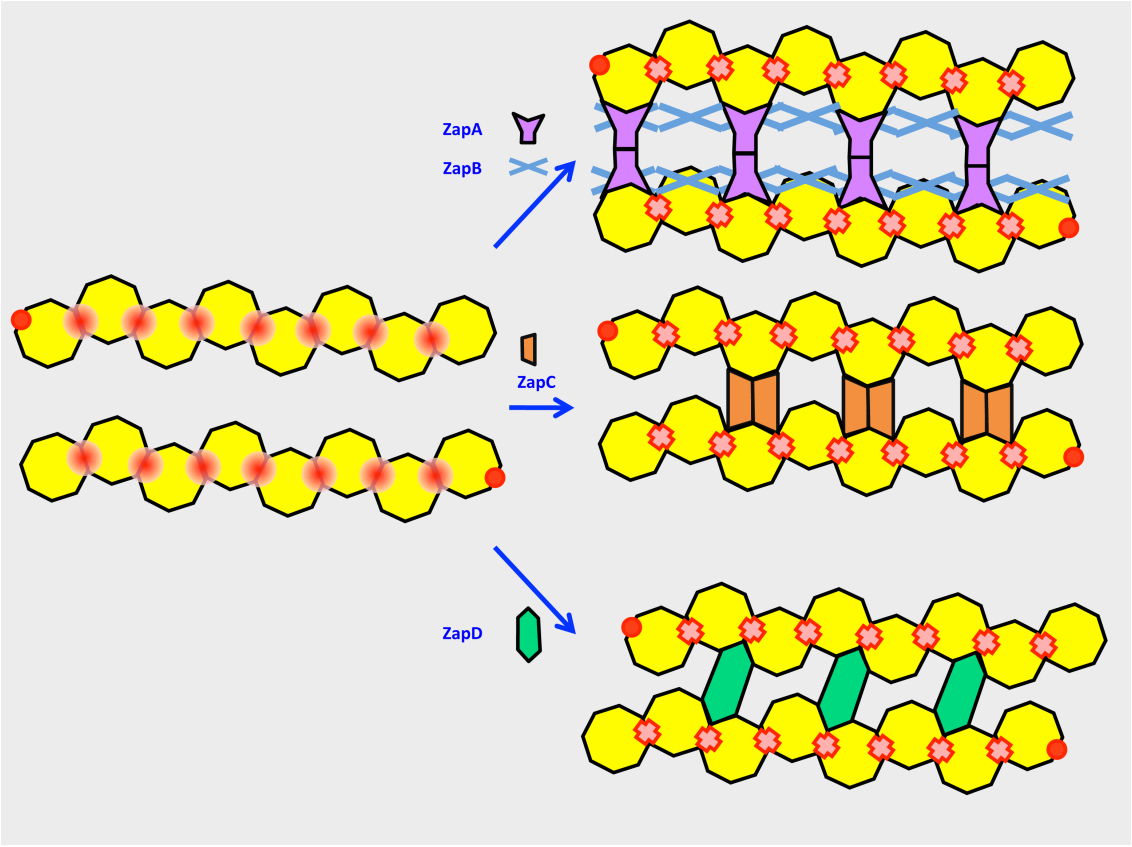

Figure 4. Bundling of the FtsZ protofilaments assisted by the Zap proteins. ZapA binds to the FtsZ filament (the simplest model involving monomers is represented, see text for further details). Two ZapA monomers, each attached to a FtsZ polymer, self-interacts to form a dimer acting as a bridge that promotes lateral interactions between two FtsZ polymers. ZapB assembles to form a network of filaments that interact with ZapA and together stabilize FtsZ polymers and favour the formation of FtsZ bundles. The GTPase activity is reduced upon bundling (represented as a cross). ZapC interacts with FtsZ polymers reducing their GTPase activity and making them more stable. ZapD also promotes the formation of FtsZ bundles establishing lateral interactions between FtsZ polymers and reducing the GTPase activity.

Contrary to the Zap proteins described above, the ZapE protein destabilizes the FtsZ polymers. It was identified in *Shigella flexneri*, an enterobacteria, under low oxygen growth conditions (Marteyn, *et al*., 2014). A mutant in the the analogous *E. coli zapE* gene causes a lethal phenotype when grown in anaerobiosis. ZapE contains an ATP binding domain and has ATPase activity. In the presence of ATP this activity results in the loss of stability of FtsZ polymers *in vitro*. Equally, the overproduction of ZapE reduces FtsZ-ring stability inducing filamentation *in vivo* (Marteyn, *et al*., 2014). Also in contrast to the other Zap proteins, which act at early cell division steps, ZapE acts later interacting perhaps with the late assembly divisome proteins FtsQ, FtsL, FtsI and FtsN (Marteyn, *et al*., 2014). It is important to note that these late assembling proteins, FtsN in particular, play a key role in the stability of the already assembled proto-ring (Rico, *et al*., 2004).

OBJECTIVES

Objectives

Our aim is to investigate the assembly of the bacterial cell division protein FtsZ, focus on the interactions of FtsZ with itself and other divisome elements established during its assembly. We will use a set of biochemical, biophysical and *in vivo* approaches in an effort to understand the following objectives:

Study *in vitro* the polymerization of FtsZ in the presence of different divalent cations. We will describe the biochemical properties of FtsZ assembly when the essential divalent magnesium is replaced by manganese, a divalent cation with similar biochemical properties.

Crystallization of the FtsZ protein from *E. coli*. We will try to crystallize the FtsZ dimer to further study how the nucleotide and the divalent cation are arranged in the interface between the two monomers.

Study the molecular interaction of the associated protein ZapC with FtsZ. Crystallographic studies on ZapC and site-directed mutagenesis will help to define the role of ZapC in cell division.

Finally, we will evaluate if the cell phenotype caused by ZapC overproduction can be counteract by the overproduction of another cell division protein.

MATERIALS & METHODS

1. Materials

1.1. *Escherichia coli* strains

The bacterial strains used in this study are described in Table 1.

Table 1. Strains used in this work

Strain	Relevant characteristics	Source or reference
DH5α	*endA1, gyrA, hsdR17, relA, recA1, supE44, thi1, Δ(lacaya-argF)U169, ϕ80(lacZΔM15), F-*	(Hanahan, 1983)
C41	*F- ompT, hsdS$_B$(r_B- m_B-), gal, dcm (DE3)*	Invitrogen
CH59	TB28, *zapC<>frt*	(Hale *et al*., 2011)

1.2. Plasmids

The plasmids used in this study, their relevant properties and markers are shown in Table 2.

Table 2. Plasmids used in this work.

Plasmid	Relevant characteristics and markers	Source or reference
pBAD22	Cloning vector, contains P_{BAD} promoter, Amp_r	(Guzman, *et al*., 1995)
pBAD33	Cloning vector, contains P_{BAD} promoter, Cam_r	(Guzman *et al*., 1995)
pDSW210	pTrc99A, down mutations in -35, -10, Amp_r	(Weiss *et al*., 1999)
pHis17	Expression plasmid for C-terminal his-tag. P_{T7} promoter, Amp_r	(Van den Ent and Löwe 2000)
pMFV56	*ftsZ* cloned in the MCS of pET28a, kan_r	Laboratory Stock
$pMinC^N$	*minC* $_{1\text{-}115aa}$ cloned in MCS of pTXB1, Amp_r	D. Ghosal, MRC-LMB
pPNV40	pTrc99A-*ftsA*, Amp_r	Laboratory Stock

pPZV33	pTrc99A-*ftsA**, Amp_r	Laboratory Stock
pSGV33	*Mtb ftsZ* cloned in MCS pET28a, Kan_r	Laboratory Stock
pSGV34	*Msm ftsZ* cloned in MCS pET28a, Kan_r	Laboratory Stock
pCOV1	*ftsZΔC5* cloned in MCS of pET28a, Kan_r	This work
pCOV2	*ftsZΔC10* cloned in MCS of pET28a, Kan_r	This work
pCOV3	*ftsZΔC30* cloned in MCS of pET28a, Kan_r	This work
pCOV4	pZapC with a point mutation M28D, Amp_r	This work
pCOV5	pZapC with a point mutation F58D, Amp_r	This work
pCOV6	$pZapC_{his}$ with a point mutation M28D, Amp_r	This work
pCOV7	$pZapC_{his}$ with a point mutation F58D, Amp_r	This work
pCOV13	pBAD22-*$zapC_{his}$ M28D* , Amp_r	This work
pCOV14	pBAD22-*$zapC_{his}$ F58D* , Amp_r	This work
pCOV15	pBAD22-*$zapC_{his}$* , Amp_r	This work
pCOV17	pBAD22-*$zapC_{his}$ M28D-F58D*, Amp_r	This work
pCOV19	pZapC *M28D-F58D*, Amp_r	This work
pCOV20	$pZapC_{his}$ *M28D-F58D*, Amp_r	This work
pCOV21	*ftsZ* $_{1\text{-}317aa}$ cloned in MCS of pET28a, Kan_r	This work
pCOV22	*ftsZ* $_{1\text{-}314aa}$ cloned in MCS of pET28a, Kan_r	This work
pCOV23	*ftsZ* $_{1\text{-}311aa}$ cloned in MCS of pET28a, Kan_r	This work

pCOV24	*ftsZ* $_{1\text{-}307aa}$ cloned in MCS of pET28a, Kan_r	This work
pCOV25	*ftsZ* $_{7\text{-}317aa}$ cloned in MCS of pET28a, Kan_r	This work
pCOV26	*ftsZ* $_{7\text{-}314aa}$ cloned in MCS of pET28a, Kan_r	This work
pCOV27	*ftsZ* $_{7\text{-}311aa}$ cloned in MCS of pET28a, Kan_r	This work
pCOV28	*ftsZ* $_{7\text{-}307aa}$ cloned in MCS of pET28a, Kan_r	This work
pCOV29	*ftsZ* $_{11\text{-}317aa}$ cloned in MCS of pET28a, Kan_r	This work
pCOV30	*ftsZ* $_{11\text{-}314aa}$ cloned in MCS of pET28a, Kan_r	This work
pCOV31	*ftsZ* $_{11\text{-}307aa}$ cloned in MCS of pET28a, Kan_r	This work
pCOV32	*ftsZ* $_{13\text{-}317aa}$ cloned in MCS of pET28a, Kan_r	This work
pCOV33	*ftsZ* $_{13\text{-}314aa}$ cloned in MCS of pET28a, Kan_r	This work
pCOV34	*ftsZ* $_{13\text{-}311aa}$ cloned in MCS of pET28a, Kan_r	This work
pCOV35	*ftsZ* $_{13\text{-}307aa}$ cloned in MCS of pET28a, Kan_r	This work
pCOV36	pBAD33-*zapC*$_{his}$, Cam_r	This work

1.3 Antisera

The polyclonal antisera used in this work are described in Table 3.

Table 3. Antisera used in this work

Target protein	Antibody	Dilution (IF)	Dilution (WB)	Source or reference
FtsZ	MVJ9	1:350	1:20000	Pla *et al*., 1991

Histidine	Anti-histidine	1:2000	1:40000	Sigma
ZapC	Anti-ZapC	ND	1:50	This work
FtsA	MVM1	N/A	1:500	Laboratory stock

ND: not determine N/A: not applicable

1.4. Primers

Oligonucleotide primers used in this work are listed in Table 4.

Table 4. Primers used in this work

Primer	Sequence 5'- 3'	Orientation	Target
CO1	GGTCATATGTTTGAACCAATGGAACTTACCAATGACGCGG	Fw[a]	*ftsZ*
CO2	GGTGGATCCTTACAGGAATGCTGGGATATCCAGATAATCC	Rv[b]	*ftsZ*ΔC5[c]
CO3	GGTGGATCCTTAATCCAGATAATCCGGCTCTTTCGCAG	Rv	*ftsZ*ΔC10
CO4	GGTGGATCCTTACGGCTTCTGCTCCTGGGTCA	Rv	*ftsZ*ΔC30
CO5	GGTCATATGCGAATTAAACCAGACGATAACT	Fw	*zapC*
CO6	GGTGGATCCTTAGACTGCCTGTTCGAGGCTGTT	Rv	*zapC*
CO7	CGATTTAGCCAATGGTGATCTATTTCGCTCACG	Fw	*zapC M28D*
CO8	CGTGAGCGAAATAGATCACCATTGGCTAAATCG	Rv	*zapC M28D*

CO9	CGACGCCGCGCTCTATGATTCTTTTGAAGAAAA GTGC	Fw	*zapC F58D*
CO10	GCACTTTTCTTCAAAAGAATCATAGAGCGCGGC GTCG	Rv	*zapC F58D*
CO11	GGTCATATGCTTACCAATGACGCGGTGATT	Fw	*ftsZ*ΔN7
CO12	GGTCATATGGCGGTGATTAAAGTCATCGG	Fw	*ftsZ*ΔN11
CO13	GGTCATATGATTAAAGTCATCGGCGTCGG	Fw	*ftsZ*ΔN13
CO14	GGTGGATCCCATGCCGATACCTGTCGCA	Rv	*ftsZ*ΔC66
CO15	GGTGGATCCACCTGTCGCAACAACGGTTA	Rv	*ftsZ*ΔC69
CO16	GGTGGATCCAACAACGGTTACGCGCAGC	Rv	*ftsZ*ΔC72
CO17	GGTGGATCCGCGCAGCTCGTCATTCATAT	Rv	*ftsZ*ΔC76

[a] Forward (Fw) [b] Reverse (Rv) [c] ΔC5= deletion of the last 5 amino acid residues from the C-terminus

1.5. Chemical reagents

Chemical reagents used in this work are listed in the Table 5.

Table 5. Chemicals used in this work

Product	Utility	Supplier
Acrilamide: N, N'-methyl bisacrilamide	Protein electrphoresis	BioRad
Agar	Preparation of LB plates	Pronadisa
Agarose	DNA electrophoresis	Pronadisa

Alexa-594 conjugated anti-rabbit serum	Secondary antibody (immunofluorescence)	Molecular Probes
Antibiotics (ampicillin, kanamacyn, chloramphenicol, tetracycline)	Selection marker	Roche
Arabinose	Protein overproduction	Merck
BM Chemiluminiscence Blotting Substrate (POD)	Inmunoblotting	Roche
Bradford reagent	Protein quantification	BioRad
BCA Protein Assay Kit	Protein quantification	Life Technologies
DNA marker	DNA electrophoresis	Promega
Filters (0.22 μm pore diameter)	Transfer of cultures to different medium	Millipore
General Chemical Reagents	Prepare Buffer solution	Merck, Sigma
Glucose	Protein repression	Merck
Inmobilon-P membrane, PVDF	Inmunoblotting	Millipore
Isopropyl β-D-1-thiogalactopyranoside (IPTG)	Protein induction	Roche
Kodak Biomax XAR film	Inmunoblotting	Sigma
Miniprep Kit	Plasmid DNA isolation	Qiagen, Promega
Precision Plus Protein Standars Dual Color	Protein electrophoresis	BioRad

Protein-A Horseradish peroxidase	Inmunoblotting	BioRad
Pfu DNA polymerase	PCR	New England Biolabs
Taq DNA polymerase	PCR	Roche
Uranil Acetate 2%	Negative stain Electron microscopy	EMS
Vectashield	Fluorescence microscopy	Vector Laboratories

2. Methods

2.1. Bacterial growth conditions

Escherichia coli strains listed in Table 1, if not indicated otherwise, were culture at 37ºC in Luria Bertani broth (LB) or LB agar plates (Sambrook *et al*., 1989), supplemented with antibiotics when required (ampicillin [100 μg/ml], tetracycline [20 μg/ml], kanamycin [50 μg/ml], chloramphenicol [50 μg/ml]). Liquid cultures were grown in an orbital shaker at 250 rpm and 200 rpm for protein induction. The optical density at 600 nm (OD_{600}) was measured using a CO8000 Cell Density Meter WPA biowave. To induce ZapC and ZapC variants (Table 2) cells were grown overnight at 37ºC in a shaking water bath with aeration and then diluted 1:200. The optical density was measured periodically and kept below 0.3 by serial dilutions with prewarmed medium. In this way, the growth rate was constant. When the balance growth was constant, cells were shifted to 0.2% arabinose allowing the expression of *zapC* and its variants. Samples were taken at different time points and processed for SDS-PAGE and inmunoblot.

2.2. Cell parameter measurements

Cell samples were obtained at the times indicated and processed for checking cell number and cell volume after inducing ZapC, ZapC variants, FtsA and FtsA* expression with 0.2% arabinose. Fixed cells (0.75% formaldehyde) were counted with a multichannel analyzer Beckman Coulter Multisizer 3 equipped with a 30-μm-diameter orifice.

2.3. Phase-contrast and fluorescence microscopy

For phase-contrast microscopy cells were spotted on an agarose-padded microscope slide and images were taken with an Olympus DP70 camera coupled to an Olympus BX61 microscope, equipped with a 100X immersion oil lens and the filters. Cells images were captured with the analysis imaging software (Olympus) and further processed with Adobe Photoshop CS5 and the Huygens professional deconvolution software package (Scientific Volume Imaging bv, Hilversum, The Nederlands). Immunofluorescence microscopy was prepared as described by Addinal *et al*., 1996. To localize FtsZ and ZapC-his and variants the primary antibodies were MVJ9 and Anti-histidine (Table 3). As secondary antibodies, Alexa-594 anti-rabbit was used to detect FtsZ and Alexa-488 anti-mouse was used to detect histidine tag fused to ZapC. The coverslip was mounted together with the addition of Vectashield Mounting medium and DAPI on the slide. The coverslip was sealed with transparent nail polish to protect sample from drying during microscopy.

2.4. SDS-PAGE and immunoblot

SDS-PAGE (Laemmli, 1970) and immunoblot (Western-blot) analysis (Towbin, *et al*., 1979) were performed according to standard procedures. For SDS-PAGE, bacterial culture pellets and purify proteins were resuspended in SDS-PAGE lysis buffer and boiled for 10 minutes at 100ºC and 0.1 OD_{600} of bacterial cells was loaded per lane. Blood serum or purified primary antibodies (Table 3) were used for specific protein detection and horseradish peroxidase coupled protein A, the BM Chemiluminescence

blotting substrate, Kodak Biomax XAR film were used for the development of the luminescence signals on PVDF membranes.

2.5. Production of anti ZapC-his antibody

The *zapC* gene was amplified by PCR and cloned into the pHis17 vector (Table 2) fused to a C-terminal histidine tag, producing the plasmid pZapC$_{his}$. The *zapC* gene was amplified from *E. coli* MG1655 chromosomal DNA using CO5 and CO6 as primers. ZapC-his was overproduced and purified according to the standard procedures described in section "Protein purification". Purified ZapC-his was blotted on the PVDF membrane and send for the production of rabbit blood serum (ProteoGenix SAS, Schiltigheim, France) containing polyclonal antibodies that recognize ZapC-his.

2.6. Protein expression and purification

***E. coli* FtsZ.** Untagged full-length FtsZ and all FtsZ variants were purified from 12 litres culture of the expression plasmids (Table 2) transformed in *E. coli* C41(DE3) cells and grown at 37ºC until OD_{600} 0.5, then 1 mM IPTG was added to induce the cultures during 3 hours at 37ºC. Cells were centrifuge and pellets were stored at -80ºC. FtsZ purification was done as described (Mukherjee & Lutkenhaus, 1998) with the following modifications. The frozen pellets were thawed and resuspended in Buffer A (50 mM Tris-HCl pH 8.0, 50 mM KCl, 10 mM EDTA, 10% glycerol) supplemented with DNAse I (Sigma) and Protease Inhibitors (Roche, Germany). The lysate was passed through the cell disruptor (Constant Systems) at 25 kpsi and was spun 30 min, 40000 rpm, 4ºC in Beckman 45Ti Rotor. The supernatant was taken and 30% ammonium sulfate was added to precipitate soluble proteins. The precipitant was recovered by centrifugation at 28000 rpm, 30 min, 4ºC, resuspended in the same buffer A and dialysed extensively against the same buffer. The dialysed sample was passed through a HiTrap Q HP (GE Healthcare, bed volumen, 5 ml), equilibrated with Buffer A, washed with 8 volumes of Buffer A and eluted with a gradient of 1 M KCl in the same buffer. The protein eluted around 300 mM KCl, concentrated up to 5 ml using Vivaspin 20 column (Sartorius) and loaded into HiPrep 16/60 Sephacryl S200 (GE Healthcare) gel filtration column to elute the protein in buffer 50 mM Tris-HCl pH 7.5, 300 mM KCl, 1

mM EDTA, 10% glycerol. The pooled fractions were concentrated up to 10 mg/ml, aliquoted and stored frozen at -80ºC.

***E. coli* ZapC.** Untagged full-length ZapC protein was purified from 12 litres bacterial culture from the plasmid pZapC transformed in *E. coli* C41(DE3) cells and grown at 37ºC to an optical density OD_{600} of 0.5, at which point expression of ZapC was induced with 1mM IPTG during 3 hours at 37ºC. Cells were centrifuged at 4000 rpm, 20 min, and 4ºC in Beckman 45Ti Rotor. Pellets were resuspended in buffer A (50 mM Tris-HCl pH 8.0, 50 mM KCl, 10% glycerol) supplemented with DNAse I (Sigma) and Protease Inhibitors (Roche, Germany). Cell lysate was passed through cell disruptor (Constant Systems) at 25 kpsi and was spun 30 min, 40000 rpm, 4ºC. Supernatant was taken and loaded into HiTrap Q HP (GE Healthcare, bed volume, 5 ml), previously equilibrated in Buffer A. The column was washed 8 volumes with Buffer A and ZapC was eluted in a gradient of 1 M KCl in the same Buffer. ZapC eluted at 300 mM KCl. Peak fractions were pooled together and concentrated up to 5 ml to be loaded into HiPrep 16/60 Sephacryl S200 (GE Healthcare) gel filtration column to elute the protein in buffer 50 mM Tris-HCl pH 7.5, 250 mM KCl, 1 mM EDTA, 10% glycerol. The pooled fractions were concentrated up to 5 mg/ml, aliquoted and stored frozen at -80ºC.

***E. coli* ZapC-his**. C-terminal histidine tag ZapC protein was purified from 12 litres bacterial culture from the plasmid $pZapC_{his}$ transformed in *E. coli* C41(DE3) cells and grown at 37ºC to an optical density 0.5 OD_{600} the expression was induced by adding 1 mM IPTG during 3 hours at 37ºC. Cells were centrifuge and pellets were stored at -80ºC. Pellets were resuspended in buffer A (50 mM Tris-HCl pH 8.0, 5 mM Imidazole, 200 mM KCl, 10% glycerol) supplemented with DNAse I (Sigma) and Protease Inhibitors (Roche, Germany). Cell lysate was passed through cell disruptor (Constant Systems) at 25 kpsi and was spun 30 min, 40000 rpm, 4ºC. Supernatant was taken and loaded into HisTrap FF (GE Healthcare, bed volume, 5 ml), previously equilibrated in Buffer A. The column was washed 8 volumes with Buffer A and ZapC-his was eluted in a gradient of 1 M Imidazole in the same Buffer. ZapC-his eluted at 250mM imidazole. Peak fractions were pooled together and concentrated up to 5 ml to be loaded into HiPrep 16/60 Sephacryl S200 (GE Healthcare) gel filtration column to elute the protein in buffer 50mM Tris-HCl pH 7.5, 250mM KCl, 1mM EDTA, 10% glycerol. The pooled fractions were concentrated up to 5 mg/ml, aliquoted and stored frozen at -80ºC.

***E. coli* MinC^N.** The N-terminal part (1-115 amino acid reisudes) of MinC protein fused to an intein/chitin-binding domain was purified from 12 litres bacterial culture from the plasmid pTXB1-MinC^N transformed in *E. coli* C41(DE3) cells. The bacterial culture grew until 0.5 OD_{600} then, adding 1 mM IPTG during 3 hours at 37ºC induced the expression. Cells were centrifuge and pellets were stored at -80ºC. Pellets were resuspended in buffer A (20mM Tris-HCl pH 8.5, 1mM EDTA, 1mM NaN_3, 100mM KCl) supplemented with DNAse I (Sigma) and Protease Inhibitors (Roche, Germany). Cell lysate was passed through cell disruptor (Constant Systems) at 25 kpsi and was spun 30 min, 45000 rpm, 4ºC. The supernatant was loaded on a chitin affinity column. The protein was cleaved on the column by incubating with 50 mM dithiothreitol overnight at 4ºC and the eluted protein was concentrated up to 2ml in Vivaspin 20 (Sartorius) to be loaded into HiPrep 26/60 Sephacryl S200 (GE Healthcare) gel filtration column. The eluted protein was concentrated up to 10 mg/ml in Vivaspin 20 (Sartorius) and stored in aliquots at -80ºC.

***Mycobacterial* FtsZ.** *Mycobacterium tuberculosis* and *Mycobacterium smegmatis* FtsZ proteins fused to N-terminal histidine tag (*Mtb*FtsZ and *Msm*FtsZ) were purified from 12 litres bacterial culture from the plasmids pSGV33 and pSGV34 respectively transformed in *E. coli* C41(DE3) cells. The bacterial culture grew until 0.5 OD_{600} then, adding 1 mM IPTG during 3 hours at 37ºC induced the expression. Cells were centrifuge and pellets were stored at -80ºC. FtsZ purification was done as described (White *et al*., 2000) with the following modifications. Pellets were resuspended in Buffer A (20mM Tris-HCl pH 7.4, 300mM KCl, 5mM imidazole, 10% glycerol) supplemented with DNAse I (Sigma) and Protease Inhibitors (Roche, Germany). Cell lysate was passed through cell disruptor (Constant Systems) at 25 kpsi and was spun 30 min, 45000 rpm, 4ºC in Beckman 45Ti Rotor. Supernatant was taken and loaded into HisTrap FF (GE Healthcare, bed volume, 5 ml), previously equilibrated in Buffer A. The column was washed 8 volumes in Buffer A + 60mM imidazole and the protein eluted in a gradient of 1M imidazole. *Mtb*his-FtsZ and *Msm*his-FtsZ eluted in buffer A at 250mM imidazole. Proteins were concentrated up to 5 ml using Vivaspin 20 column (Sartorius) and loaded into HiPrep 16/60 Sephacryl S200 (GE Healthcare) gel filtration column to elute the protein in Buffer B (20mM Tris-HCl pH 7.4, 300mM KCl, 10% glycerol). The N-terminal histidine tag was removed by digestion for 2 hours with 3 U

of thrombin (Novagen)/ml of FtsZ. Thrombin was removed using Streptavidin Agarose (Novagen). The sample was dialyzed against 50mM MES-KOH pH 6.5, 150mM KCl, 10% glycerol, and then concentrated using Vivaspin 6 (Sartorius) to 2 mg/ml.

2.7. 90º Light Scattering assay

Light scattering assays were carried out to characterize FtsZ polymerization according to (Mukherjee & Lutkenhaus, 1999). A Fluorescence Spectrophotometer F-7000 (HITACHI) was used to analysed FtsZ polymerization levels with both the excitation and emission wavelengths setting at 350nm in a 100 μl Quartz cuvette (cell, 2 by 10mm; Hellma), with slit widths of 2.5nm and 1cm path length fluoremeter cuvette. In *Chapter 1*, purified FtsZ proteins were added to the cuvette to a final concentration of 400 μg/ml (10μM) in buffer 50mM MES-KOH pH=6.5, 10mM $MgCl_2$ or 10mM $MnCl_2$, 150mM KCl (*Mycobacterial* FtsZ) in buffer 50mM Tris-HCl pH=7.5, 10mM $MgCl_2$ or $MnCl_2$, 150mM KCl (*E. coli* FtsZ). The cuvette was then placed in the cuvette chamber and data were collected for 1min to establish the basal line. Then the cuvette was removed, and 1mM GTP was added to achieve a final reaction volume of 100 μl. The reaction mixture was stirred with a pipette tip, and the cuvette was returned to the chamber for data collection for a specified period of time. In *Chapter 2*, purified $FtsZ_{10}$ variant was added to the cuvette to a final concentration of 120 μg/ml (3μM) in buffer 50mM Tris-HCl pH=7.5, 10mM $MgCl_2$, 300mM KCl. Polymerization was triggered after 1mM GTP addition. Data collection was monitored at the specified time. In *Chapter 3*, purified full-length FtsZ, FtsZ C-terminal truncates and ZapC were added to a final concentration of 200 μg/ml (5μM) for FtsZ and its truncates and 100 μg/ml (5μM) for ZapC. All proteins were diluted in buffer 50mM Tris-HCl pH=7.5, 10mM $MgCl_2$, 300mM KCl. FtsZ polymerization was triggered after 0.5mM GTP addition. Data collection was monitored at the specified time.

2.8. Negative stain electron microscopy

Purified proteins used for light scattering assays were analysed using transmission electron microscopy. Polymerized FtsZ proteins were applied to glow-discharged EM grids covered with continuous carbon. After 30 s, excess sample was blotted away, and the grid was washed twice with 2% (w/v) uranyl acetate in water and stained for up to

5 s. Samples were dried and transferred into a Tecnai T12 electron microscope (FEI Company) operated at 120 kV and imaged on a CCD camera. The software used for image capture was Gatan Digital Micrograph 1.8.0 and Adobe Photoshop CS2 was used for image processing.

2.9. GTPase assay

All chemicals need to be freshly made and stored (up to two weeks, unless stated otherwise) in new plastic ware (no glass, not reused), as detergents interfere with the assay due to their phosphate contents. A malachite green-sodium molybdate assay is used to measure production of inorganic phosphate (Hoenig, *et al*., 1989). We prepare the GTPase reactions in a final volume of 100μl. The optimal conditions are:
10μM *Ec*FtsZ previously in 10mM Tris pH 7, 250mM KCl, 10mM $MgCl_2$/10mM $MnCl_2$. Reactions start with the addition of 1mM GTP.
10μl are taken at 7 time intervals (usually from 0.5min to 7min) and added to 90μl of stop solution (same than reaction solution + 25mM EDTA) in a 96-wells plate. $NaPO_4$ buffer was used to create a standard curve, and the reaction was normalized by including a control without FtsZ (to avoid any signal due to the spontaneous degradation of the GTP).
10μl of the stopped reaction is added to 60μl $H_2O_{destilled}$ in a 96-wells plate.
Blank contained 70μl of $H_2O_{destilled}$ and 180μl of the detection solution is added into each well. Absorption readings were made with a microplate reader using a 620nm filter after 2min.

2.10. Analytical ultracentrifugation

Proteins samples at concentrations of 1-3 mg/ml in 50 mM Tris-HCl, pH 7.5, 250 mM KCl, 1 mM EDTA, 10 % (v/v) glycerol) were centrifuged at 50,000 rpm at 20°C using 12 mm double sector cells in an An60Ti rotor, while monitoring interference in a Beckman Optima XL-I analytical ultracentrifuge. The sedimentation coefficient distribution function, c(s), was analyzed using the SEDFIT program, version 13.0 (Schuck, 2000) with a frictional ratio (f/f_o) of 1.20-1.23. The partial-specific volume (v-bar), solvent density and viscosity were calculated using SEDNTERP (Laue *et al*.

1992). The calculated v-bar was corrected for the effect of the presence of glycerol using the formula:

$$\frac{\Delta vbar}{\Delta\%\ vol\ glycerol} = 3.33\ x\ 10^{-4}$$

derived from the data of Gekko and Timasheff (Gekko & Timasheff, 1981). Data were plotted using GUSSI (by Dr Chad Brautigam, http://biophysics.swmed.edu/MBR/software.html).

2.11. Isothermal titration calorimetry

Isothermal titration calorimetry (ITC) experiments were carried out using a MicroCal iTC200 instrument (Malvern Instruments) at 20 °C. Titrations consisted of 19 consecutive 2 μL injections of protein ligand (following a pre-injection of 0.5 μL) into the buffer or protein sample in the cell at 120 s intervals. Experiments consisted of injecting 2 mM FtsZ peptide into ZapC (100 μM) in 50 mM Tris-HCl, pH 7.4, 150 mM KCl, 1 mM EDTA, 2 mM $MgCl_2$. The resulting integrated heats were corrected for the heat of dilution, then fitted to a one-site binding model and binding constants calculated using the Origin software (OriginLab).

2.12. Crystallization

Crystallisation conditions were found using our in house high-throughput crystallisation platform, mixing 100 nl ZapC solution at 5 mg/ml with 100 nl of 1920 different crystallisation reagents in MRC vapour diffusion sitting drop crystallisation plates (Stock, *et al*., 2005). For data collection, SeMet-substituted ZapC crystals were grown at 19˚C by using the following final crystallisation solution: 0.58 M ammonium tartrate, 0.01 M sodium acetate, pH 4.6, and was mixed again 1:1 with protein solution. Crystals were flash frozen for data collection by adding 20 % (v/v) glycerol as a cryo-protectant.

2.13. Structure determination of ZapC

Dr. Jan Löwe at the MRC-Laboratory of Molecular Biology, Cambridge, UK, carried

out structure determination. Since crystals were thin, long needles we used Diamond micro focus beamline I24 for data collection. Using un-attenuated beam and 100 ms exposure time, good diffraction to better than 3.0 Å at the selenium edge could be achieved but crystals would die rapidly under those conditions. We therefore adopted a data collection strategy by which 16 wedges from 3 independent crystals were collected, translating the beam along the crystals for the wedges that came from the same crystals. In this way, a complete dataset to 2.9Å with very good anomalous signal could be obtained (Table 6). Selenium sites were found with SHELXCD and initial maps were obtained by PHASER in SAD mode. It was immediately recognised that the electron density maps contain a local twofold axis and the axis was localised using PHENIX.FIND_NCS. Adding the NCS symmetry to solvent flattening after PHASER produced a good map that BUCCANEER could build into. BUCCANEER was forced to recognise the local twofold axis by re-arranging chains manually and finally REFMAC and manual model building/correcting in MAIN 2014 was employed to produce a fully-refined model of the *E. coli* ZapC dimer. Data collection and refinement statistics are listed in Table 6. The experimental structure factors amd refined coordinates have been deposited in the Protein Data Bank (PDB) with accession code XXXX.

Table 6. Crystallographic data

Statistics	
Protein	***E. coli ZapC***
UniProt ID	P75862.2
Data collection	
Beamline	Diamond I24
Wavelength (Å)	0.97858
Method Crystal	SeMet SAD

Space group	$P4_32_12$
Cell (Å)	87.4, 87.4, 118.3
Scaling	
Resolution (Å)	2.9
Completeness (%)[1]	100.0 (100.0)
Multiplicity[1]	41.8 (40.7) 16 wedges from 3 crystals
(I) / σ(I) [1]	17.0 (3.9)
$\mathbf{R_{merge}}$ [1]	0.302 (1.758)
$\mathbf{R_{pim}}$ [1]	0.064 (0.378)
Refinement	
R / $\mathbf{R_{free}}$ [2]	0.223 (0.249)
Model	2 monomers: A: 1-168; B: 1-168, 0 H_2O
Bond length rmsd (Å)	0.015
Bond angle rmsd (º)	2.001
Favoured (%)[3]	99.6
Disallowed (%)[3]	0.0
MOLPROBITY percentile	76th
PDB ID	XXXX

RESULTS

1. Replacement of the divalent cation magnesium in FtsZ assembly

The tubulin-like protein FtsZ is a GTPase that polymerizes in the presence of GTP (Mingorance *et al*., 2001). The basic FtsZ polymer is a single stranded filament, in which the GTPase activity requires a divalent cation magnesium (Mg^{2+}) and it is stimulated by a monovalent cation, potassium (K^{+}) (Mukherjee & Lutkenhaus, 1999) (Mendieta *et al*., 2009).

The most frequent biological role of Mg^{2+} is to bind a nucleotide triphosphate within the catalytic pocket of an enzyme. When GTP is bound in the active site of FtsZ, Mg^{2+} activates the phosphate ester to adopt a conformation favouring the hydrolysis (Mendieta *et al*., 2009). The role of magnesium in FtsZ assembly became evident when FtsZ polymers were able to assemble but no GTP hydrolysis was detected (Mukherjee & Lutkenhaus, 1999) (de Boer *et al*., 1992). Given the importance of magnesium in FtsZ assembly we planned to replace it by other divalent cation that shares similar chemical characteristics.

Manganese (Mn^{2+}) is described as the most common substitute that can replace Mg^{2+} in the majority of enzymes (Maguire & Cowan, 2002). Manganese ion has similar ligand preferences as magnesium. However, Mn^{2+} is significantly larger than Mg^{2+} (R_{ionic} Mn^{2+} 0.8 Å and R_{ionic} Mg^{2+} 0.65 Å), and this could lead to some differences in biochemical interactions as for example to fit into binding sites designed by evolution for Mg^{2+} (Maguire & Cowan, 2002).

To investigate the possibility that manganese could replace the divalent magnesium in the active site of FtsZ, we used three different FtsZ bacterial proteins purified from *E. coli*. FtsZ from *E. coli* (*Ec*FtsZ), *M. tuberculosis* (*Mtb*FtsZ) and *M. smegmatis* (*Msm*FtsZ) will be used to assay the assembly of FtsZ in the presence of both divalent cation.

1.1 Requirement of magnesium for *Mycobacterial* FtsZ oligomerization

As Mukherjee & Lutkenhaus, 1999 demonstrated for *E. coli* FtsZ, we wanted to investigate if the magnesium (Mg^{2+}) cation was essential for *Mycobacterial* FtsZ polymerization. We assayed the assembly of FtsZ proteins of the pathogenic and slow-growing *Mycobacterium tuberculosis* (*Mtb*) and of the non-pathogenic and fast-growing *M. smegmatis* (*Msm*).

The dynamics of polymerization and depolymerization of *Mtb*FtsZ and *Msm*FtsZ were assayed using 90º light scattering assay (**Figure 5**). 90º light scattering assay is a measure of polymer mass, we used established ionic conditions where FtsZ forms dynamic polymers that hydrolyse GTP and disassembly upon exhaustion of GTP (Mukherjee & Lutkenhaus, 1998).

In both cases using the same ionic conditions in which magnesium was included (see Materials and Methods) FtsZ polymerization only depended on the addition of GTP and reached the maximum polymerization levels in about 10 minutes (**Figure 5**). Addition of EDTA led to depolymerization, as indicated by the drop of the light scattering signal to basal values. Nevertheless, the two proteins recovered the polymerization levels after addition of an excess of magnesium

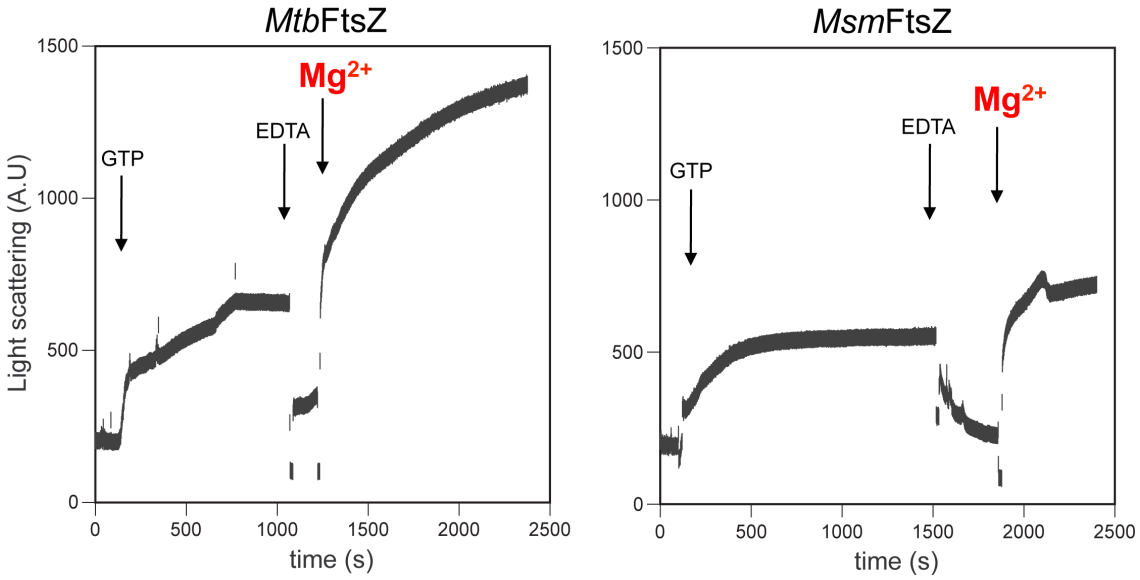

Figure 5. Polymerization dynamics of *Mycobacterial* FtsZ. *Mtb*FtsZ and *Msm*FtsZ were assayed under the same ionic conditions (see Materials & Methods). The polymerization of FtsZ was induced by 1mM GTP addition. Chelation of magnesium was achieved by adding 20mM EDTA and was reverted by an excess of 25mM $MgCl_2$ that recovered FtsZ polymerization levels. Arrowheads mark GTP, EDTA and Mg^{2+} addition.

Light scattering results indicated that *Msm*FtsZ requires GTP and Mg^{2+} to polymerize, as it was already shown for *Mtb*FtsZ (White, *et al*., 2000). These results already differed from *Ec*FtsZ, where polymers have been visualized in the absence of Mg^{2+}, however no dynamic polymerization-depolymerization has been detected (Mukherjee & Lutkenhaus, 1999).

We further analysed the *Mycobacterial* FtsZ polymers by electron microscopy (**Figure 6**). Both FtsZ proteins were analysed under the same ionic condition used in the light scattering assay. Electron microscopy images confirmed the light scattering results, in which no FtsZ polymerization was detected when magnesium was not presented in the polymerization buffer. In contrast, both *Mycobacterial* FtsZ proteins polymerized into long single and double stranded filaments when magnesium was included in the polymerization buffer.

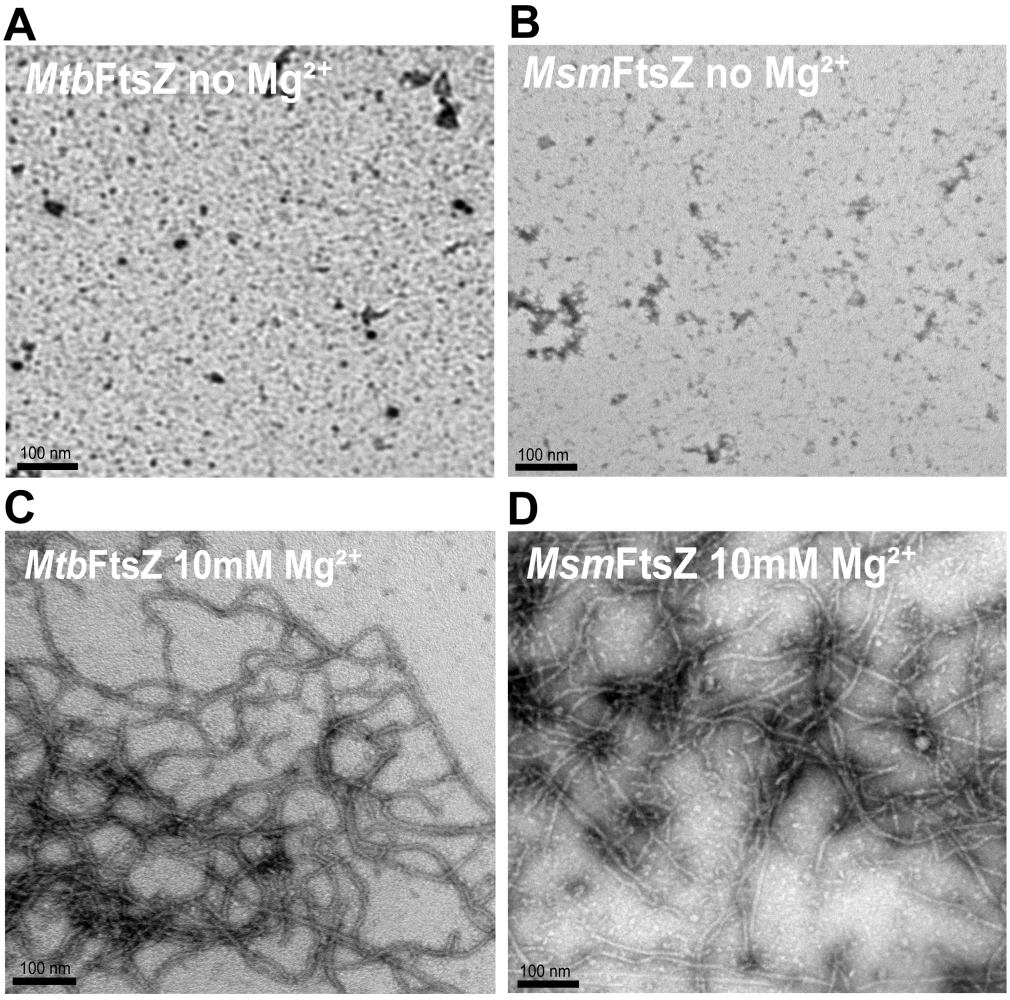

Figure 6. Electron microscopy images of *Mycobacterial* FtsZ polymers. Negative stain transmission electron microscopy images of *Mtb*FtsZ and *Msm*FtsZ in the absence and presence of magnesium. **A.** and

B. show images of the FtsZ proteins in the absence of magnesium. **C.** and **D.** FtsZ proteins in the presence of magnesium. The left column is *Mtb*FtsZ, the right column is *Msm*FtsZ. Scale bar: 100nm.

1.2 Polymerization of FtsZ in the presence of manganese

To compare the polymerization of FtsZ in the presence of either magnesium or manganese, two different polymerization buffers were prepared, in which magnesium and manganese were included. Upon addition of GTP an increased in 90º light scattering signal was detected immediately in the two cases (**Figure 7**).

Results obtained for *Ec*FtsZ were comparable to the reported by Mukherjee & Lutkenhaus, 1999 in which the dynamic of polymerization and depolymerization of the *E. coli* FtsZ protein is described to be very fast. In fact, immediately after GTP addition, *Ec*FtsZ reached the maximum polymerization level and 10 minutes later, the polymerization levels dropped to basal levels indicating the disassembly of the FtsZ polymers. In contrast, after GTP addition, *Mtb*FtsZ and *Msm*FtsZ required approximately 10 minutes to reach the maximum polymerization levels and the polymers remained stable during 25 minutes (**Figure 7**, *left column*).

To determine how polymerization levels are when magnesium is replaced by manganese, FtsZ proteins were incubated in the polymerization buffer with manganese. FtsZ polymerization was triggered by addition of GTP. Surprisingly, *Ec*FtsZ polymerization levels were completely different with manganese than with magnesium. In the presence of manganese, *Ec*FtsZ polymers remained stable during 25 minutes. We did not detect depolymerisation of the *Ec*FtsZ polymers as we did before with magnesium. On the other hand, polymerization levels of *Mtb*FtsZ and *Msm*FtsZ proteins in the presence of manganese were comparable to the ones observed before in the presence of magnesium (**Figure 7**, *right column*). There were no significant changes in the polymerization levels of the *Mycobacterial* proteins.

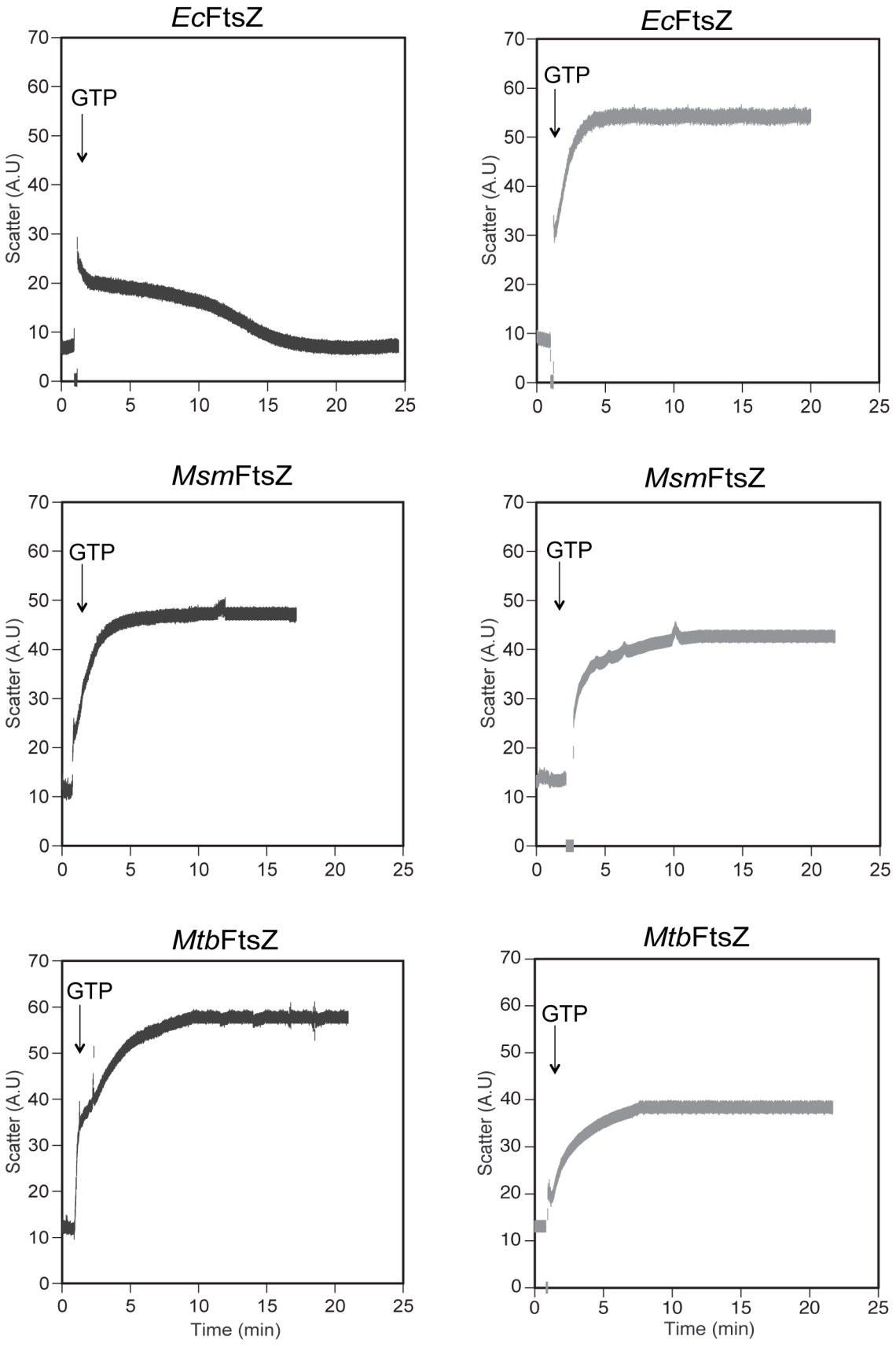

Figure 7. FtsZ polymerization levels in the presence of different divalent cations. 90º light scattering measurements of FtsZ proteins (10μM) after 1mM GTP addition. *Left column*. Polymerization levels of

FtsZ proteins incubated in polymerization buffer with 10mM Mg^{2+}. *Right column*. Polymerization levels of FtsZ proteins in the presence of Mn^{2+}. An arrowhead marks GTP addition.

As *Ec*FtsZ polymerization levels detected in light scattering were so different when magnesium was replaced by manganese we analysed the polymers by electron microscopy (**Figure 8**). FtsZ polymers formed in the presence of magnesium assembled mostly in single filaments, with few FtsZ filaments forming lateral interactions leading to doublets (**Figure 8**, left). In contrast, the *Ec*FtsZ polymers formed in the presence of manganese were rigid straight bundles (**Figure 8**, right). These FtsZ polymeric structures formed by *E. coli* FtsZ never were found in *Mtb*FtsZ and *Msm*FtsZ filaments (**Figure 8**, right).

It has been shown that FtsZ is a polymorphic protein, which *in vitro* can assembles into a variety of different polymer structures as rings, toroids, sheets or bundles depending on the pH and the ionic conditions (Popp et al., 2009). However, we found that the replacement of magnesium by manganese induced stable and rigid *Ec*FtsZ polymers that have been found previously when FtsZ polymerization was assayed using crowding agents or multivalent cations (Popp et al., 2009).

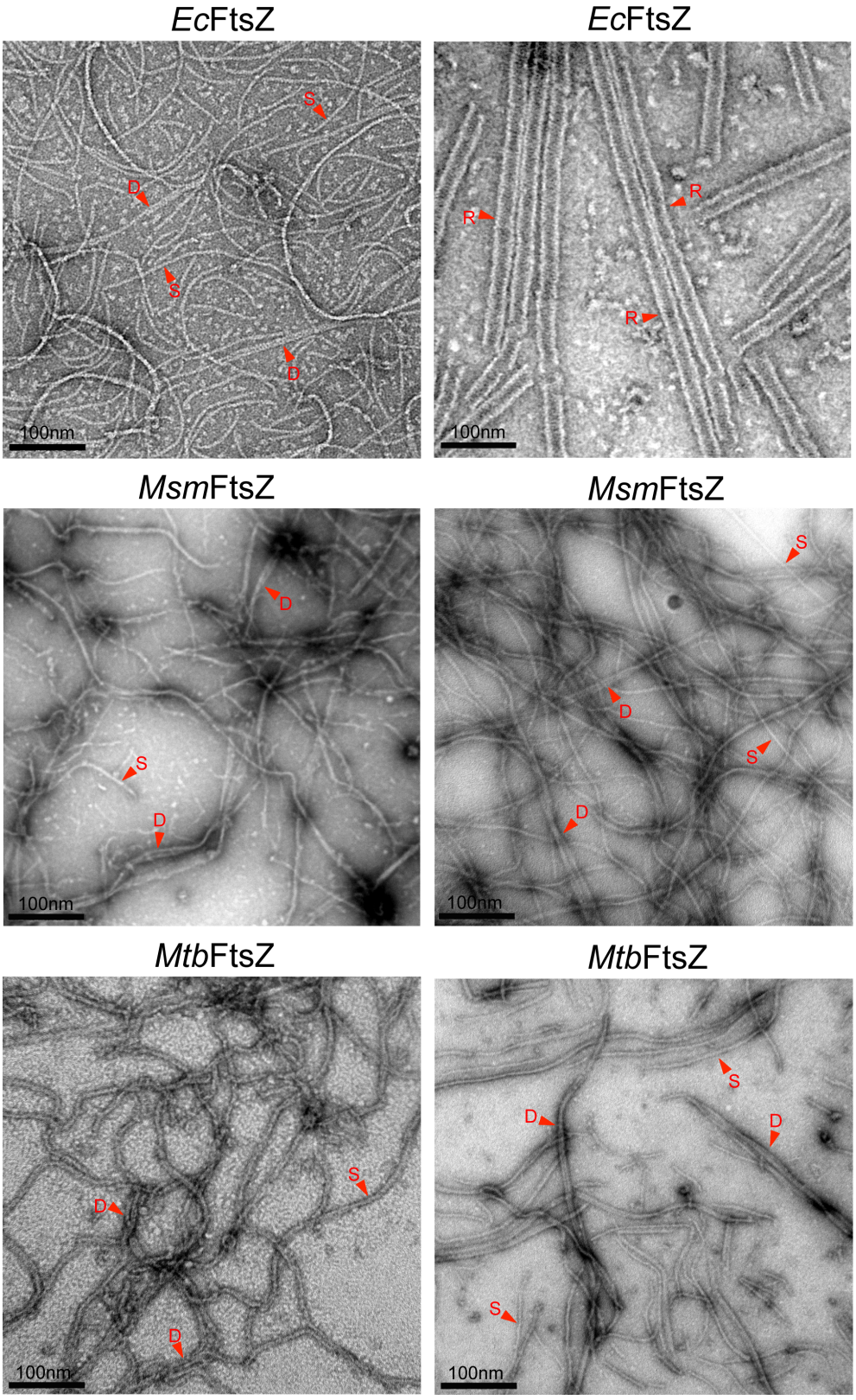

Figure 8. Electron microscopy images of FtsZ filaments formed in the presence of either magnesium or manganese. FtsZ filaments were visualized using negative stain electron microscopy and under the same ionic conditions used for light scattering assay. *Left*, FtsZ polymers formed in the presence of 10mM Mg^{2+}. *Right*, FtsZ polymers formed in the presence of 10mM Mn^{2+}. Red arrowheads

mark representative sections of *S*, single filaments, *D*, double filaments and *R*, rigid bundles). Scale bar: 100nm.

1.3 The hydrolytic activity of *Ec*FtsZ polymers in the presence of manganese

In order to investigate the biochemical parameters that are affected in *Ec*FtsZ assembly by the replacement of magnesium by manganese, we determined if the GTP hydrolysis is different when manganese was present. The hydrolytic activity of FtsZ was assayed using the same ionic conditions used for the light scattering assay so we prepared two polymerization buffers with magnesium and manganese. Previous results have shown that GTPase activity of *Ec*FtsZ fluctuates depending on pH, K^+ ion and protein concentration (Mingorance *et al*., 2001), (Mukherjee & Lutkenhaus, 1999).

The GTPase activity was quantified using the colorimetric assay, Malachite green (see Materials & Methods). As Mg^{2+} is necessary for GTP turnover in FtsZ polymers and, in the absence of Mg^{2+} FtsZ does not hydrolyse GTP, a sample with no Mg^{2+} was the right control in these experiments.

We first measured the GTPase activity with magnesium and then with manganese. The GTPase activity of *Ec*FtsZ was approximately 9 nmol Pi/nmol FtsZ.min and the *Mycobacterial* FtsZ was 0.6 nmol Pi/nmol FtsZ.min. These results were comparable to the previously reported for *Mtb*FtsZ (White *et al*., 2000). The GTPase activity of *Ec*FtsZ was reduced up to 4 nmol Pi/nmol FtsZ.min with manganese. In *Mycobacteria* FtsZ, the hydrolytic activity of the polymers in the presence of manganese did not change.

Our results show that the GTPase activity of *Ec*FtsZ was 2.5 times lower when manganese was used instead of magnesium.

Previous studies have shown that GTP hydrolysis of *Ec*FtsZ could be also reduced by the presence of other divalent cations as Ca^{2+}, which induced lateral associations of the FtsZ filaments (Yu & Margolin, 1997), (Mukherjee & Lutkenhaus, 1999). However, we have replaced the magnesium ion in the active centre of the FtsZ protein by manganese. This replacement has not been done before given the requirement of FtsZ to polymerize in the presence of magnesium.

2. Crystallization of *Escherichia coli* FtsZ

The absence of structural data on FtsZ from *E. coli* makes it difficult to study the FtsZ interactions with itself and with the other division proteins. As an alternative to approximate the biochemistry of the *Ec*FtsZ protein, we use the FtsZ crystal structures from other organisms.

The first FtsZ structure solved was from the hyperthermophilic methanogen *Methanococcus jannaschii* (Löwe and Amos, 1998). The three dimensional structure of FtsZ was then compared to the structure of the eukaryotic tubulin. The amino acid sequence of FtsZ and tubulin show no obvious homology, however, both show a significant structural homology. Crystal structures from several FtsZ proteins, *B. subtilis*, *P. aeruginosa*, *A. aeolicus* and *T. maritima* show similar folding between them (Oliva, *et al*., 2007). A globular domain formed by the N-terminal part including the nucleotide-binding site and the C-terminal domain. Both domains are connected by the central H7 alpha helix that, together with the insertion of the catalytic T7 loop into the nucleotide-binding site may activates the GTPase activity of FtsZ.

A missing part in all FtsZ structures is the linker of the core C-terminal domain of the protein. It has been shown that the C-terminal domain of FtsZ is highly variable between bacterial species and is not represented in any of the available FtsZ structures (Buske and Levin, 2013). The length of the linker varies from 50 to 60 amino acids residues in *E. coli* and *B. subtilis,* up to 300 amino acids residues in *C. crescentus*. The last 11 amino acids residues have been crystallized in complex with other division proteins. This short alpha helix is known as the central hub of FtsZ and in *E. coli* it is critical for the interaction with a number of cell division proteins, as FtsA or Zip. Both FtsA and ZipA serve to tether FtsZ to the cytoplasmic membrane. Also the cell division inhibitors, MinC and SlmA require the central hub of FtsZ to interact (Ortiz, *et al*., 2015).

In order to attempt the crystallization of *E. coli* FtsZ we have put together all the available structural data from the solved FtsZ structures. We have used bioinformatics predictions and multiple sequence alignments to designed the different *Ec*FtsZ variants that will be use in the crystallization attempts. We will further test the possibility to crystallize FtsZ in complex with the MinC protein.

2. 1 Bioinformatic analysis of *E. coli* FtsZ

Based on the available FtsZ crystal structures in which the C-terminal flexible linkers are missing, to crystallize *Ec*FtsZ we first investigated which were the appropriate FtsZ variants to construct.

We used *Ec*FtsZ amino acid sequence as a query protein to carry out a multiple sequence alignment to the amino acid sequences of the available bacterial FtsZ proteins whose three-dimensional structures are known **(Figure 9)**. Results from the multiple sequence alignment (NCBI, protein Blast tool) showed that *Pseudomonas aeruginosa* FtsZ (*Pa*FtsZ) shares a 57% homology at the amino acid level with the full-length *Ec*FtsZ. This value was the highest between all FtsZ proteins.

FtsZ protein	Length (aas residues)	Identity (%)	Query cover (%)
Bacillus subtilis	382	47	92
Pseudomonas aeruginosa	394	57	93
Aquifex aeolicus	367	46	77
Staphylococcus aerous	390	51	81
Thermotoga maritima	351	49	82
Methanococcus jannaschii	364	47	82
Mycobacterium tuberculosis	379	45	93

Figure 9. Multiple sequence alignment of the bacterial FtsZ proteins against *E. coli* FtsZ. *Ec*FtsZ is the query protein used to carry out the multiple alignments. Results from the multiple alignments of the different FtsZ proteins against *Ec*FtsZ. The table shows the length of the proteins, the percentage of identity that they share with *Ec*FtsZ and the percentage of query cover. *Pseudomonas aeruginosa* FtsZ is highlighted in green due to share the highest value of identity with *Ec*FtsZ.

The secondary structure of a protein can be defined by the pattern of hydrogen bonds of the protein, such as alpha helices and beta sheets. Accurate secondary structure prediction is a key element in the prediction of tertiary structure of the protein. We chose then the *Pa*FtsZ as a footprint to carry out the bioinformatic analysis of the secondary structure prediction of *Ec*FtsZ (Psipred Protein Sequence tool) **(Figure 10A)**.

Results from the secondary structure revealed that both *Ec*FtsZ and *Pa*FtsZ are highly similar. Both alpha helices and beta sheets from the two proteins are located in the same amino acids positions.

Data derived from the secondary structure prediction also revealed the disordered and binding regions of the two proteins **(Figure 10B)**. Results showed that the C-terminal domain was highly disordered (residues 300-383). Also, the first amino acids residues from the N-terminal domain (residues 1-10) were disordered.

Based on the bioinformatic predictions, we will construct different *Ec*FtsZ variants which will lack of the C-terminal domain (residues 300-383) and the first amino acids from the N-terminal domain (residues 1-10).

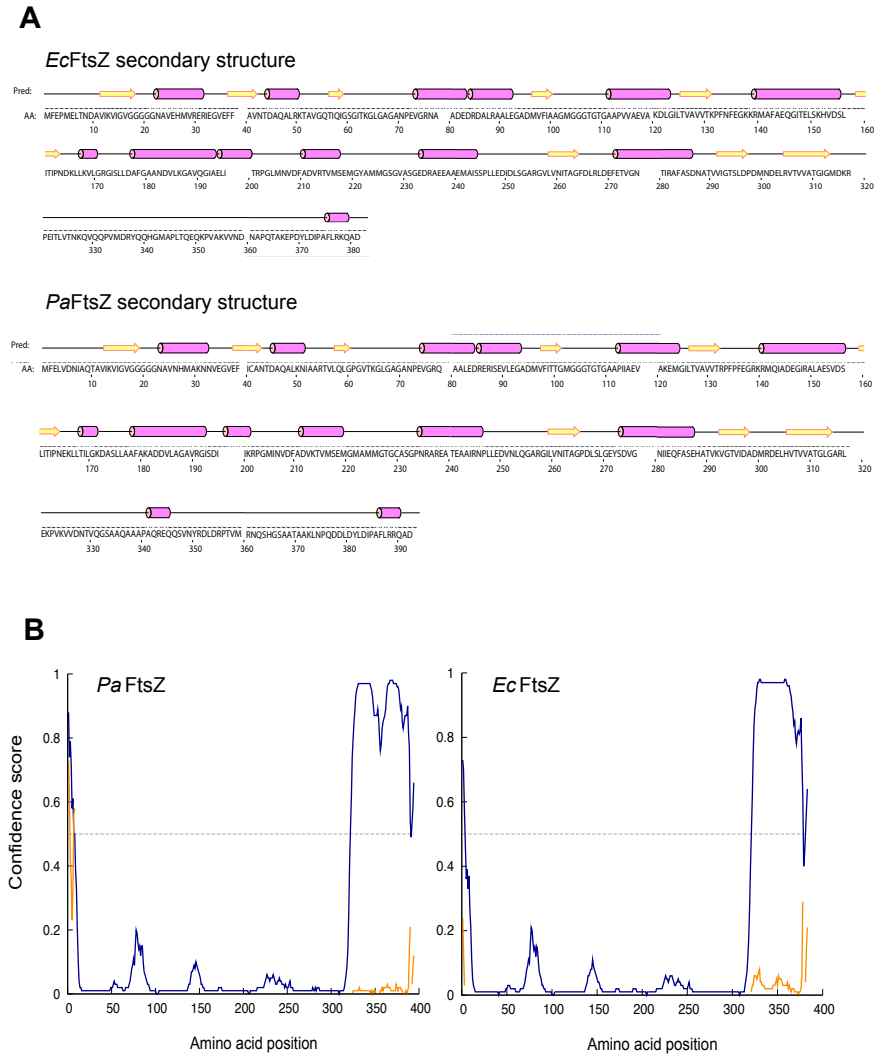

Figure 10. Bioinformatics prediction of the secondary structure and the disordered domains in *Ec*FtsZ and *Pa*FtsZ. A. Prediction of the secondary structure of *Ec*FtsZ and *Pa*FtsZ (Psipred prediction

protein tool). Yellow arrows represent β-strands, pink cylinders represent α-helix and the black line represents the coil domains. **B.** Prediction of the intrinsic disorder profile of both proteins. The amino

acids that are considered disordered when the blue line is above the grey dashed line, that is the confidence score is higher than 0.5. The yellow line shows the confidence of disordered protein binding residue predictions.

2.2 Screening of *E. coli* FtsZ variants

We designed different *Ec*FtsZ variants based on the bioinformatic predictions results. In order to produce a stable protein, we deleted the highly variable C-terminal domain in combination with the first amino acids residues from the N-terminal domain, which also was shown to be disordered. We always kept intact the GTP-binding domain of FtsZ (^{16}-GVGGGGG-^{23}) in all the variants. Our objective to attempt the crystallization of *Ec*FtsZ was to obtain the structure of the FtsZ dimer. We then needed to design FtsZ variants, which are able to polymerize in the presence of GTP.

We designed 16 different *Ec*FtsZ variants in which we removed the amino acid residues from the C-terminal domain and the N-terminal. The *Ec*FtsZ variants were then analysed to determine the percentage of identity with its homologue *Pa*FtsZ **(Figure 11)**. The alignment results showed that deletion of the C-terminal domain increased the percentage of identity up to 67% in comparison with the full-length *Ec*FtsZ and *Pa*FtsZ proteins that shared the 57%.

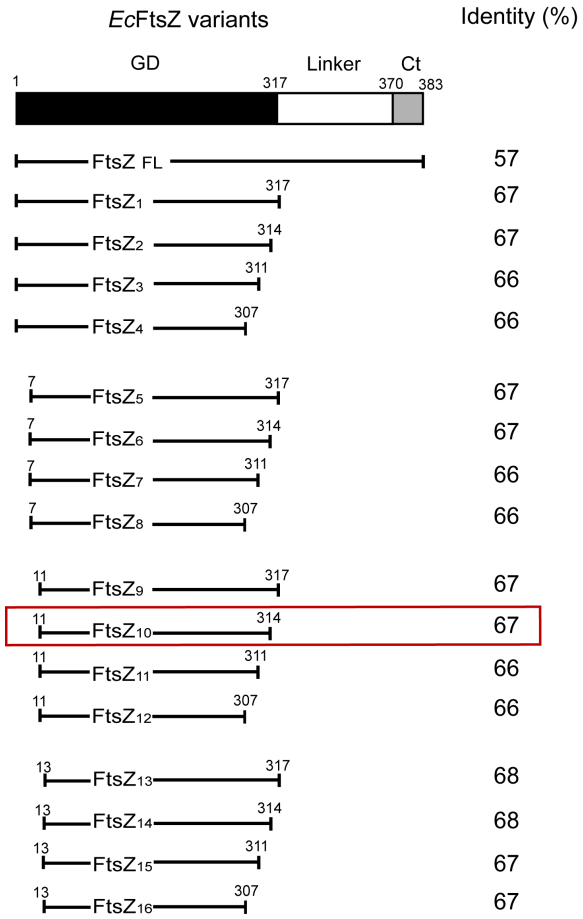

Figure 11. Schematic representation of the different *Ec*FtsZ variants and its sequence identity with *Pa*FtsZ. *Ec*FtsZ structural domains (*GD*, globular domain; *linker*, unstructured C-terminal domain; *Ct*, C-terminal end) and the different variants constructed to crystallised FtsZ. Percentage of identity of FtsZ variants when they are compared to the amino acid sequence of *Pa*FtsZ. The single FtsZ variant that was induced as a soluble protein, $FtsZ_{10}$, is highlight inside a red rectangle, which includes the percentage of identity with *Pa*FtsZ.

One of the most important conditions to crystallize a protein is to obtain enough amount of pure protein. We carry out an induction screening of the FtsZ variants to detect which of them could be produce by the bacteria as a soluble protein to further purify it. Our results showed that only the $FtsZ_{10}$ variant could be purified as a soluble protein (**Figure 11**, highlighted in red). Unfortunately, the other 15 FtsZ variants we constructed were produced by the bacteria as inclusion bodies so we did not purify these constructions. Although we constructed FtsZ variants that showed highest values of sequence identity, we did not want to take the risk to purify these constructions from the inclusion bodies.

We then purified the soluble $FtsZ_{10}$ variant and analysed its activity by 90º light scattering assay and visualised the polymers using electron microscopy **(Figure 12)**.

The results showed that the amount of purify protein was pure enough to attempt the crystallization. Also we confirmed that *Ec*FtsZ$_{10}$ was able to polymerize in the presence of GTP and assemble it into filaments. We obtained a yield of 28 mg/ml of *Ec*FtsZ$_{10}$.

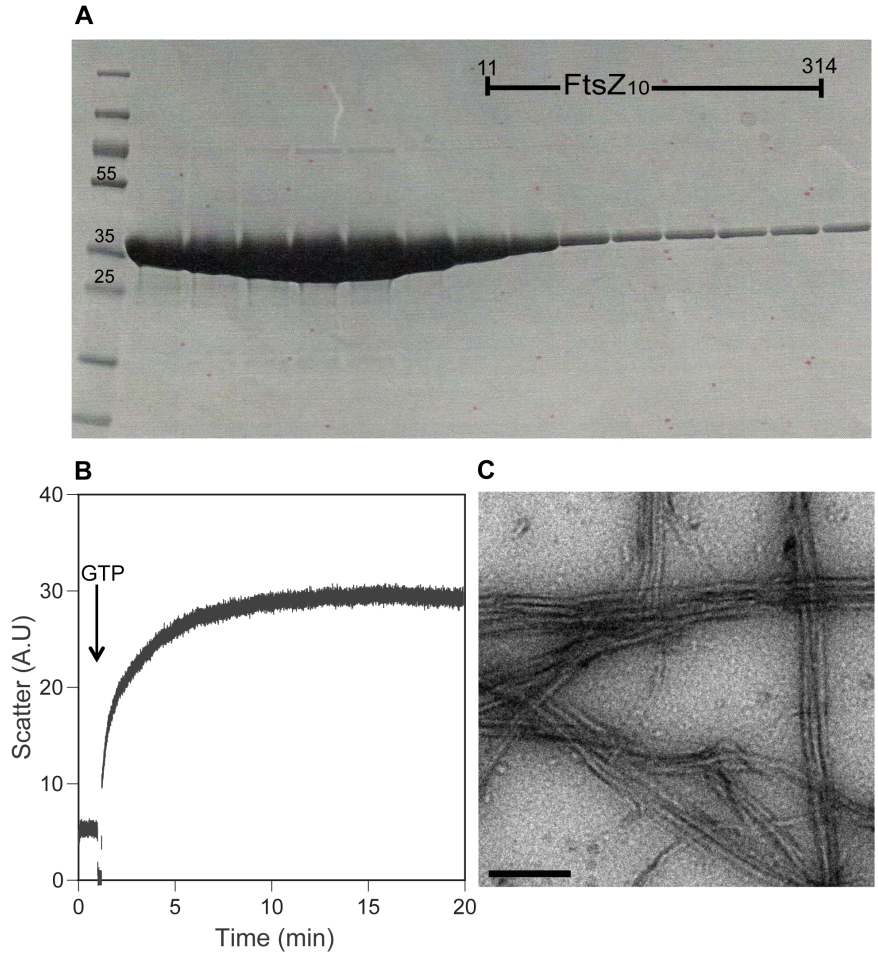

Figure 12. Purification of FtsZ$_{10}$ variant and its *in vitro* analysis. (A) Coomassie stained 12% SDS-PAGE gel of purified FtsZ$_{10}$ after gel filtration column. Molecular weights standard is shown in the left line. **(B)** 90º light scattering measurement of 3 μM FtsZ$_{10}$ in the presence of 1mM GTP. **(C)** Negative stain electron microscopy image of the FtsZ$_{10}$ polymers. Scale bar: 100nm.

2.3 *Ec*FtsZ$_{10}$ crystals

Crystallisation of FtsZ was carried out according to the standard protocol used by the high-throughput crystallization screening at the MRC-Laboratory of Molecular Biology (see Materials & Methods). Each screening contained 1920 different conditions in which the protein could crystallize (96 wells, LMB1-LMB17 plates). FtsZ$_{10}$ was concentrated up to 28 mg/ml and then, different nucleotides and divalent cations were added to induce the assembly of the protein (**Figure 13**). We first used GTPγS, the non-hydrolyzable analogue of GTP that induces the assembly of FtsZ. GDP; the product of

the GTP dephosphorylation was also used and the C8-morpholino-GTP, which has been characterized as a potent inhibitor of FtsZ polymerization (Lappchen, *et al*., 2008). Previous results have shown that the C8-morpholino-GTP allowed the crystallisation of *Aquifex aeolicus* FtsZ (Oliva *et al*., 2007). Apart from magnesium, which it has been shown, that is required for a fully functional FtsZ protein, we included the manganese ion in the screening, since our previous results showed the ability of FtsZ to polymerize into these stable rigid bundles (**Figure 8**, *section 1*).

Protein	Nucleotide	Divalent cation
$FtsZ_{10}$	2mM GTPγS	4mM Mg^{2+}
$FtsZ_{10}$	2mM GTPγS	4mM Mn^{2+}
$FtsZ_{10}$	2mM GDP	4mM Mg^{2+}
$FtsZ_{10}$	2mM GDP	4mM Mn^{2+}
$FtsZ_{10}$	8-Morpho-GTP	4mM Mg^{2+}
$FtsZ_{10}$	8-Morpho-GTP	4mM Mn^{2+}

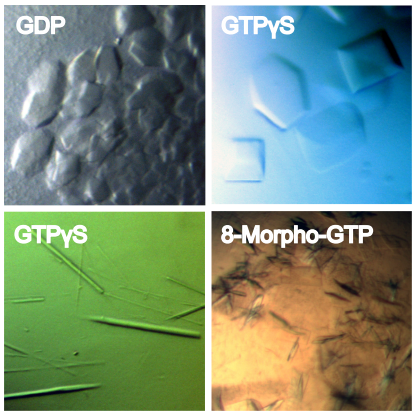

Figure 13. Crystallization conditions used for $FtsZ_{10}$. The table summarizes the crystallization conditions for $FtsZ_{10}$, the nucleotides and the divalent cation used. Protein concentration was 28 mg/ml and each condition was used for the complete screening (1920 conditions). Crystal pictures obtained from the different conditions used in $FtsZ_{10}$ crystallization.

The crystallization plates were incubating at 19ºC during at least 3 days and then visualized under the microscope. Although we obtained different protein crystals (**Figure 13**), the quality of them was not enough to obtain diffraction pattern. Also we had negative results from the screening that contained the manganese cation since we did not visualize any protein crystal.

Our objective was to look for the crystal structure of the FtsZ dimer. However, our results showed that FtsZ did not produce strong crystals with the nucleotides that should induce the dimerization, which were GTPγS and GDP with magnesium. The inhibitor C8-morpholino-GTP that binds to the GTP-binding site of FtsZ and blocks the dimerization did not show a good diffraction pattern.

2.4 Crystals of the MinC-FtsZ complex

In order to make FtsZ a more stable protein and in a last attempt to crystallize FtsZ, we used the N-terminal domain of *E. coli* MinC ($MinC^N$) as the binding protein of FtsZ to crystallize the complex FtsZ-$MinC^N$.

MinC protein consists of two domains: the N-terminal domain ($MinC^N$), which binds to the alpha helix 10 (H10) of FtsZ, which is located at the interface between the FtsZ subunits and inhibits FtsZ polymerization (Shen & Lutkenhaus, 2010), and the C-terminal domain ($MinC^C$) that binds to the C-terminal tail, the central hub of FtsZ (Shen & Lutkenhaus, 2009). We chose the N-terminal domain of MinC to crystallize in complex with FtsZ because the FtsZ variant we used lacked that C-terminal domain which is required for the interaction with the C-terminal domain of MinC.

We carried out the same crystallization screening using to crystallize FtsZ alone (96 wells, LMB1-LMB17 plates). The nucleotides and divalent cations used to crystallize the complex are summarize in the **Figure 14** as well as the protein ratio concentration used to form the complex (**Figure 14**). The plates were incubated at 19ºC during and crystal formation was checked after 3 days.

Results from the crystallization screening showed that there were protein crystals in the conditions were the complex MinC-FtsZ was assayed at a protein ratio (1:3), with GDP and magnesium. Protein crystals were needles as the picture shows. We chose the bigger ones and, we freeze them in liquid nitrogen with a cryoprotectant solution, which avoids ice crystals formation that would damage the protein crystals, we send them to the synchrotron. Dr. Jan Löwe analysed the diffraction pattern. Results from the diffraction pattern corresponded only to the $MinC^N$ protein. FtsZ protein did not crystallize, although the protein ratio was 3 times more amount of FtsZ protein that MinC.

Protein ratio	Nucleotide	Divalent cation
$MinC^{N}$-$FtsZ_{10}$ (1:1)	2mM GTPγS	4mM Mg^{2+}
$MinC^{N}$-$FtsZ_{10}$ (1:1)	2mM GDP	4mM Mg^{2+}
$MinC^{N}$-$FtsZ_{10}$ (3:1)	2mM GTPγS	4mM Mg^{2+}
$MinC^{N}$-$FtsZ_{10}$ (3:1)	2mM GDP	4mM Mg^{2+}
$MinC^{N}$-$FtsZ_{10}$ (1:3)	2mM GTPγS	4mM Mg^{2+}
$MinC^{N}$-$FtsZ_{10}$ (1:3)	2mM GDP	4mM Mg^{2+}

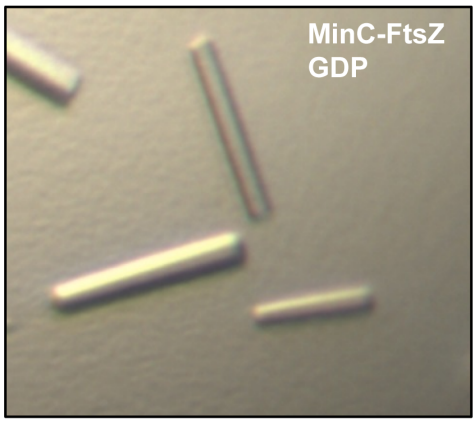

Figure 14. Crystallization conditions used to crystallize the protein complex $MinC^{N}$-$FtsZ_{10}$. The table summarizes the different conditions used to crystallize $MinC^{N}$-$FtsZ_{10}$. Crystal picture of the crystals formed in the presence of GDP. The diffraction pattern revealed that all the crystals were only from by the $MinC^{N}$ protein.

3. Molecular interaction of the cell division proteins ZapC and FtsZ in *E. coli*

In vitro experiments have shown that ZapC interacts directly with FtsZ decreasing the GTPase activity on the polymers by producing the FtsZ bundling effect (Hale *et al*., 2011). *In vivo* results shown that deletion of the *zapC* leads to a mild division-defective phenotype and ZapC localization only depended on the FtsZ presence, neither FtsA, ZipA, ZapA nor ZapB were needed to localize ZapC at the midcell (Hale *et al*., 2011). However, ZapC overproduction caused cell filamentation by inhibiting cell division and the FtsZ-ring appeared delocalized forming aberrant structures (Hale *et al*., 2011).

It has been also speculated that the C-terminal tail of FtsZ was unlikely the binding site of ZapC on FtsZ (Durand-Heredia, *et al*., 2011). And recent results have explored the mechanism of binding between ZapC and FtsZ (Bhattacharya, *et al*., 2015), finding out that ZapC does not bind to the C-terminal tail of FtsZ. When a C-terminal FtsZ truncation was used to assay its interaction with ZapC the authors found and increased in the FtsZ bundling measured by an increased in the fluorescence (Bhattacharya *et al*., 2015).

In order to investigate the interaction of the cell division proteins ZapC and FtsZ, we will carry out *in vitro* experiments that will suggest that ZapC requires at least the C-terminal tail of FtsZ, the central hub, to detect the bundling effect of FtsZ polymers. We will use X-ray crystallography to solve the ZapC crystal structure at a resolution of 2.9Å. Biophysical experiments will show that ZapC behaves in solution as a monomer-dimer and a FtsZ central hub peptide will bind to ZapC. Also, our studies will be extended to *in vivo* experiments that will implicate site-directed mutagenesis on ZapC and the analysis of the lethal phenotype caused by the excess of ZapC. Our results will provide new insights in the molecular interaction of ZapC and FtsZ.

3.1 *In vitro* interaction between ZapC and FtsZ

To investigate *in vitro* the effect of ZapC on FtsZ bundling, we constructed two carboxy terminal end truncations of the FtsZ protein (**Figure 15A**). We confirmed the *in vitro* bundling induced by ZapC on FtsZ polymers (Hale *et al*., 2011). 90ºlight scattering experiment was used to reflect the assembly of FtsZ polymers from FtsZ full length and its truncations after addition of GTP (**Figure 15B**). After 5 min of FtsZ polymerisation, ZapC was added to the assembled FtsZ polymers. A pronounce increase in the scatter signal was detected when ZapC was added to the FtsZ full-length protein (**Figure 15B**). In contrast, when ZapC was added to the FtsZ carboxy terminal end truncates, no change in the scatter signal was detected (**Figure 15B**). As a consequence, both FtsZ carboxy terminal end truncates polymerised and depolymerised as the full-length FtsZ (**Figure 15B**). These results suggest that, *in vitro*, the carboxy terminal end of FtsZ is needed to observe a bundling effect induced by ZapC.

These results were confirmed analysing the structure of the FtsZ polymers in the presence of ZapC by electron microscopy (**Figure 15C**). Electron micrographs revealed single stranded FtsZ polymers in the presence of GTP and bundles of FtsZ polymers when ZapC was added to them (**Figure 15C**). The FtsZ carboxy terminal end truncates did not show visible bundles in the presence of ZapC (**Figure 15C**).

Results from light scattering experiments in Figure 15B, show that FtsZ polymers form higher order bundling in the presence of ZapC. Deletions in the carboxy terminal end of FtsZ comprising the last 5 amino acids (Δ5) and the last 30 amino acids (Δ30) residues resulted in the absence of bundling when ZapC was added to them. These results suggest that FtsZ bundling by ZapC may involve the FtsZ central hub.

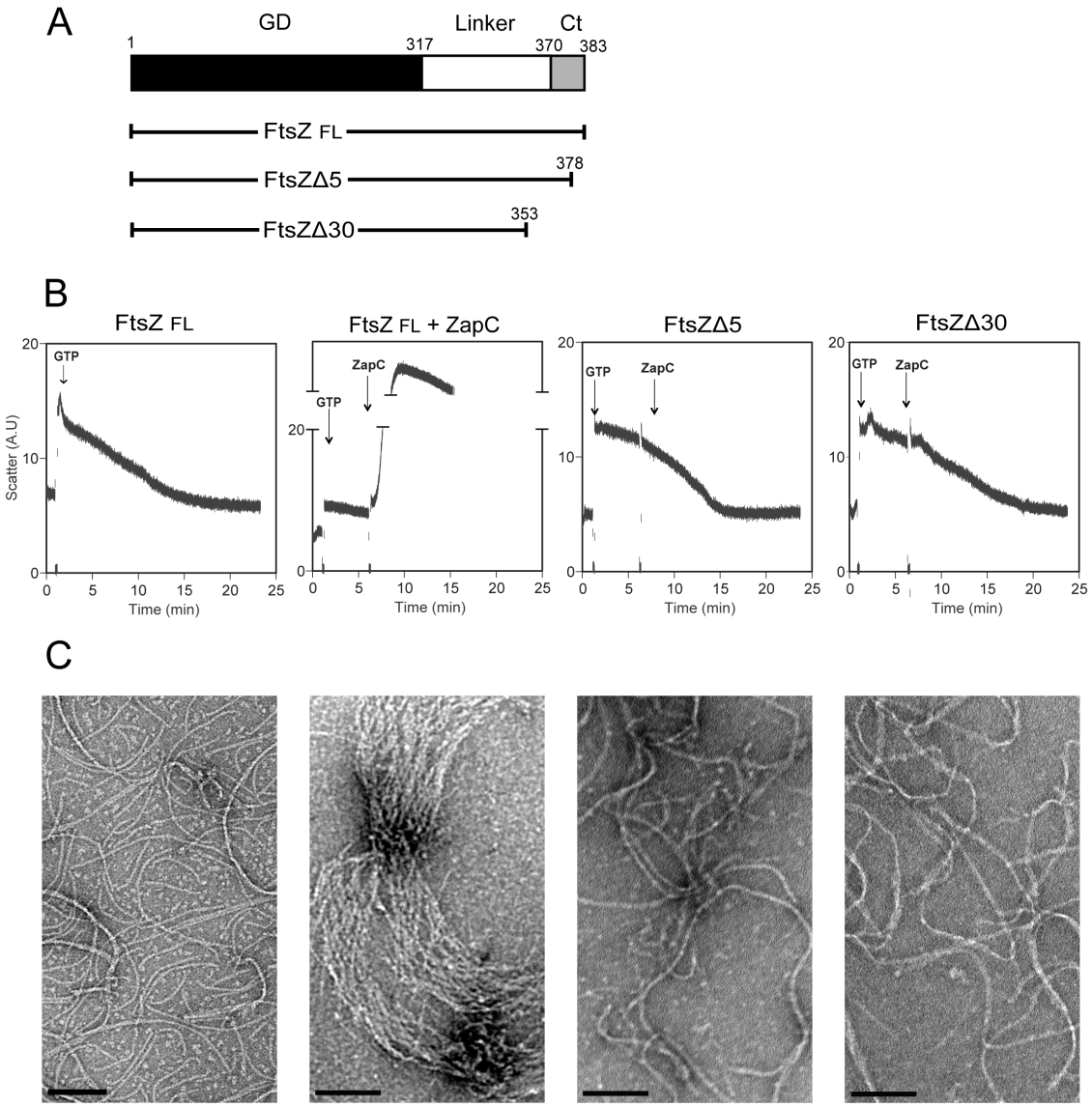

Figure 15. ZapC effect on polymers formed by different carboxy terminal end FtsZ truncations. A. Diagram showing the different FtsZ constructions used in the experiment: *GD*, globular domain; *linker*, unstructured carboxy terminal linker; *Ct*, carboxy terminal end. **B.** 90º light scattering assay using purified FtsZ proteins depicted in (A). In all experiments FtsZ proteins (5µM) were incubated in the polymerisation buffer (see *Materials and Methods*) and polymerisation was initiated by addition of GTP (0.5mM). After 5 min, indicated by an arrow, ZapC (5µM) was added to each reaction mixture. **C.** Electron micrographs of each reaction analysed in (B). Samples were taken after ZapC addition, negatively stained and observed by electron microscopy. Scale bar: 200nm and 100nm.

3.2 Measurement of the thermodynamics parameters of ZapC and FtsZ interaction

Since our *in vitro* experiments showed that the interaction between ZapC and FtsZ could involve the central hub of FtsZ; these results are already different to the one reported by Bhattacharya *et al*., 2015. We wanted to confirm what we observed in light

scattering and electron microscopy using a direct measurement technique, isothermal titration calorimetry (ITC).

ITC is a physical technique used to determine the thermodynamic parameters of an interaction in solution. It is a quantitative technique that can determine the binding affinity (k_a), enthalpy changes (ΔH) and binding stoichiometry (n) of the interaction between two molecules. In the experiment, 12 amino acids residues peptide was designed (^{372}-LDIPAFLRKQAD-^{383}) that belongs to the central hub of FtsZ to measure the binding affinity to the target, ZapC (**Figure 16**). A first injection of the peptide is injected in the chamber where ZapC is found in solution and it is bound to the protein. The signal returns to baseline before the next injection. A second injection is made and again the FtsZ peptide becomes bound to ZapC. As the injections continue, the ZapC protein becomes saturated with the peptide, so less binding occurs and the heat change starts to decrease (**Figure 16**).

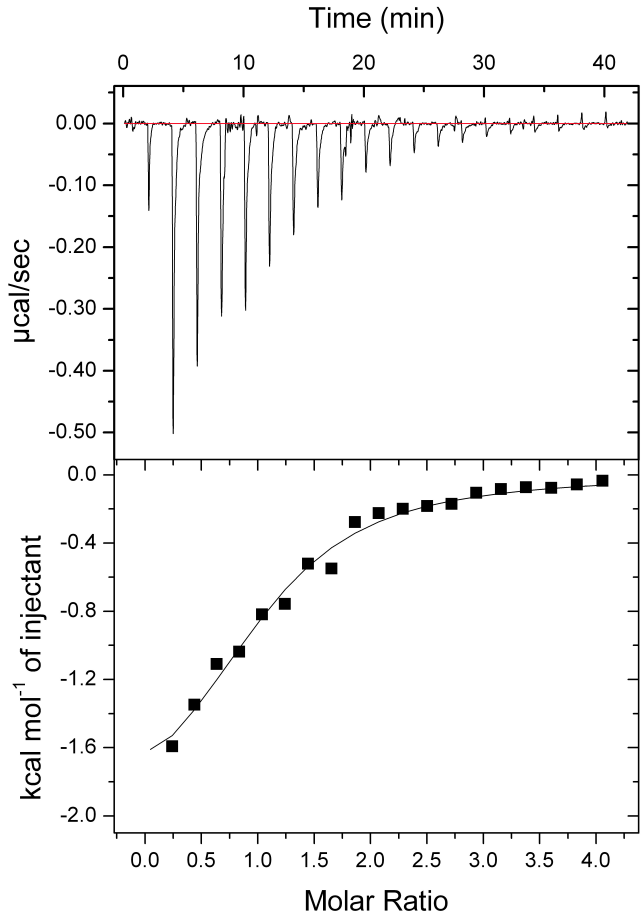

Figure 16. Binding of FtsZ peptide to ZapC. Raw heats measured during injections of FtsZ peptide into ZapC by ITC (top) were integrated and fitted to a single-site binding model (bottom) yielding a stoichiometry of 1.0 with an enthalpy of -2.1 kcal/mol.

Results obtained from ITC showed that the FtsZ peptide binds to ZapC with a 1:1 stoichiometry. That means, that the FtsZ peptide has one binding site, but ZapC can have more than one binding site. This interaction was also showed to be enthalpically favourable (ΔH=-2.1 kcal/mol). The negative value for ΔH indicates favouring the binding by bonds broken and created. On the other hand, the calculated binding of the FtsZ peptide to ZapC was determine to be in the micromolar range with a k_a of 32 ± 6 μM. This moderate binding affinity of the FtsZ peptide was a direct measurement that probe that the central hub of FtsZ binds to ZapC. Of course we cannot exclude that ZapC has other binding surfaces on FtsZ that could potentially lead to the nanomolar affinity as has been reported previously (Bhattacharya *et al*., 2015).

3.3 Crystal structure of the cell division protein ZapC from *E. coli*

We cloned and expressed *zapC* from *E. coli* in *E. coli*, adding a histidine tag at the C-terminus to circumvent low expression levels. ZapC is a 20,6kDa cytoplasmic protein that after purification to homogeneity by metal affinity and size exclusion chromatography (**Figure 17A**), we routinely produced 3 mg from 12 litres of culture. ZapC proved to be a difficult protein when we tried to concentrate it as the protein precipitated in most buffers but we found it to be manageable in a buffer at pH 7.5 and higher (Materials & Methods). Crystallisation trials yielded needle-shaped crystals (**Figure 17B**) that diffracted well enough but were difficult to grow bigger. Structure determination from seleno-methionine substituted crystals by SeMet SAD hence utilised a microfocus beamline (I24, Diamond Light Source, Harwell, UK), using three needle-shaped crystals and 16 wedges collected from different spots along the crystals. This yielded a highly redundant dataset suitable for phasing (**Table 6**, *Materials & Methods*). Phasing, automated and manual model building, and refinement produced an atomic model of very good quality, resolving residues 1-168 of ZapC, with two molecules in the asymmetric unit, at 2.9 Å resolution.

The structure of the ZapC monomer shows it to be composed of alpha helices and two small beta sheets (**Figure 17C**). The protein contains two separate domains that are linked by a long, extended and irregular linker reaching almost all the way around the molecule (residues 88-109). This is presumably because the folds of two domains place their C- and N-termini at opposite ends of the molecule (**Figure 17D**, linker in yellow).

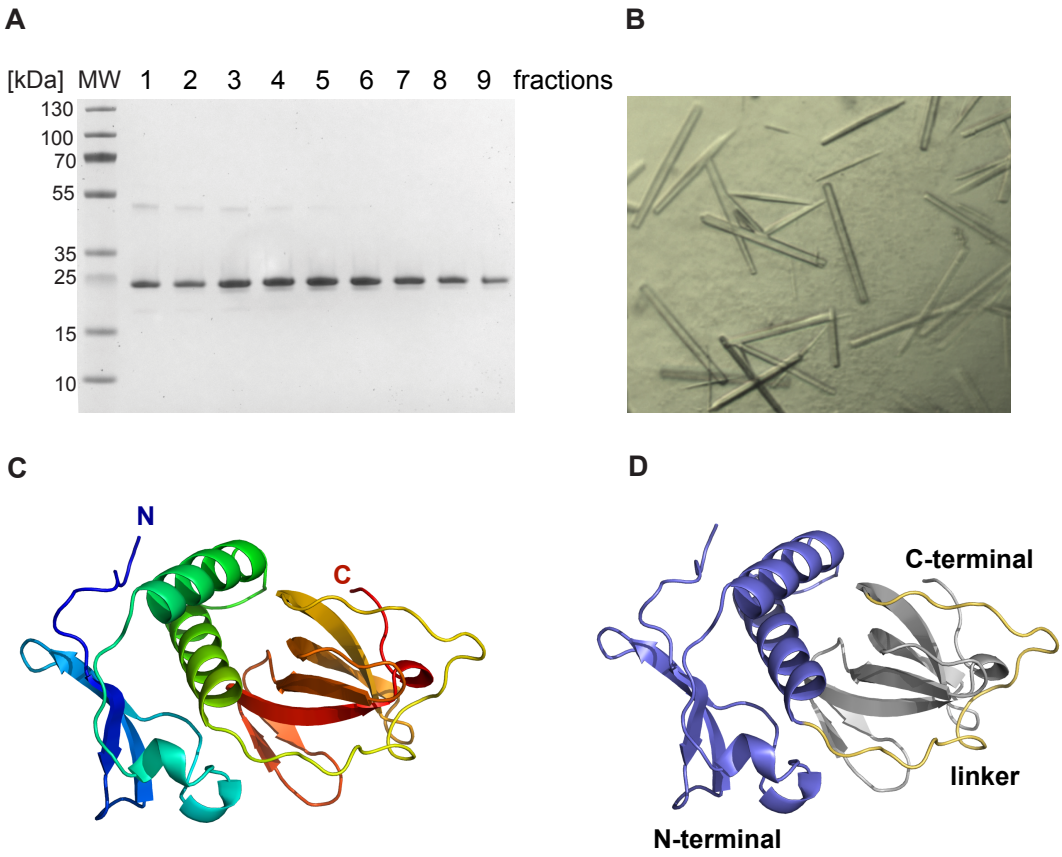

Figure 17. Purification, crystals and structure of ZapC. A. Coomassie-stained SDS-PAGE gel showing fractions after size exclusion chromatography of *E. coli* ZapC. **B.** Typical crystals of *E. coli* ZapC after optimisation as used in this study. The needles were typically less than 20 μm in diameter, leading to weak diffraction and strong decay in the X-ray beam during data collection. **C.** Ribbon plot (PyMOL, Schrödinger) outlining the crystal structure of ZapC at 2.9 Å resolution. The structure is shown in rainbow colours from the N-terminus in blue to the C-terminus in red. **D.** ZapC contains two fairly separate domains that are connected via a long linker, shown in yellow. The N-terminal domain is shown in light blue, the C-terminal domain in grey.

3.4 ZapC structure and its homology to the Royal superfamily

ZapC structural N and C-terminal domains are related to chromo and Tudor domains respectively (**Figure 18B** and **D**). The C-terminal domain of ZapC is related to Tudor domains (Ballare, *et al.*, 2012). For example, ZapC can be superimposed on subunit Phf19 of the polycomb repressive complex 2 (PRC2, PDB 4BD3) with an RMSD of 1.5 Å over 51 Ca atoms (**Figure 18B**). In fact, all top DALI structural similarity search hits were Tudor domains, indicating a high significance of this finding. Although the fit is good, ZapC contains an extra beta hairpin (residues 141-154) that is not normally present in Tudor domains (**Figure 18C**).

The N-terminal domain is distantly related to chromo domains as was found when comparing ZapC to all entries in the Protein Data Bank (PDB) (**Figure 18D**). For example, the N-terminal domain of ZapC can be superimposed on chromobox homolog 7 (CBX7, PDB 4MN3) with an RMSD of 3.3 Å over 42 Ca atoms (**Figure 18D**). The fit is not as good as for the N-terminal domain and Tudor domains and the angles of all secondary structural elements are slightly different between chromo domains and the N-terminal ZapC. When compared to canonical chromo domains, an extra helical loop and helix are found in the ZapC N-terminal domain (residues 32-71). The last helix of the ZapC chromo domain (residues 72-87) is longer than in canonical chromo domains and is connected via the long linker (**Figure 18C**) to the N-terminus of ZapC's Tudor domain.

Tudor domains are closely related to the chromo domains, which together form the Royal domain superfamily that typically recognizes arginine- or lysine-methylated ligands (Chen, *et al*., 2011). These domains have important roles in many cellular processes, including the DNA damage response, histone modification and chromatin remodelling. This means that ZapC contains two distantly related domains that are part of a superfamily of domains known for their ability to sense arginise and lysine-methylated peptides. (Ballare, *et al*., 2012) have reported structural data showing that Tudor domains binds with high affinity to methylated lysine-36 (K36Me3). We investigated the structure of the putative canonical peptide binding sites in both the N-terminal chromo domain and C-terminal Tudor domain. In both cases, the binding sites seem to be occluded. In the Tudor domain of ZapC, the extra beta hairpin (residues 141-154) covers the very hydrophobic pocket that in canonical Tudor domains binds the methylated arginine-containing peptide (**Figure 18E**, cyan peptide). In the N-terminal chromo domain of ZapC, the binding site is not quite as occluded but the hydrophobic pocket is not very accessible either (**Figure 18E**, yellow peptide). In both cases, however, it seems plausible that the domains could eventually undergo conformational changes allowing access to the hydrophobic pockets that are required for methylated arginine and lysine binding.

Our results from the Isothermal titration calorimetry have shown that there is a binding affinity from the peptide of FtsZ central hub to ZapC. We have found that the FtsZ

central hub contains a conserved arginine. We then hypothesize the possibility that ZapC could bind to the central hub of FtsZ through its last conserved arginine residue.

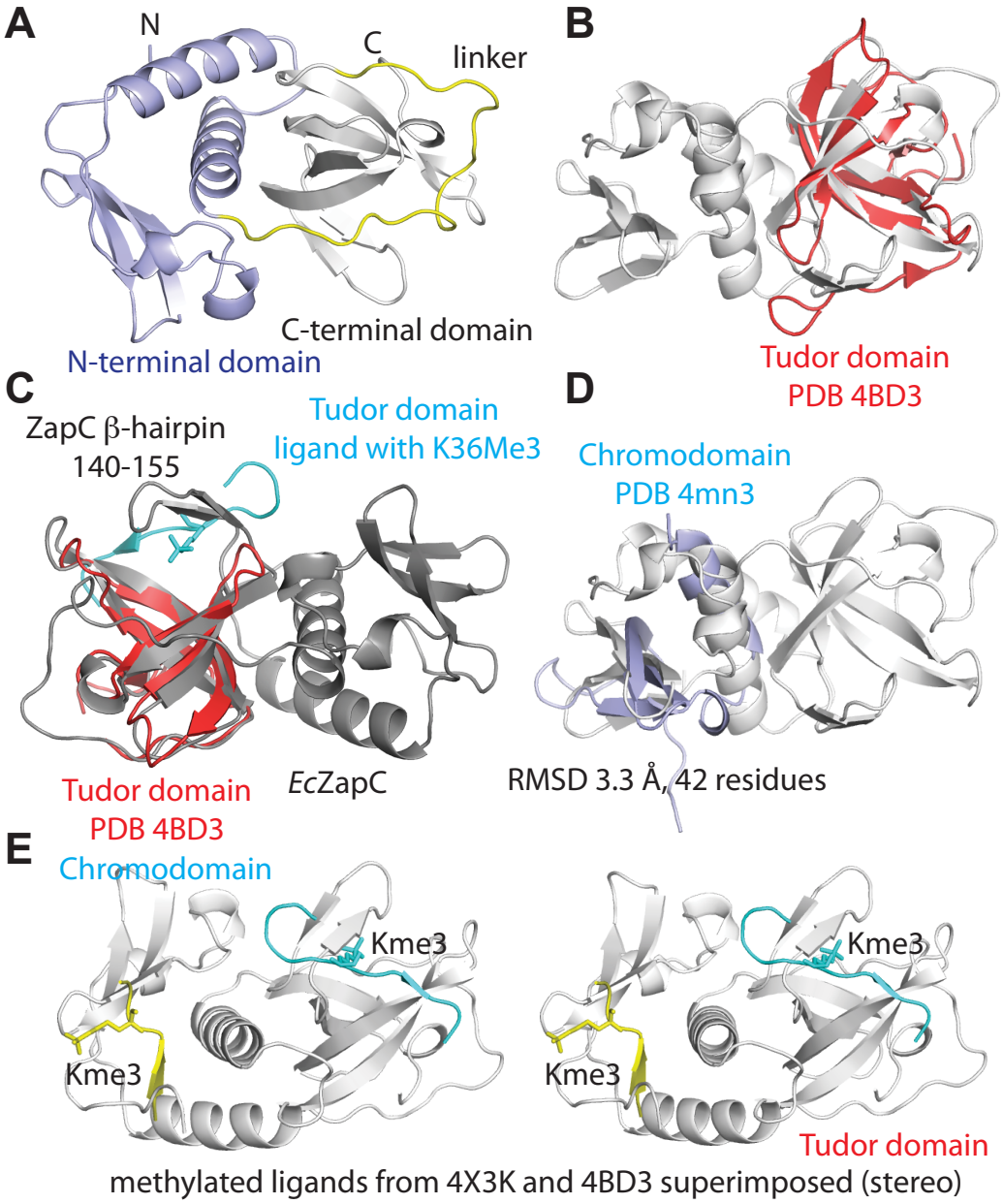

Figure 18. ZapC crystal structure and the structural homology to a Royal superfamily domains. A. The crystal structure of ZapC at 2.9Å resolution. ZapC contains two fairly separate domains that are connected via a long linker shown in yellow. The N-terminal domain is shown in light blue, the C-terminal domain in grey. **B.** The C-terminal domain of ZapC is related to Tudor domains (DALI server). A superposition between PDB 4BD3 (PHD finger protein 19, red, RMSD 1.5Å over 51Cα) and ZapC C-terminal Tudor domain is shown. **C.** Tudor domains are known to preferentially bind to peptides containing methylated arginines and lysines. The superposition in B is repeated here with the methylated histone tail peptide ligand shown in cyan. The same binding pocket in ZapC is occluded by a small β-hairpin comprising residues 143-154. **D.** The N-terminal domain of ZapC is distantly related to the chromodomains. A superposition between PDB 4MN3 (CBX7, chromobox homologue 7, light blue, RMSD 3.3Å over 42 Cα) and ZapC chromodomain is shown. **E.** Stereo plot showing both superpositions

(B, C and D) with their lysine-methylated peptide ligands, only (yellow: chromodomain, cyan: tudor domain). As for the tudor domain, the canonical peptide pocket in ZapC chromodomain is probably occluded by a different orientation of the first strand and a small helical segment between residues 44 and 50.

3.5 ZapC oligomerization

The structure of the ZapC crystals described here contains two monomers per asymmetric unit. Although there are two other contacts in the lattice, the one shown in **Figure 19A** has the largest interface, buries a number of hydrophobic side chains and completes the otherwise open beta sheet of the N-terminal chromo domain forming an eight-stranded beta sheet across the two monomers. (**Figure 19A**). This particular dimer was also selected computationally by PISA (PDBe PISA, www.ebi.ac.uk/pdbe/pisa) as the most likely assembly. The dimer interface buries a contact area of approximately 1500 $Å^2$ (out of 8900 $Å^2$ of each monomer). In order to clarify the oligomeric state of the protein in solution, we performed analytical ultracentrifugation (**Figure 19B**) finding that ZapC runs as three species, and the two major species corresponded very well with theoretical values for ZapC monomers and dimers (**Figure 19C**). There is a minor species of higher S value but this varies between different concentrations corresponding to masses between a trimer or tetramer. This may be due to aggregration as found during analytical ultracentrifugation in the absence of glycerol.

The concentration of the monomers and dimers can be measured from integration of the baseline-separated distributions, giving an estimate for the dissociation constant of approximately K_D 30 μM for the monomer-dimer equilibrium.

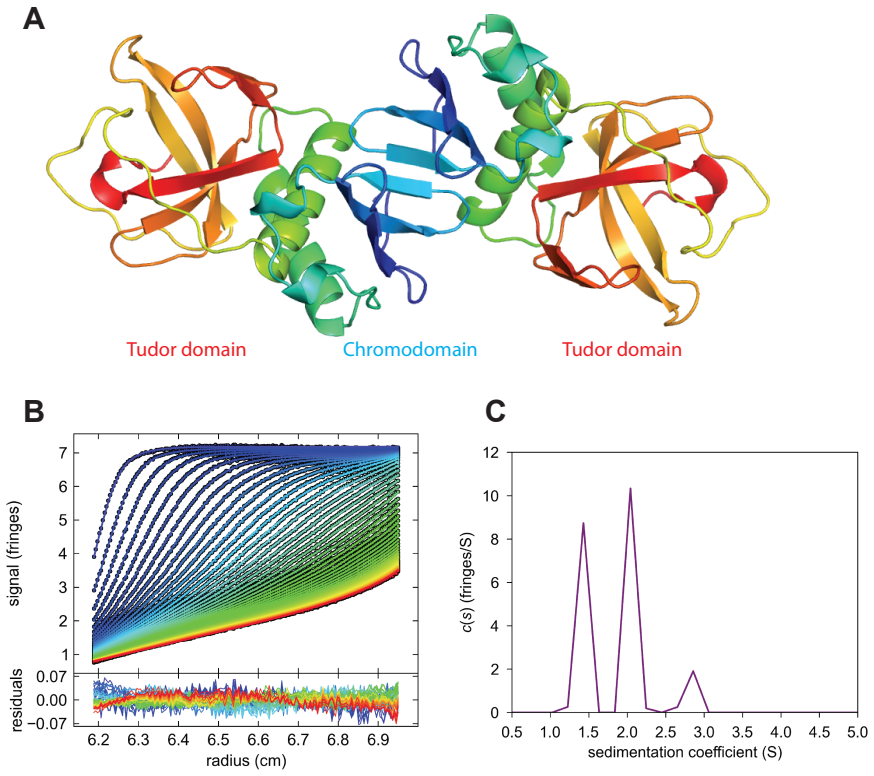

Figure 19. Oligomeric state of ZapC. A. Structure of ZapC dimer as suggested by crystal packing. The strands of the N-terminal chromodomain come together to form an eight-stranded sheet. **B.** Analysis of the loigomeric status of ZapC from sedimentation velocity analytical ultracentrifugation (AUC). Interference scans (symbols) and best-fit c(s) model at different points in time indicated by colour temperature with residuals to the fit below. **C.** c(s) sedimentation coefficient distribution showing peaks for monomer, dimer and higher oligomer.

3.6 Effects of high ZapC levels on growth and division

We have investigated if dimerization of ZapC as shown by its crystal structure, has any effect on division and growth *in vivo*. We constructed ZapC single M28D and F58D, and double, M28D-F58D mutants. These residues were chosen because they are the most conserved ones within the dimerisation interface in the ZapC sequences of gammaproteobacteria (**Figure 20**). Since our objective is to disrupt the dimerization interface of ZapC, both amino acids, Methionine (M) and Phenylalanine (F) that contain hydrophobic side chains have been mutated to an Aspartic Acid (D), which has a negative charged side chain.

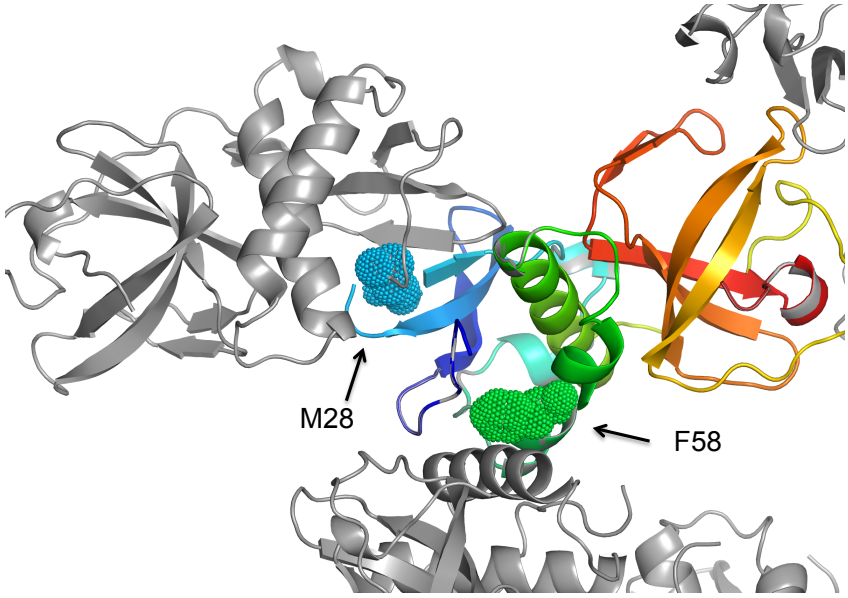

Figure 20. ZapC point mutations. The selected point mutations were chosen based on ZapC crystal contacts and the conservation of the residues. ZapC M28 and F58 are shown as spheres coloured in blue and green respectively. An arrow marks the specific site were both residues localise. M28 is located in the interface of the β-sheets between two ZapC monomers. F58 is allocated in the contact interface between two alpha helices.

An *in vitro* analysis of the ZapC mutants on FtsZ polymerisation make it impossible due to the aggregation into inclusion bodies of all of them. Then, we investigate the effect of the overproduction of the ZapC variants (M28D, F58D and M28D-F58D) in *E. coli* cells. Samples from all cell cultures were taken at indicated times to analyse the protein levels of FtsZ and all ZapC constructions (**Figure 21**). Western blot analysis revealed that intracellular FtsZ levels were not altered when ZapC and its variants were overproduced. *E. coli* Δ*zapC* strain was used as a genetic background to overproduce ZapC and ZapC variants (see Table 2, Materials & Methods).

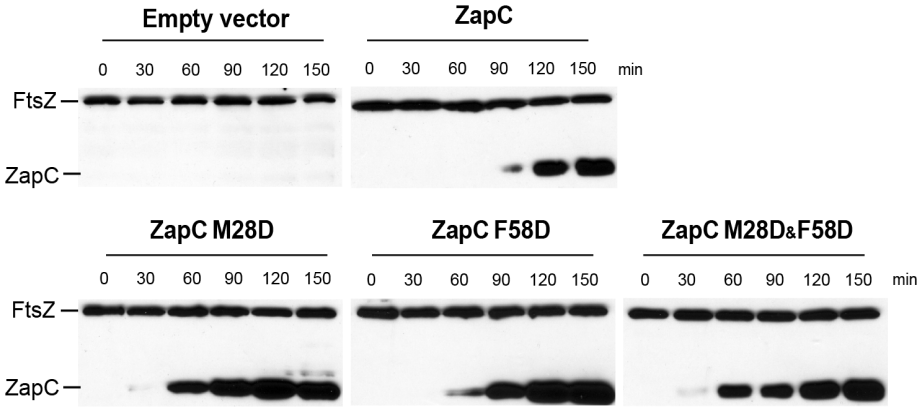

Figure 21. Levels of intracellular FtsZ and ZapC following induction of different *zapC* variants. The empty expression vector pBAD22, *zapChis wt*, *zapChis M28D*, *zapChis F58D* and *zapChis M28D&F58D* transformed in *ΔzapC E.coli* strain were induced during 150 min. Samples were withdrawn at the

indicated times and western blot analysis was developed using α-FtsZ and anti-Histidine antibodies to detect the intracellular amount of FtsZ and the induced ZapC and its variants..

To examine the effect of the overproduced ZapC constructions in *E. coli* cells we grew cell cultures as is described in Materials & Methods. At the indicated times, each sample was taken and processed to analyse it with the Cell Counter.

Results in **Figure 22** show that optical density (OD) from all the cultures increased at a constant rate. However, after 150 min induction, the expression of ZapC blocked cell growth. Phase-contrast microscopy images obtained after 150 min induction showed that the ZapC double M28D-F58D mutant did not affect cell growth or division, whereas the single ZapC mutations, M28D and F58D, produced filamentation and the cells producing ZapC showed evident signs of lysis. We also quantified the levels of the ZapC proteins produced at several times by the plasmids containing the different constructions used in our experiment (**Figure 21**). We found that the cell lysis effect caused by ZapC is not likely due to higher levels of the protein as the inert double ZapC M28D-F58D mutant was produced, under the same conditions, at 134% the amount of the wild type ZapC. Similarly, the single ZapC M28D and F58D mutants, showing a partial phenotype resulting in filamentation, were produced at 84 and 129% levels respectively. We reason then that the deleterious effect of high amounts ZapC is due to an excess in activity rather than in amount.

We then tested if high levels of the ZapC variants may affect particle increase (particles per ml) (**Figure 22**). Similarly to their effects on cell morphology we found that ZapC significantly decreased the rate of particle increase after one mass doubling. As expected from the morphological changes ZapC single mutants, M28D and F58D also affected particle increased although at times between one and two mass doublings. On the other hand the overproduction of the double mutant M28D-F58D had no effect on particle increase.

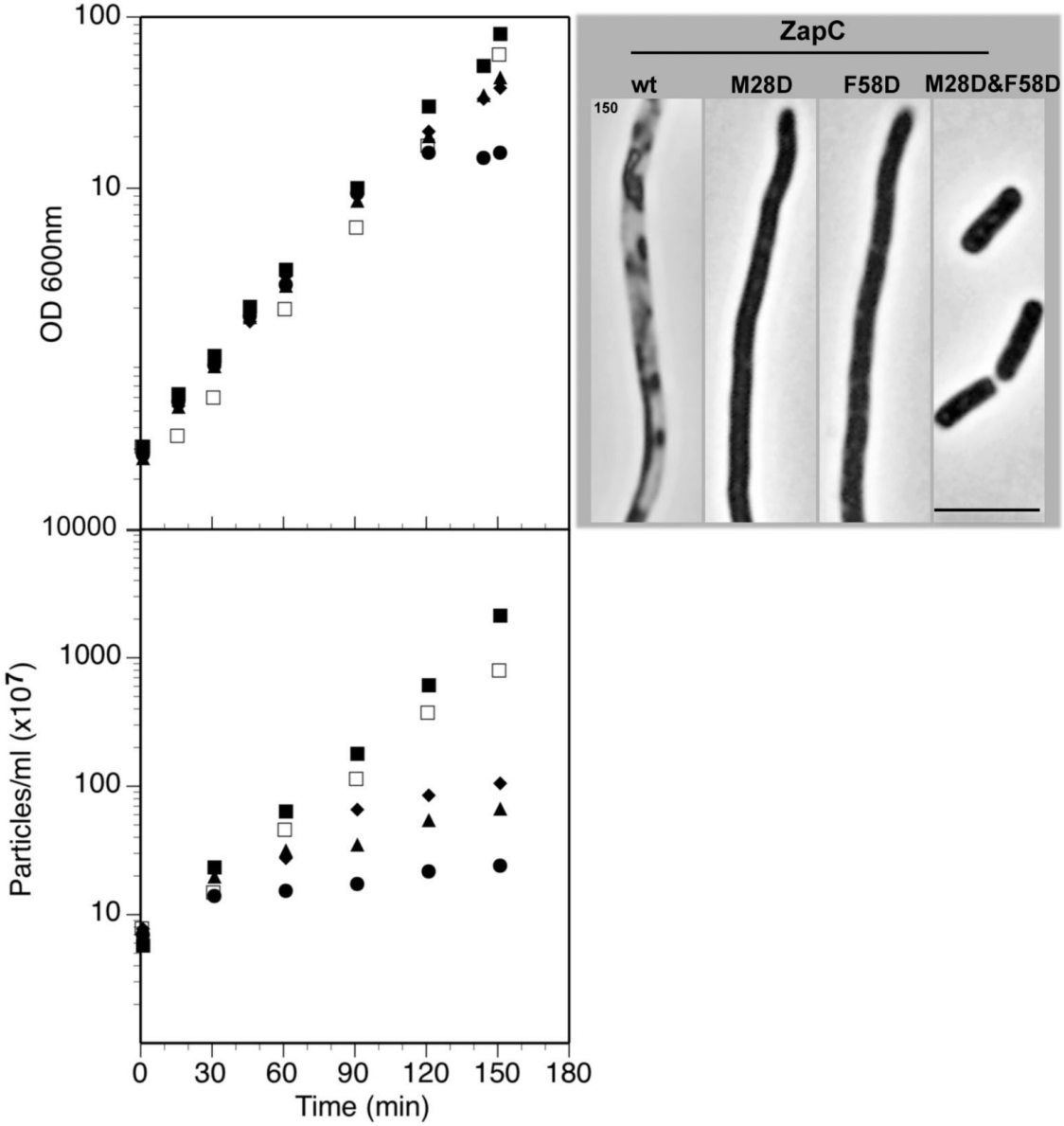

Figure 22. Effect of *zapC* overexpression on growth and division. Cultures of CH59 (*ΔzapC*) containing pBAD22 (empty vector; ■), pCOV15 (*zapC*; ●), pCOV13 (*zapC M28D*; u), pCOV14 (*zapC F58D;* ▲) and pCOV17 (*zapC M28D-F58D;* □) were grown in glucose-containing medium as indicated in the text. At time zero 0.2 % arabinose was added for induction. OD (600 nm), and particle increases were measured at the times indicated. A sample of each culture was withdrawn at 150 minutes and observed by phase-contrast microscopy (right hand panel). Scale bar: 5 μm.

3.7 Effect of high levels of ZapC variants on the localization of the FtsZ-ring

To test the stability of the FtsZ-ring *in vivo*, we expressed the different ZapC variants in the *E. coli* Δ*zapC* strain. Cell samples were taken at different time points to immunolocalise the intracellular FtsZ and the induced ZapC using specific antibodies against FtsZ and against the histidine tag fused to ZapC variants (**Figure 23**). Control

cells transformed with the empty expression vector showed that FtsZ localised at the midcell forming the typical ring-like structure (**Figure 24**). Localisation pattern of overproduced ZapC and its variants was dispersed along the cell length (**Figure 23**). At 60 min after ZapC induction, the FtsZ-ring appeared completely disorganised and dispersed along the cytoplasm co-localising with ZapC as the merge image shows (**Figure 23A**). This FtsZ-ring disorganisation was not observed when ZapC variants induced at this time (**Figure 23C** and **23D**). High amounts of either ZapC, M28D or F58D resulted in a more dispersed localisation of FtsZ that did not form regular rings. As expected, production of the ZapC double M28D-F58D mutant had no effect on the localisation of the FtsZ-rings (**Figure 23B**).

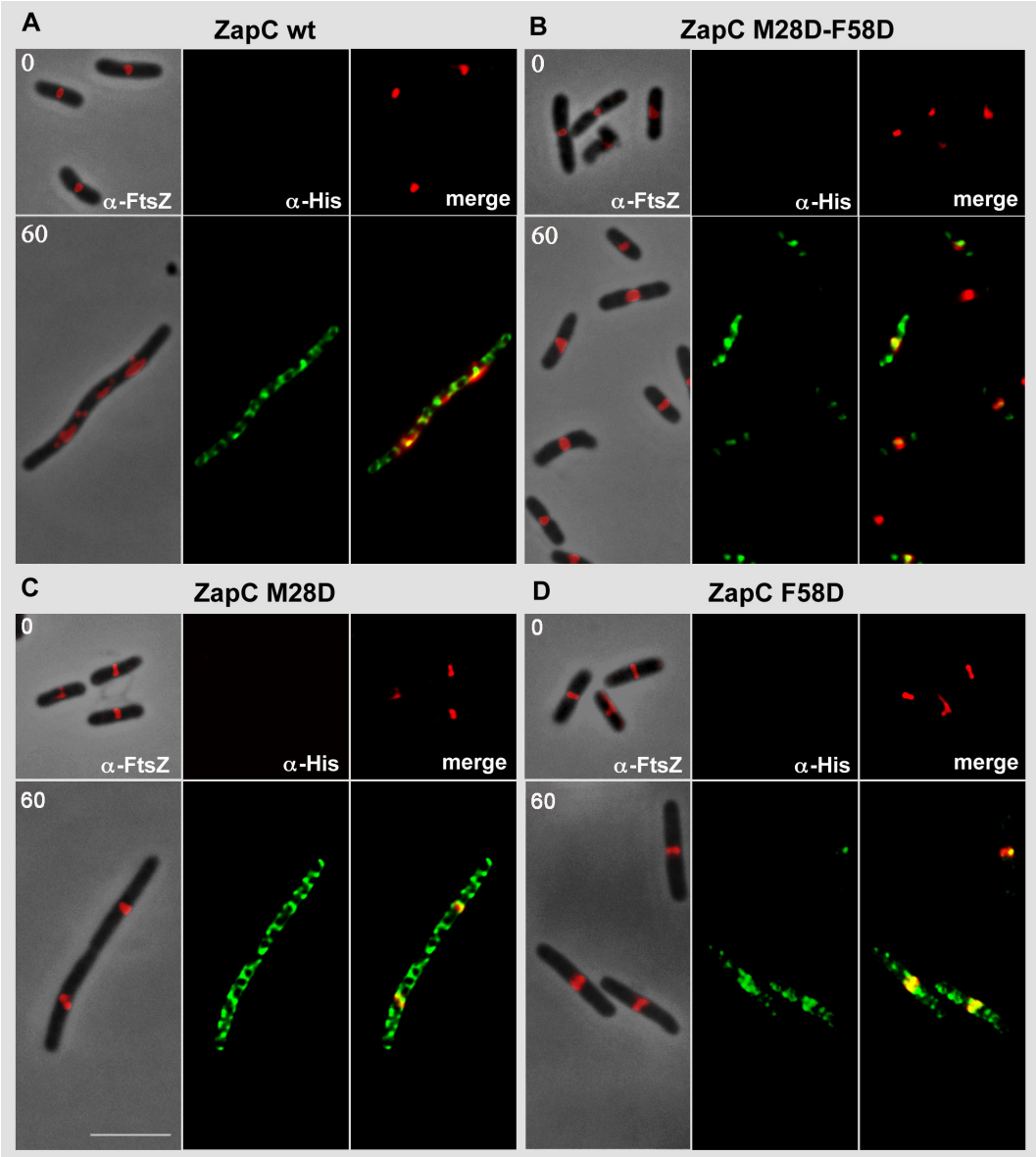

Figure 23. Effect of high levels of ZapC variants on the FtsZ-ring. Samples from the cultures shown in Figure 3 were withdrawn at the times indicated. Visualisation of FtsZ was done using α-FtsZ and Alexa 594 conjugated secondary anti-rabbit antibody (red signal). ZapC-His was revealed by α-Histidine and Alexa 488 conjugated anti-mouse secondary antibody (green signal). The third column shows merged images. Scale bar: 5 μm.

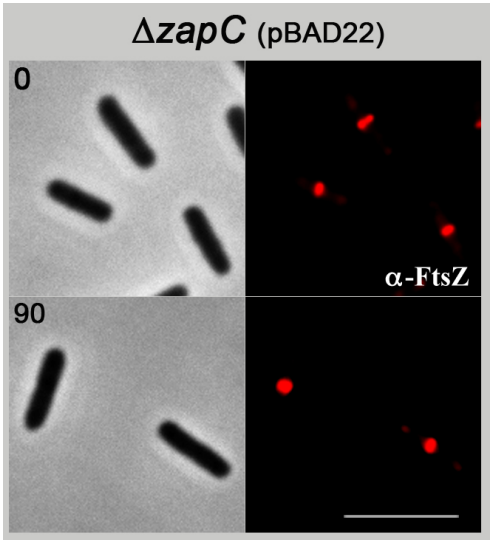

Figure 24. Immunolocalisation of FtsZ in *E. coli* cells transformed with the empty expression vector pBAD22. *E. coli* strain CH59 (*ΔzapC*) was transformed with the empty pBAD22 vector and grown as describe in the legend to Figure 22. At the indicated times samples were withdrawn and the cells were fixed and stained with α-FtsZ plus secondary Alexa 594 conjugated anti-rabbit antibodies. Scale bar: 5 μm.

3.8 Effect on growth and division of FtsA overproduction in *E. coli* cells overexpressing *zapC*

Our previous results have shown the toxic effect that overproduction of ZapC causes in both growth and cell division in *E. coli* cells. These results agree with the previously published by (Hale *et al*., 2011). It has been also shown that ZapC localization depends only on the presence of FtsZ and neither FtsA, ZipA, ZapA nor ZapB is required to localize ZapC. However, we want to investigate if this lethal phenotype caused by ZapC overproduction can be rescued by the induction of any other cell division protein.

The same experiments were carried out to determine the effect in growth and division of *ftsA* overexpression together with *zapC*. Results showed in **Figure 25**, showed that induction of FtsA produced a severe effect in both growth and cell division as it has been previously reported (Dai & Lutkenhaus, 1992). Results from the culture cooverproducing both plasmids, FtsA and ZapC, showed similar defects in growth and division. Size measurements showed that only after 60 min induction of FtsA and FtsA

together with ZapC produced long filamentous cells and, after 90 min cells were so long that cell counter machine could not continued the measurements.

We analysed also by western blot the induction levels of the three proteins. As we observed before, FtsZ levels remained constant during all time points. FtsA levels immediately increased after its induction and ZapC induction levels were lower compared to FtsA. However, the effect of ZapC induction in the cells was comparable to the observed in FtsA cultures. We reason then that the deleterious effect of high amounts ZapC is due to an excess in activity rather than in amount.

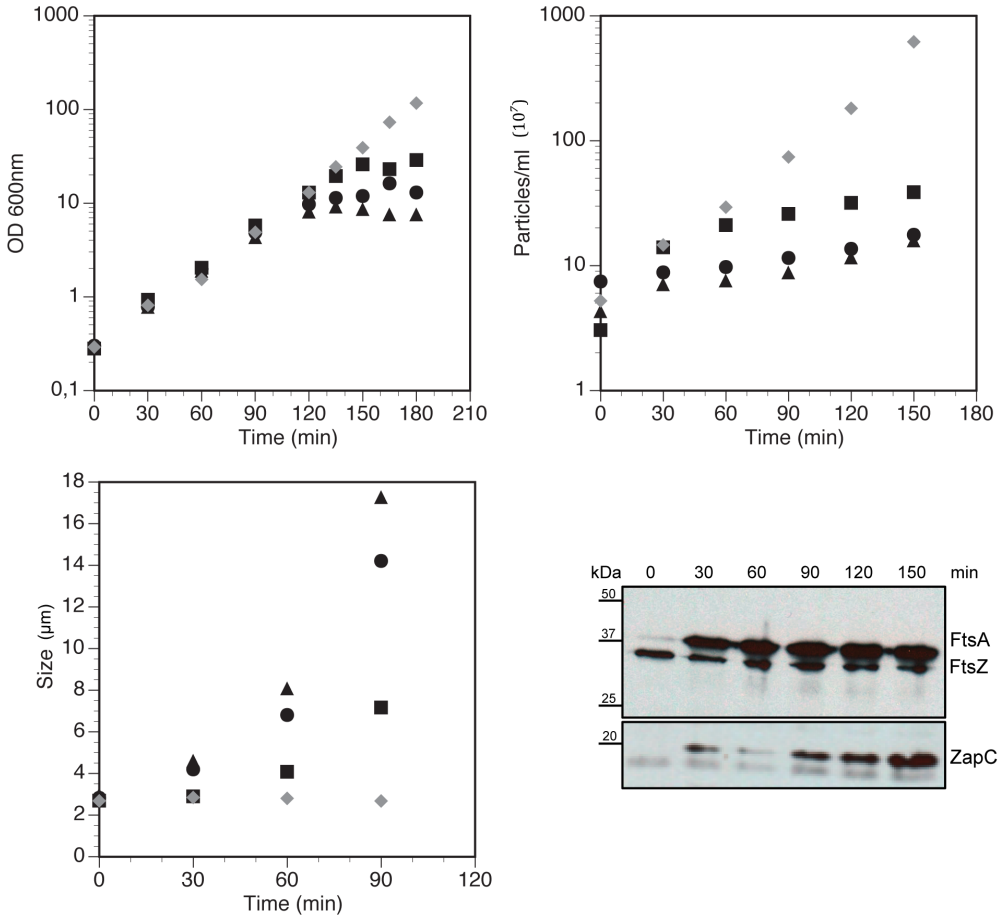

Figure 25. Effect of *ftsA* and *zapC* overexpression on growth and division and levels of FtsZ, FtsA and ZapC following induction of different plasmids. Cultures of CH59 (*ΔzapC*) containing pBAD33 (empty vector; ▲), pCOV36 (*zapC* ■), pPNV40 (*ftsA* ▲), (*zapC* and *ftsA* ●) were grown in glucose-containing medium. At time zero 0.2 % arabinose and 0.5mM IPTG were added for induction. OD (600 nm), particle increases and cell size was measured at the times indicated. Samples were withdrawn at the indicated times and western blot analysis was developed using α-FtsZ, α-FtsA and α-ZapC antibodies to detect the intracellular amount of FtsZ and the induced FtsA and ZapC.

3.9 Effect of the FtsA* gain-of-function overproduction

We wanted to investigate if the FtsA* gain-of-function could rescued the stop in growth and division in *E. coli* cells overexpressing *zapC*. It has been reported that FtsA* bypasses the requirement of ZipA *in vivo* and, it interacts more strongly with FtsZ compared to FtsA, maintaining the FtsZ-ring (Geissler *et al*., 2003), (Geissler *et al*., 2007). We investigate if this characteristic of FtsA* to interact strongly with FtsZ, could rescue the toxicity caused by ZapC overproduction.

We have transformed the *E. coli* Δ*zapC* strain with ZapC and FtsA* plasmids to cooverproduced and analyse the effect on growth and division (**Figure 26**). Optical density (OD) measurement showed that all cultures grew at a constant rate with the exception of *zapC* expression culture that stopped growing after 150 min. We found that ZapC and FtsA* separately, decreased the rate of particle increase after one mass doubling. In contrast, the culture which cooverproduced ZapC and FtsA* divided as the control. Size measurements showed that induction of FtsA* and ZapC together produced similar cells as the control strain. Western blot analysis revealed that FtsZ protein levels were constant and both FtsA* and ZapC proteins increased their levels after induction. These results suggest that the cooverproduction of FtsA* and ZapC allowed the growth and division of *E. coli* cells.

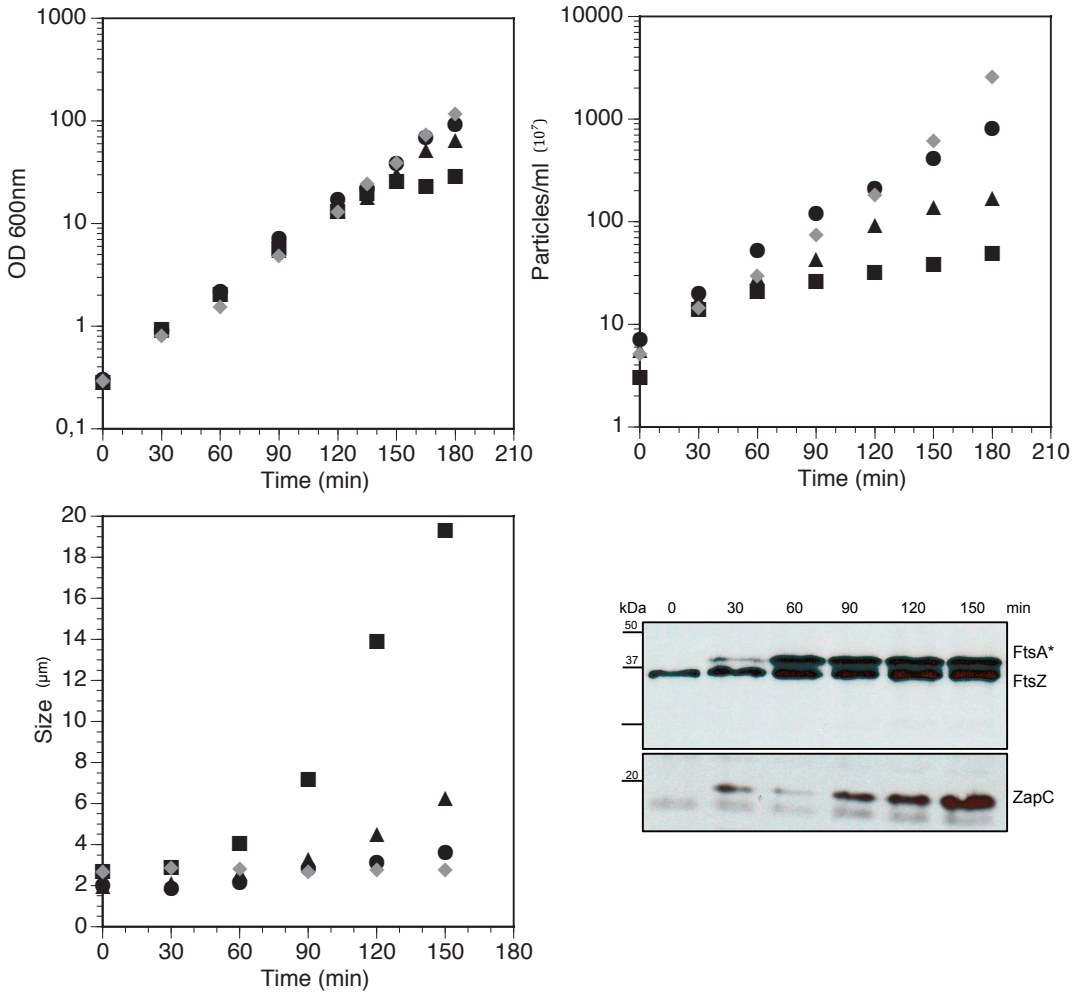

Figure 26. Effect of *ftsA and *zapC* overexpression on growth and division and levels of FtsZ, FtsA* and ZapC following induction of different plasmids.** Cultures of CH59 (*ΔzapC*) containing pBAD33 (empty vector; ▲), pCOV36 (*zapC* ■), pPZV33 (*ftsA** ▲), (*zapC* and *ftsA** ●) were grown in glucose-containing medium. At time zero 0.2 % arabinose and 0.5mM IPTG were added for induction. OD (600 nm), particle increases and cell size was measured at the times indicated. Samples were withdrawn at the indicated times and western blot analysis was developed using α-FtsZ, α-FtsA and α-ZapC antibodies to detect the intracellular amount of FtsZ and the induced FtsA and ZapC.

3.10 Effect of FtsA and FtsA* overproduction on the localization of the FtsZ-ring in cells overexpressing *zapC*

To test the stability of the FtsZ-ring *in vivo*, we expressed the different FtsA and FtsA* plasmids in the *E. coli* Δ*zapC* strain. Cell samples were taken at different time points to immunolocalise the intracellular FtsZ (**Figure 27**). At time 0, localisation pattern of FtsZ in all strains was at the midcell forming the FtsZ-ring. At 60 min after ZapC induction, the FtsZ-ring appeared completely dispersed along the cytoplasm in almost all cells. At 120 min, we observed long filamentous cells with FtsZ completely

disorganised along the cytoplasm. An immediate FtsZ-ring delocalisation was observed upon FtsA induction. Surprisingly, when the FtsZ-ring was localised in cells cooverproducing both ZapC and FtsA we did not detect the disorganisation previously observed by the induction of these proteins. In contrast, the FtsZ-ring was properly localised at the potential division sites along the filament.

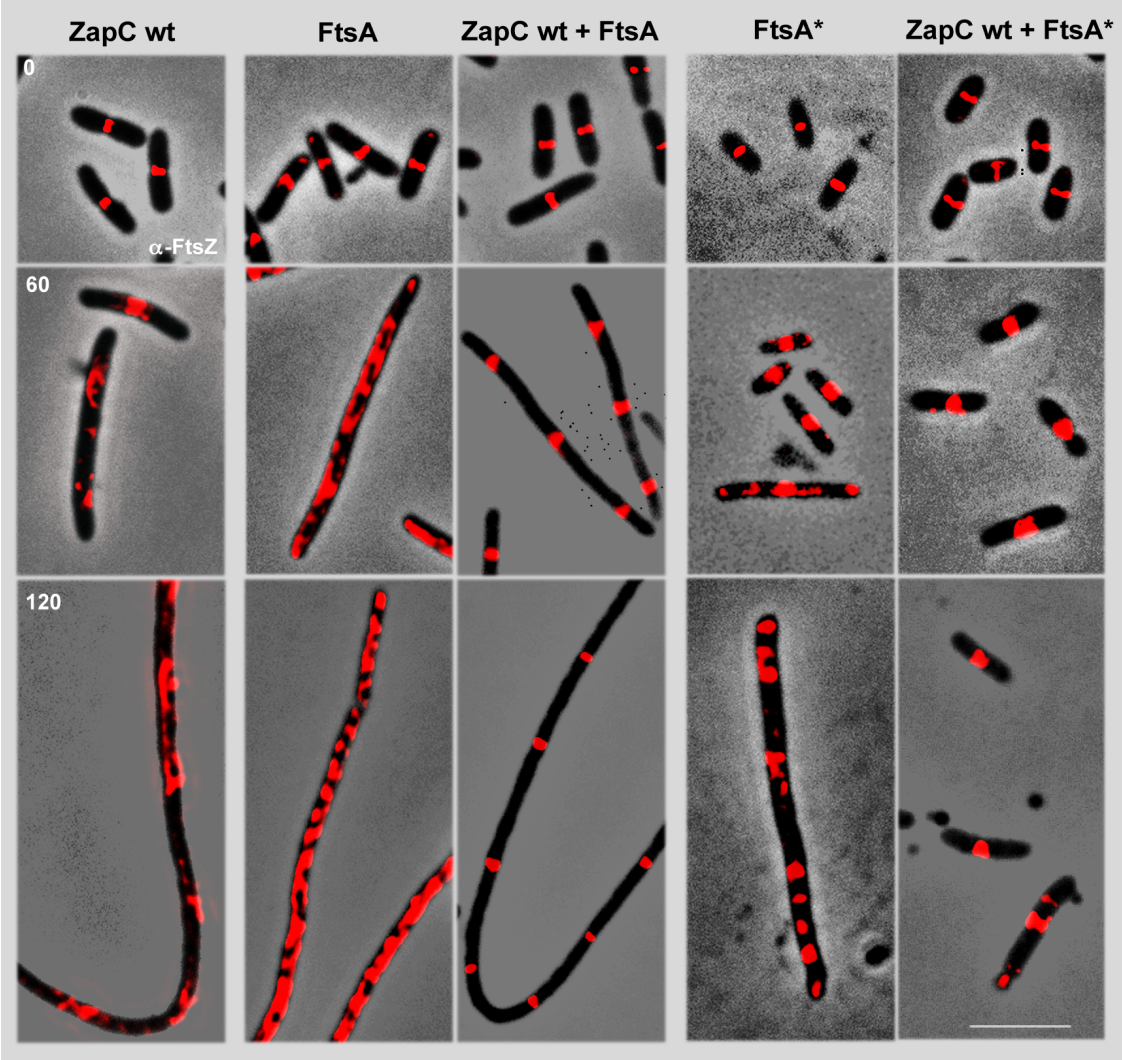

Figure 27. Effect of the overproduction of ZapC, FtsA and FtsA* on the FtsZ-ring localization. Samples from the cultures shown in Figure X and Figure X were withdrawn at the times indicated. Visualisation of FtsZ in all the cultures was done using α-FtsZ and Alexa 594 conjugated secondary anti-rabbit antibody (red signal). Scale bar: 5 μm.

According to the reported results from Geissler *et al*., 2007, cells transformed with FtsA* are shorter than the wild type because FtsA* accelerates assembly of the FtsZ-ring. However, the FtsZ-ring is positioning at midcell and after 120 min FtsA* induction we observed the FtsZ-ring disorganisation. As expected from the results

obtained in OD and particles experiments, the localisation of the FtsZ-ring in cells cooverproducing FtsA* and ZapC was perfectly positioned at midcell and cell size could be comparable to cells that have the FtsZ-ring completely functional to grow and divide

DISCUSSION

1. Manganese as a substitute of magnesium in FtsZ assembly

The studies carried out by Mukherjee & Lutkenhaus in 1999 with the FtsZ protein from *E. coli* revealed one important characteristic of the biochemistry of the protein. They showed that GTP hydrolysis was required for the FtsZ polymers to depolymerize. This dynamic behaviour of the FtsZ filament formation which is probably one of the most important processes in cell division, is carry out by the divalent magnesium ion (Mukherjee & Lutkenhaus, 1999). In the same study, they also showed that FtsZ filament formation is affected by pH between 6.5 and 7.9.

Since then, *in vitro* FtsZ polymerization has been extensively studied and the majority of the data have shown FtsZ as a polymorphic protein, whose polymers are able to assembly in a variety of structures such as rings, spirals, toroids or bundles when are in the presence of crowding agents as Ficoll or methyl cellulose, polycations as hexammine cobalt, divalent cations like Ca^{2+} and different pHs (Popp *et al.*, 2009). Since no available image of the arrangement of the FtsZ filaments inside the living cell, which of these FtsZ polymeric structures are significant *in vivo* is still a matter of discussion. As no available FtsZ structure from *E. coli* exists, we have used to visualize the active centre of the protein, FtsZ from *M. jannaschii* (**Figure 28**). A closer look to the active site of the FtsZ dimer reveals that the coordination sphere of Mg^{2+} involves the phosphates of the GTP and the Aspartic Acid in position 72.

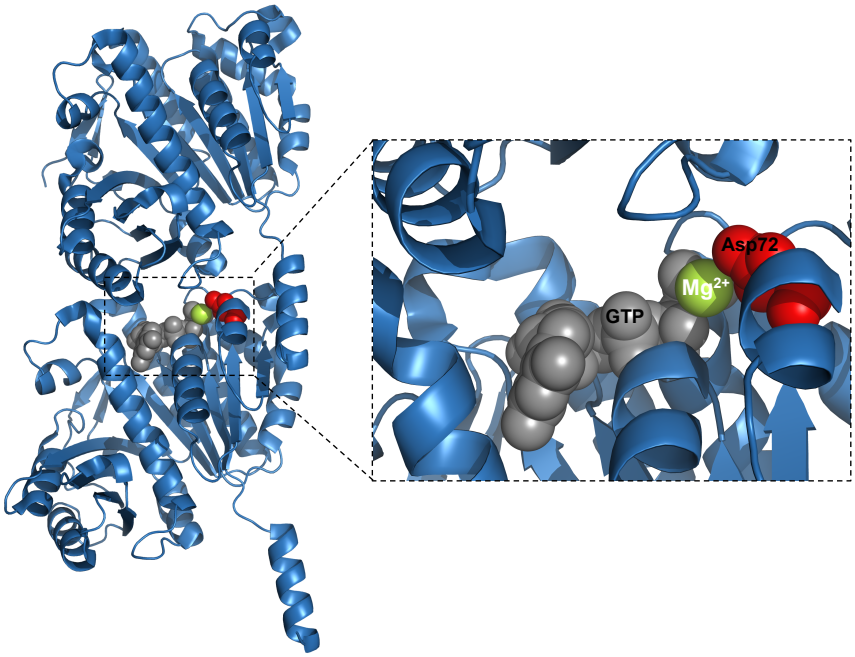

Figure 28. Crystal structure of FtsZ dimer from *Methanococcus jannaschii*. The FtsZ dimer (adapted from the Protein Data Bank (PDB) entry 1W5A) shows both FtsZ folded monomers coloured in blue. The full structure of the GTP-binding site is formed by the overlp of the top monomer in which the bottom surface provides the top surface of the complete active site. The divalent cation Mg^{2+} (green sphere) bound to the phosphates of the nucleotide, GTP (grey spheres) and to the Aspartic Acid-72 (red spheres) activates the hydrolysis of the GTP producing the oligomerization of FtsZ. *Inset*, expanded view of the active site formed by the two monomers. It shows the Mg^{2+}-coordination sphere with the GTP and the Aspartic Acid-72.

It has been shown that there are a group of enzymes, superoxide dismutase (SOD), whose catalytic activity depends on the acquisition of a metal ion (Tainer *et al*., 1982). In *E. coli* the crystal structure of SOD enzyme has been solved showing the manganese ion in the active site between two SOD subunits. The active site of the SOD showed that the coordination sphere of Mn^{2+} involved an Aspartic Acid in position 167 (Whittaker, *et al*., 2011). FtsZ and SOD are two proteins completely different which are not related either structurally or enzymatically, however both enzymes activity rely on the binding of a divalent magnesium and manganese.

Our objective was studied if the divalent cation manganese could replace the essential role of the magnesium ion previously described in FtsZ polymerization.

We have studied the *in vitro* assembly of the FtsZ proteins from three different bacterial species, *E. coli* the bacterial model to study cell division, *M. tuberculosis* and *M. smegmatis*. We found that, although the three FtsZ proteins were able to polymerize with manganese, the *Ec*FtsZ protein did not exhibit the dynamic behaviour previously showed with magnesium (**Figure 7**, *Section 1*). *Ec*FtsZ filaments did not depolymerize and, they assembled into rigid straight bundles with a reduced GTPase activity.

Interestingly, results obtained in 90º light scattering and electron microscopy from the FtsZ proteins from *M. tuberculosis* and *M. smegmatis* were comparable when both magnesium and manganese ions were present in the polymerization buffers (**Figure 7**, *section 1*). Given the results obtained, the question that arises is why the manganese ion affects only the *Ec*FtsZ polymerization. One possible strategy to investigate, will be study the assembly of other known FtsZ proteins from *Bacillus subtilis*, *Methanococcus jannaschii*, *Pseudomonas aeruginosa* and determine if the effect of manganese observed for *Ec*FtsZ filaments is also affecting other FtsZ polymerizations.

Computer simulations using molecular dynamics have suggested that, at neutral pH, one K^+ ion is located at a stable position between the phosphate of GTP and the top monomer. This ion holds a water molecule in position for the catalytic attack on the

phosphate bond (Mendieta *et al*., 2009). It is known that the ionic radius (R_{ionic}) of Mn^{2+} is larger than the Mg^{2+} (0.8 Å and 0.65 Å respectively) (Maguire and Cowan, 2002). It could be possible that manganese ion could disturb the position of the K^+ ion which has been described to position the catalytic water to drive GTP hydrolysis, then the hydrolytic activity of the FtsZ protein can be affected.

Although it has been reported that manganese coordination sphere can also bind an Aspartic Acid and the phosphates of the nucleotide, the difference on the ionic radius (R_{ionic}) could disturb the bond distances between manganese and Aspartic Acid and GTP.

Although, the question why the replacement of magnesium by manganese only affected *Ec*FtsZ has not been solved, the polymeric structures that *Ec*FtsZ formed in the presence of manganese whose GTPase activity is reduced led us to attempt the crystallization of *E. coli* FtsZ exists. We then decided to test if these structures were amenable for a crystallographic analysis to determine the FtsZ structure of *E. coli*.

2. Crystallization of *Escherichia coli* FtsZ

A prerequisite to solve the tridimensional structure of a protein is the production of protein crystals of suitable quality and, in the specific case of FtsZ this was the rate-limiting step in the process. Our results show that the effectiveness of a crystallization experiment was not proportional to the number of conditions tested (**Figure 13**, *section 2*). Finally, the three dimensional structure of *E. coli* FtsZ continues being a problem in the future since the quality of the obtained crystals was not enough to get a good diffraction pattern.

One general aspect of protein crystallization is that rigid, stable proteins are much more likely to crystallize than proteins that are internally flexible or have dynamic surfaces. We designed C-terminal deletions of FtsZ, which have been shown to be a good strategy to improve protein crystallization. In fact, all available FtsZ structures lack of the C-terminal flexible linker. In addition to these FtsZ C-terminal deletions, we added different nucleotides that bind the GTP binding site of the protein to make it more stable (**Figure 13**, *section 2*). However, the absence of results led us to alter our initial objective to crystallize FtsZ as a dimer and the possibility to investigate the active centre formed by the association of the two monomers.

It is well known that FtsZ is a highly dynamic protein with a fast rate of polymerization-depolymerization. This property of FtsZ could be the reason why the obtained FtsZ crystals with GTPγS, the slowly hydrolyzable analogous of GTP or GDP, were poorly diffracting crystals. Although were able to get better crystals when we used the C8-morpholino-GTP, which inhibits FtsZ polymerization and, as a consequence, blocks FtsZ monomers association, the diffraction pattern we obtained did not give us the resolution to solve the structure. Even the presence of divalent cation Mn^{2+}, which showed to reduce the GTPase activity of the protein (*Results in section 1*), only formed salt crystals.

It has been also shown that there are proteins that have crystallized only when they form complexes with other proteins (Davis *et al*., 1990). Since we have used an FtsZ variant that lacked the C-terminal flexible linker that included the central hub, on one hand, we made a more stable protein by deleting the C-terminal part of FtsZ, which is highly disordered (**Figure 10**, *section 2*), but on the other hand we could not use the set of

regulatory proteins that bind to the central hub of FtsZ to try crystallize FtsZ as a complex (Ortiz *et al*., 2015).

However, we did try to crystallize FtsZ in complex with $MinC^N$, which has been shown to bind the body of FtsZ (Shen & Lutkenhaus, 2010). Unfortunately, the obtained crystals only contained the $MinC^N$ protein (**Figure 14**, *section 2*).

In order to make more rigid and stable the formation of the complex, one alternative could be used the full length FtsZ protein in complex with the full length MinC protein, which binds to the central hub ($MinC^C$) and the body of FtsZ ($MinC^N$). Another possibility should try the complex FtsZ-SlmA. As it has been reported that SlmA binds the central hub of FtsZ and also the body of the protein (Du & Lutkenhaus, 2014). Together with MinC and SlmA proteins, SulA will complete the group of proteins known as the inhibitors of FtsZ assembly. The crystal structure of the *P. aeruginosa* SulA has been shown to bind FtsZ exclusively in the catalytic T7 loop needed for GTP hydrolysis (Cordell *et al*., 2003).

The case of *E. coli* FtsZ is extremely recalcitrant since already there are seven FtsZ crystal structures available (Löwe and Amos, 1998, Oliva *et al*., 2007). Bioinformatic predictions have shown that FtsZ proteins are highly similar between them at the amino acid level to *Pa*FtsZ (**Figure 9**, *section 2*). When we have analysed the amino acid sequences between *Ec*FtsZ and *Pa*FtsZ we have detected that both proteins differed in just few amino acids residues, which some of them are located on the surface of the protein (**Figure 29**). There are 97 amino acids residues that are different between both FtsZ proteins. Among them, only 52 amino acids residues are completely different comparing the polarity and the charge of the amino acid group, and the rest, 45 amino acids although they are different they still belong to the same charged group.

One possible strategy to finally obtain a workable *Ec*FtsZ crystal could be work with the *Pa*FtsZ protein that crystallization conditions are known and can be reproduced (Oliva *et al*., 2007). As we have identified in *Pa*FtsZ the amino acids residues that are different to *Ec*FtsZ (**Figure 29A**), the experiment will consist in mutagenize one by one all the residues that are different between the proteins, starting from those, which are located on the surface and in the loops of the protein (**Figure 29B** and **C**). The residues that are located in the loop are the most flexible ones and mutate them could help to decreased the flexibility of the protein.

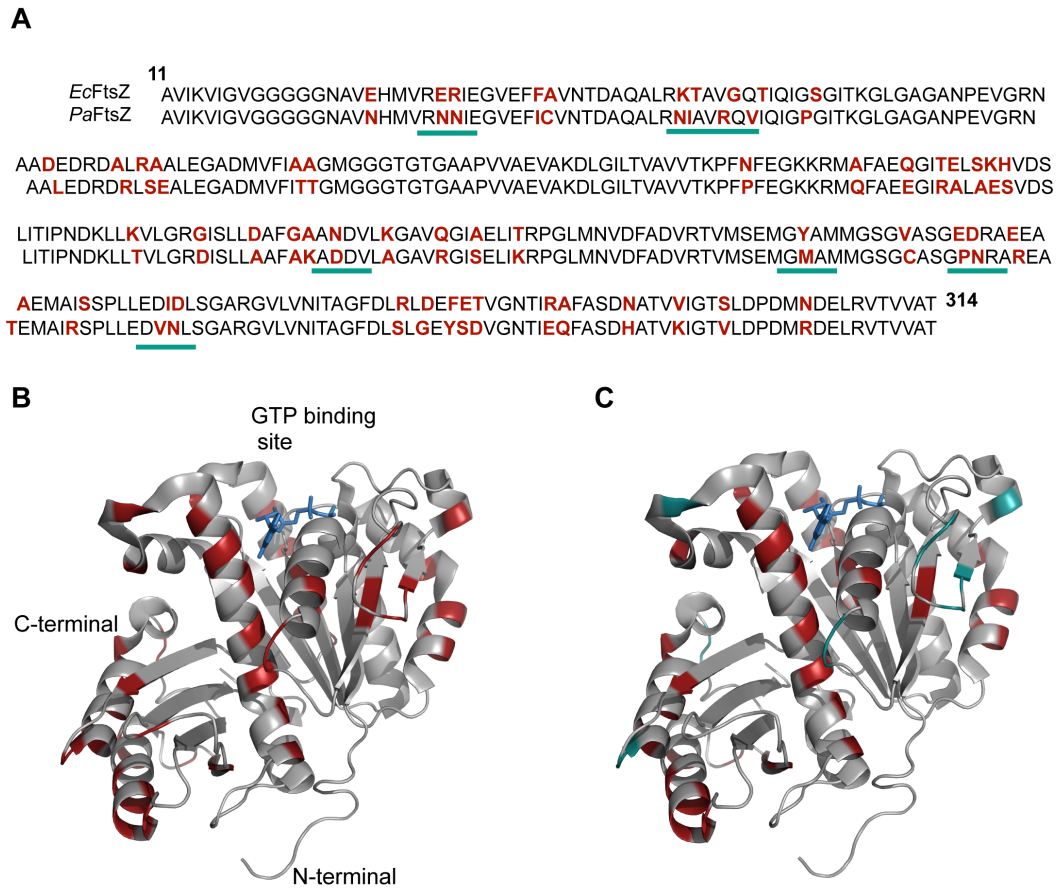

Figure 29. Amino acid homology between *Ec*FtsZ and *Pa*FtsZ. A. Comparison of the amino acids sequences of *Ec*FtsZ and *Pa*FtsZ in which are highlighted in red the amino acids residues that are completely different. The residues that are underlined in green are located in the loop of the protein. **B.** The *Pa*FtsZ monomer (adapted from the Protein Data Bank (PDB) entry 2VAW) shows the body of the protein from the N-terminal to the C-terminal part colour in grey. The GTP-binding site is located on the top surface of the N-terminal domain (nucleotide in blue). Residues that are coloured in red shows the amino acids that are different between both proteins. **C.** Same as **B** but the amino acids coloured in green are located in the loops of the protein.

3. Crystal structure of the FtsZ associated cell division protein ZapC

We have confirmed previous *in vitro* results that showed ZapC as the stabilizer of FtsZ filaments by bundling FtsZ polymers (**Figure 15**, *section 3*) (Hale *et al*., 2011). We have also found that the bundling effect promoted by ZapC addition was dependent on the presence of the central hub of FtsZ (**Figure 15**, *section 3*). However, recent results suggest that ZapC most likely binds to the body of FtsZ, not the central hub, although the study used mostly pelleting conditions and fluorescence changes as a readout, both of which we would consider indirect and prone to problems because the assays involve sedimentation (Bhattacharya *et al*., 2015). We therefore probed the direct interaction of a peptide derived from the central hub of FtsZ with ZapC by ITC (isothermal titration calorimetry) and obtained a K_D of 30 μM, as expected for binding of a short peptide (**Figure 16**, *section 3*). Of course we cannot exclude that ZapC has other binding surfaces on FtsZ that could potentially lead to the nanomolar affinity as has been reported previously (Bhattacharya *et al*., 2015).

Furthermore we present the tridimensional structure of ZapC (**Figure 18**, *section 3*). We showed that both N- and C-terminal ZapC domains are related to the so-called Royal superfamily that comprises Tudor, chromo, MBT and Agenet domains (Chen, *et al*., 2011). Interestingly, all those domains are known to often bind methylated lysines and arginines and they are probably best known for their sensing of methylated histone tails in eukaryotes. This means that ZapC contains two distantly related domains that are part of a superfamily of domains known for their ability to sense arginine and lysine-methylated peptides.

It appears striking to us that a bacterial cell division protein contains two domains of the Royal superfamily. Could ZapC be involved in binding methylated regions of FtsZ? Previously, it has been suggested that methylation might be required for progression of cell division as determined by reducing methylation co-factor availability (Wang, *et al*., 2005). What would those regions in FtsZ be? FtsZ contains a C-terminal tail (central hub) that is highly conserved, about 10 amino acids long and is spaced away from the folded body of the protein by a long flexible linker (**Figure 30B**). The tail of FtsZ does contain a highly conserved arginine, R379 (**Figure 30A**).

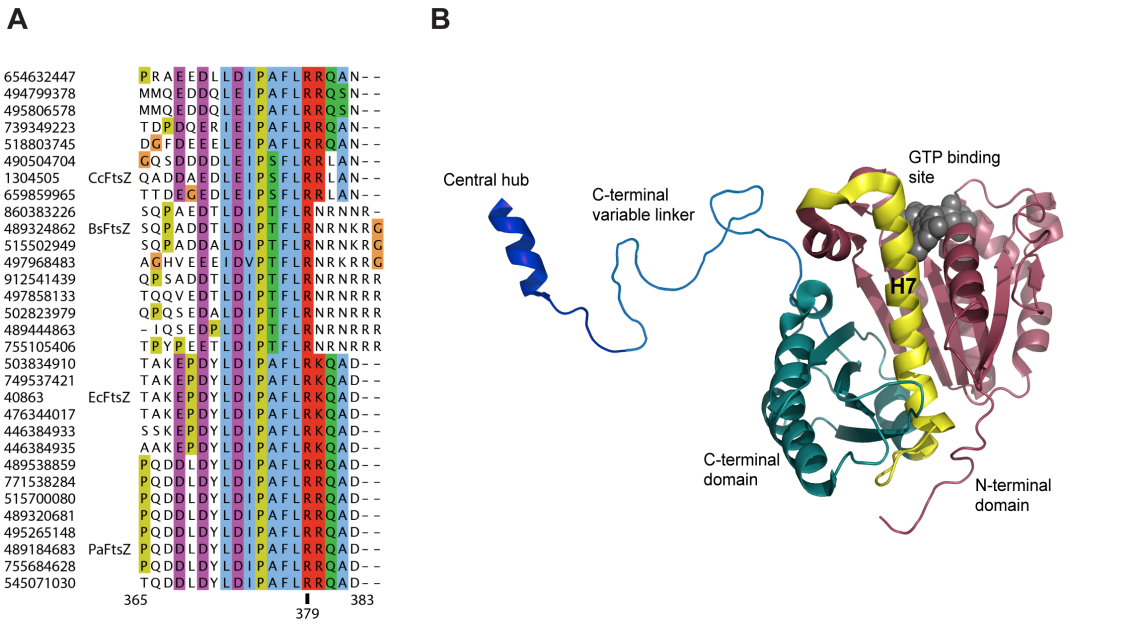

Figure 30. The central hub of FtsZ. A. Multiple sequence alignment (Clustal Omega, www.clustal.org) showing conservation within the C-terminal tails of various FtsZ proteins. A maximum of ten sequences were collected from each BLAST search with FtsZ sequences from *E. coli*, *B. subtilis*, *C. crescentus* and *P. aeruginosa* (Ec, Bs, Cc, PaFtsZ) sampled evenly up to the point where percentage of sequence cover and identify dropped below 95 % and 40 %, respectively. Totally conserved arginine residue 379 is highlighted and numbering corresponds to *Ec*FtsZ. **B.** FtsZ monomer modelled from the *Pa*FtsZ (PDB 2VWA) in which the N-terminal domain is coloured in dark red, the helix H7 in yellow, the C-terminal domain in green, the C-terminal variable linker is depicted as an unstructured polypeptide chain (blue) and the central hub of FtsZ (blue) is based on the structure of the interacting region of the *E. coli* FtsZ protein with the globular domain of ZipA (PDB 1F47).

The ZapC crystals described here contain two monomers per asymmetric unit. In order to clarify the oligomeric state of the protein in solution, we performed analytical ultracentrifugation (AUC) (**Figure 19**, section 3). Results showed that the two major species corresponded very well with theoretical values for ZapC monomers and dimers. We hypothesized that if one FtsZ tail binds one ZapC monomer, as indicated here by ITC (**Figure 16**, section 3), it is expected that a dimer of ZapC would have the ability to crosslink and bundle FtsZ filaments, as has been reported (Hale *et al*., 2011). Beyond this, we can only speculate what the role of dimerisation is in the context of ZapC's interaction with FtsZ and in the wider context of bacterial cell division but it is intriguiging that a number of FtsZ-interacting proteins are dimers, including SulA, MinC, ZapA, SlmA and EzrA and all of these also bind to the central hub of FtsZ.

Any *in vivo* analysis to demonstrate that ZapC could bind to the central hub of FtsZ was impossible, since the central hub of FtsZ is essential to be anchored to the membrane by FtsA and ZipA (reviewed in Ortiz *et al*., 2015). Instead of that, we constructed point mutations of ZapC in order to disrupt the dimer interface and, in this way, determine

that the ZapC dimer is relevant for the FtsZ-ring stability. However, *in vivo* results were not definite since the overexpression of each point mutation produced finally the FtsZ-ring delocalization (**Figure 23**, *section 3*). Any attempt to purify these ZapC point mutations was impossible due to the aggregation into inclusion bodies, we can only speculate about the dimerization role of ZapC based on the crystal structure.

4. Molecular interaction between ZapC and FtsZ in *E. coli*

The gain-of-function mutant FtsA* has been shown to bypass some of the functions exerted by ZipA in the assembly and stability of the divisome, among them the need for ZipA in the assembly of the late divisome proteins (Geissler, *et al*., 2003). It has been also shown that FtsA* interacts more efficiently with FtsZ than FtsA (Geissler et al 2007).

On the other hand, previous results from ZapC overproduction have shown to produce a (Hale *et al*., 2011).

This idea prompted us to test if the toxic effect caused by the induction of ZapC, could be supresses by the induction of other cell division protein.

Although structurally different, ZipA and ZapC share a common function: stabilize the FtsZ-ring. *In vitro* both proteins bundle FtsZ filaments. From our results we can deduced that the balance between FtsZ assembly and FtsZ disassembly which is disrupted by the induction of ZapC as well as the induction of FtsA, can be compensate by the addition of FtsA*.

In a way, our results with FtsA* could be comparable with the reported ones for ZipA. FtsA* is able to bypasses ZipA function in vivo and also supresses the toxic effects of high levels of ZipA (Geissler *et al*., 2003). Our results show that FtsA* is able to supress the ZapC induction-toxic effect allowing cells grow and divide normally.

Since FtsZ levels measured by western blot did not change during FtsA* induction, could indicated that FtsA* promotes FtsZ-ring dynamics.

However, it has been shown also that FtsA* interacts more efficiently with FtsZ than FtsA (Geissler et al 2007). This data support our idea that FtsA* is able to rescue grow and division and FtsA is only able to positioning the ring. In this case, we hypothesised that this extra-function of FtsA* may act as a destabilizer the FtsZ-ring. A possible mechanism is that FtsA can be stimulated by the over-assembly of FtsZ produce by the

excess of ZapC and acquire a role in maintaining the balance FtsZ:ZapC and being able to position the FtsZ-ring although not to rescue the division. However when we induce FtsA* we observe cells with normal grow rate and division as control cells. This role that FtsA acquires to compensate the excess ZapC, is increased in FtsA* allowing the FtsZ-ring dynamics by compensating completely the balance FtsZ:ZapC.

CONCLUSIONS

Conclusions

In vitro, polymerization from both *M. tuberculosis* and *M. smegmatis* FtsZ can be trigger by either magnesium or manganese ions. *Mtb*FtsZ and *Msm*FtsZ polymerize into long single and double filaments also polymerization levels were stable after reached the steady state, which take about 10 minutes.
Although manganese is able to prompt the polymerization of *E. coli* FtsZ, it induced the formation of rigid stable bundles of FtsZ filaments. *Ec*FtsZ polymerization was stable and FtsZ polymers did not disassembly as they do with magnesium.

The FtsZ associated protein ZapC stabilizes FtsZ filaments *in vitro*. Possibly it binds to the FtsZ central hub to stabilize the polymers. The crystal structure of ZapC reveals a protein with homology to the Royal family domains, chromo and Tudor domains, which are implicated in the binding of methylated arginines. The central hub of FtsZ contains one arginine residue highly conserved.

In vivo, the overproduction of ZapC produces a toxic effect on growth and division and FtsZ cannot assemble in the division ring. The simultaneous overproduction of FtsA and ZapC in *E. coli* cells, allow the position of the FtsZ protein at the potential cell division sites but does not restore division. The overproduction of the FtsA* gain-of-function mutant, restored both growth and division in *E. coli* cells overproducing ZapC.

CONCLUSIONES

In vitro, la polimerización de FtsZ de *M. tuberculosis* y *M. smegmatis* puede ser desencadenada tanto por el ión magnesio como el ión manganeso. *Mtb*FtsZ y *Msm*FtsZ polimerizaron en filamentos sencillos y dobles y también los niveles de polimerización fueron estables después de alcanzar el máximo de polimerización a los 10 minutos.
Aunque el ión manganeso fue capaz de provocar la polimerización de FtsZ de *E. coli,* éste indujo la formación de polímeros rígidos y estables de FtsZ, los cuales no se habían observado en presencia de magnesio. Los niveles de polimerización de FtsZ fueron también differentes, los polímeros fueron estables y no se desensamblaron como sí lo hicieron con magnesio.

La proteína asociada a FtsZ, ZapC, estabiliza los filamentos de FtsZ *in vitro*. Posiblemente se une al C-terminal de FtsZ, el central hub. La estructura cristalina de ZapC reveló que tenía homología a la familia de dominios Royal, dominios chromo y Tudor, los cuales están implicados en la union de argininas metiladas. El central hub de FtsZ contiene una arginine muy conservada entre lase species de bacterias.

In vivo, la sobre producción de ZapC produce un efecto tóxico en el crecimiento y la division y la proteinna FtsZ no puede ensamblarse en el anillo de division.The sobreproducción simultanea de FtsA y ZapC en *E. coli* permitió el posicionamiento de FtsZ, sin embargo, no restauró la division. La sobreproducción de FtsA*, un mutante punctual, fue capaz de restaurar el crecimiento y division en la células de *E. coli* que sobreprodujeron ZapC.

REFERENCES

References

Adams DW, Wu LJ & Errington J (2015) Nucleoid occlusion protein Noc recruits DNA to the bacterial cell membrane. *EMBO J* **34**: 491-501.

Addinall SG, Bi E & Lutkenhaus J (1996) FtsZ ring formation in fts mutants. *J. Bacteriol*. **178**: 3877-3884.

Anderson DE, Gueiros-Filho FJ & Erickson HP (2004) Assembly dynamics of FtsZ rings in Bacillus subtilis and Escherichia coli and effects of FtsZ-regulating proteins. *J Bacteriol* **186**: 5775-5781.

Ballare C, Lange M, Lapinaite A, *et al*. (2012) Phf19 links methylated Lys36 of histone H3 to regulation of Polycomb activity. *Nat Struct Mol Biol* **19**: 1257-1265.

Bernhardt TG & de Boer PA (2005) SlmA, a nucleoid-associated, FtsZ binding protein required for blocking septal ring assembly over Chromosomes in E. coli. *Mol Cell* **18**: 555-564.

Bhattacharya A, Ray S, Singh D, Dhaked HP & Panda D (2015) ZapC promotes assembly and stability of FtsZ filaments by binding at a different site on FtsZ than ZipA. *Int J Biol Macromol* **81**: 435-442.

Bramkamp M, Emmins R, Weston L, Donovan C, Daniel RA & Errington J (2008) A novel component of the division-site selection system of Bacillus subtilis and a new mode of action for the division inhibitor MinCD. *Mol Microbiol* **70**: 1556-1569.

Busiek KK, Eraso JM, Wang Y & Margolin W (2012) The early divisome protein FtsA interacts directly through its 1c subdomain with the cytoplasmic domain of the late divisome protein FtsN. *J Bacteriol* **194**: 1989-2000.

Buske PJ & Levin PA (2012) Extreme C terminus of bacterial cytoskeletal protein FtsZ plays fundamental role in assembly independent of modulatory proteins. *J Biol Chem* **287**: 10945-10957.

Buske PJ & Levin PA (2013) A flexible C-terminal linker is required for proper FtsZ assembly in vitro and cytokinetic ring formation in vivo. *Mol Microbiol* **89**: 249-263.

Buss J, Coltharp C, Shtengel G, Yang X, Hess H & Xiao J (2015) A multi-layered protein network stabilizes the Escherichia coli FtsZ-ring and modulates constriction dynamics. *PLoS Genet* **11**: e1005128.

Cabre EJ, Monterroso B, Alfonso C, *et al*. (2015) The Nucleoid Occlusion SlmA Protein Accelerates the Disassembly of the FtsZ Protein Polymers without Affecting Their GTPase Activity. *PLoS One* **10**: e0126434.

Cabre EJ, Sanchez-Gorostiaga A, Carrara P, *et al*. (2013) Bacterial Division Proteins FtsZ and ZipA Induce Vesicle Shrinkage and Cell Membrane Invagination. *J Biol Chem* **288**: 26625-26634.

References

Camberg JL, Hoskins JR & Wickner S (2009) ClpXP protease degrades the cytoskeletal protein, FtsZ, and modulates FtsZ polymer dynamics. *Proc Natl Acad Sci U S A* **106**: 10614-10619.

Chen C, Nott TJ, Jin J & Pawson T (2011) Deciphering arginine methylation: Tudor tells the tale. *Nat Rev Mol Cell Biol* **12**: 629-642.

Cheng I, Mikita N, Fishovitz J, Frase H, Wintrode P & Lee I (2012) Identification of a region in the N-terminus of Escherichia coli Lon that affects ATPase, substrate translocation and proteolytic activity. *J Mol Biol* **418**: 208-225.

Cho H & Bernhardt TG (2013) Identification of the SlmA active site responsible for blocking bacterial cytokinetic ring assembly over the chromosome. *PLoS Genet* **9**: e1003304.

Cho H, McManus HR, Dove SL & Bernhardt TG (2011) Nucleoid occlusion factor SlmA is a DNA-activated FtsZ polymerization antagonist. *Proc Natl Acad Sci U S A* **108**: 3773-3778.

Cordell SC, Anderson RE & Lowe J (2001) Crystal structure of the bacterial cell division inhibitor MinC. *EMBO J* **20**: 2454-2461.

Cordell SC, Robinson EJ & Löwe J (2003) Crystal structure of the SOS cell division inhibitor SulA and in complex with FtsZ. *Proc Natl Acad Sci U S A* **100**: 7889-7894.

Dai K & Lutkenhaus J (1992) The proper ratio of FtsZ to FtsA is required for cell division to occur in Escherichia coli. *J Bacteriol* **174**: 6145-6151.

Dajkovic A, Mukherjee A & Lutkenhaus J (2008) Investigation of regulation of FtsZ assembly by SulA and development of a model for FtsZ polymerization. *J Bacteriol* **190**: 2513-2526.

de Boer PA, Crossley RE & Rothfield LI (1989) A division inhibitor and a topological specificity factor coded for by the minicell locus determine proper placement of the division septum in *E. coli*. *Cell* **56**: 641-649.

de Boer PA, Crossley RE & Rothfield LI (1992) Roles of MinC and MinD in the site-specific septation block mediated by the MinCDE system of Escherichia coli. *J Bacteriol* **174**: 63-70.

Du S & Lutkenhaus J (2014) SlmA antagonism of FtsZ assembly employs a two-pronged mechanism like MinCD. *PLoS Genet* **10**: e1004460.

Du S, Park KT & Lutkenhaus J (2015) Oligomerization of FtsZ converts the FtsZ tail motif (conserved carboxy-terminal peptide) into a multivalent ligand with high avidity for partners ZipA and SlmA. *Mol Microbiol* **95**: 173-188.

Durand-Heredia J, Rivkin E, Fan G, Morales J & Janakiraman A (2012) Identification of ZapD as a cell division factor that promotes the assembly of FtsZ in Escherichia coli. *J Bacteriol* **194**: 3189-3198.

Durand-Heredia JM, Yu HH, De Carlo S, Lesser CF & Janakiraman A (2011) Identification and characterization of ZapC, a stabilizer of the FtsZ ring in Escherichia coli. *J Bacteriol* **193**: 1405-1413.

Ebersbach G, Galli E, Møller-Jensen J, Löwe J & Gerdes K (2008) Novel coiled-coil cell division factor ZapB stimulates Z ring assembly and cell division. *Mol Microbiol* **68**: 720-735.

Erickson HP (2001) The FtsZ protofilament and attachment of ZipA--structural constraints on the FtsZ power stroke. *Curr Opin Cell Biol* **13**: 55-60.

Erickson HP, Anderson DE & Osawa M (2010) FtsZ in Bacterial Cytokinesis: Cytoskeleton and Force Generator All in One. *Microbiol Mol Biol Rev* **74**: 504-528.

Espeli O, Borne R, Dupaigne P, Thiel A, Gigant E, Mercier R & Boccard F (2012) A MatP-divisome interaction coordinates chromosome segregation with cell division in E. coli. *EMBO J* **31**: 3198-3211.

Fleurie A, Lesterlin C, Manuse S, *et al*. (2014) MapZ marks the division sites and positions FtsZ rings in Streptococcus pneumoniae. *Nature* **516**: 259-262.

Fu G, Huang T, Buss J, Coltharp C, Hensel Z & Xiao J (2010) *In vivo* structure of the *E. coli* FtsZ-ring revealed by photoactivated localization microscopy (PALM). *PLoS One* **5**: e12682.

Galli E & Gerdes K (2012) FtsZ-ZapA-ZapB interactome of *Escherichia coli*. *J Bacteriol* **194**: 292-302.

Geissler B, Elraheb D & Margolin W (2003) A gain-of-function mutation in ftsA bypasses the requirement for the essential cell division gene zipA in Escherichia coli. *Proc Natl Acad Sci U S A* **100**: 4197-4202.

Geissler B, Shiomi D & Margolin W (2007) The *ftsA** gain-of-function allele of *Escherichia coli* and its effects on the stability and dynamics of the Z ring. *Microbiology* **153**: 814-825.

Gekko K & Timasheff SN (1981) Mechanism of protein stabilization by glycerol: preferential hydration in glycerol-water mixtures. *Biochemistry* **20**: 4667-4676.

Ghosal D, Trambaiolo D, Amos LA & Lowe J (2014) MinCD cell division proteins form alternating copolymeric cytomotive filaments. *Nat Commun* **5**: 5341.

Gola S, Munder T, Casonato S, Manganelli R & Vicente M (2015) The essential role of SepF in mycobacterial division. *Mol Microbiol*.

References

Gueiros-Filho FJ & Losick R (2002) A widely conserved bacterial cell division protein that promotes assembly of the tubulin-like protein FtsZ. *Genes Dev*. **16**: 2544-2556.

Guzman LM, Belin D, Carson MJ & Beckwith J (1995) Tight regulation, modulation, and high-level expression by vectors containing the arabinose PBAD promoter. *J Bacteriol* **177**: 4121-4130.

Haeusser DP, Lee AH, Weart RB & Levin PA (2009) ClpX inhibits FtsZ assembly in a manner that does not require its ATP hydrolysis-dependent chaperone activity. *J Bacteriol* **191**: 1986-1991.

Hale CA & de Boer PA (1997) Direct binding of FtsZ to ZipA, an essential component of the septal ring structure that mediates cell division in E. coli. *Cell* **88**: 175-185.

Hale CA & de Boer PA (1999) Recruitment of ZipA to the septal ring of Escherichia coli is dependent on FtsZ and independent of FtsA. *J Bacteriol* **181**: 167-176.

Hale CA, Rhee AC & de Boer PA (2000) ZipA-induced bundling of FtsZ polymers mediated by an interaction between C-terminal domains. *J. Bacteriol*. **182**: 5153-5166.
Hale CA, Shiomi D, Liu B, Bernhardt TG, Margolin W, Niki H & de Boer PA (2011) Identification of *Escherichia coli* ZapC (YcbW) as a component of the division apparatus that binds and bundles FtsZ polymers. *J Bacteriol* **193**: 1393-1404.

Hamoen LW, Meile JC, de Jong W, Noirot P & Errington J (2006) SepF, a novel FtsZ-interacting protein required for a late step in cell division. *Mol Microbiol* **59**: 989-999.

Hanahan D (1983) Studies on transformation of Escherichia coli with plasmids. *J Mol Biol* **166**: 557-580.

Hoenig M, Lee RJ & Ferguson DC (1989) A microtiter plate assay for inorganic phosphate. *J Biochem Biophys Methods* **19**: 249-251.

Holeckova N, Doubravova L, Massidda O, *et al*. (2015) LocZ is a new cell division protein involved in proper septum placement in Streptococcus pneumoniae. *MBio* **6**: e01700-01714.
Hu Z & Lutkenhaus J (2003) A conserved sequence at the C-terminus of MinD is required for binding to the membrane and targeting MinC to the septum. *Mol Microbiol* **47**: 345-355.

Hu Z, Mukherjee A, Pichoff S & Lutkenhaus J (1999) The MinC component of the division site selection system in Escherichia coli interacts with FtsZ to prevent polymerization. *Proc Natl Acad Sci U S A* **96**: 14819-14824.

Huang KH, Durand-Heredia J & Janakiraman A (2013) FtsZ ring stability: of bundles, tubules, crosslinks, and curves. *J Bacteriol* **195**: 1859-1868.

Huisman O, D'Ari R & Gottesman S (1984) Cell-division control in *Escherichia coli*: specific induction of the SOS function SfiA protein is sufficient to block septation. *Proc Natl Acad Sci U S A* **81**: 4490-4494.

Jacquier N, Frandi A, Pillonel T, Viollier PH & Greub G (2014) Cell wall precursors are required to organize the chlamydial division septum. *Nat Commun* **5**: 3578.

Jaffe A, Boye E & D'Ari R (1990) Rule governing the division pattern in Escherichia coli minB and wild-type filaments. *J Bacteriol* **172**: 3500-3502.

Koppelman CM, Aarsman ME, Postmus J, *et al*. (2004) R174 of Escherichia coli FtsZ is involved in membrane interaction and protofilament bundling, and is essential for cell division. *Mol Microbiol* **51**: 645-657.

Krol E, van Kessel SP, van Bezouwen LS, Kumar N, Boekema EJ & Scheffers DJ (2012) Bacillus subtilis SepF binds to the C-terminus of FtsZ. *PLoS One* **7**: e43293.

Krupka M, Rivas G, Rico AI & Vicente M (2012) Key role of two terminal domains in the bidirectional polymerization of FtsA protein. *J Biol Chem* **287**: 7756-7765.

Krupka M, Cabre EJ, Jimenez M, Rivas G, Rico AI & Vicente M (2014) Role of the FtsA C terminus as a switch for polymerization and membrane association. *MBio* **5**: e02221.

Laemmli UK (1970) Cleavage of structural proteins during the assembly of the head of bacteriophage T4. *Nature* **227**: 680-685.

Lappchen T, Pinas VA, Hartog AF, *et al*. (2008) Probing FtsZ and tubulin with C8-substituted GTP analogs reveals differences in their nucleotide binding sites. *Chem Biol* **15**: 189-199.

Lara B, Rico AI, Petruzzelli S, *et al*. (2005) Cell division in cocci: localization and properties of the Streptococcus pneumoniae FtsA protein. *Mol Microbiol* **55**: 699-711.

Li Z, Trimble MJ, Brun YV & Jensen GJ (2007) The structure of FtsZ filaments *in vivo* suggests a force-generating role in cell division. *Embo J* **26**: 4694-4708.

Loose M & Mitchison TJ (2014) The bacterial cell division proteins FtsA and FtsZ self-organize into dynamic cytoskeletal patterns. *Nat Cell Biol* **16**: 38-46.

Loose M, Fischer-Friedrich E, Ries J, Kruse K & Schwille P (2008) Spatial regulators for bacterial cell division self-organize into surface waves in vitro. *Science* **320**: 789-792.

López-Montero I, López-Navajas P, Mingorance J, Rivas G, Vélez M, Vicente M & Monroy F (2013) Intrinsic disorder of the bacterial cell division protein ZipA: coil-to-brush conformational transition. *FASEB J*.

References

Low HH, Moncrieffe MC & Löwe J (2004) The crystal structure of ZapA and its modulation of FtsZ polymerisation. *J Mol Biol* **341**: 839-852.

Löwe J & Amos LA (1998) Crystal structure of the bacterial cell-division protein FtsZ. *Nature* **391**: 203-206.

Lutkenhaus J, Pichoff S & Du S (2012) Bacterial cytokinesis: From Z ring to divisome. *Cytoskeleton (Hoboken)* **69**: 778-790.

Maguire ME & Cowan JA (2002) Magnesium chemistry and biochemistry. *Biometals* **15**: 203-210.

Marston AL, Thomaides HB, Edwards DH, Sharpe ME & Errington J (1998) Polar localization of the MinD protein of Bacillus subtilis and its role in selection of the mid-cell division site. *Genes Dev* **12**: 3419-3430.

Marteyn BS, Karimova G, Fenton AK, *et al*. (2014) ZapE is a novel cell division protein interacting with FtsZ and modulating the Z-ring dynamics. *MBio* **5**: e00022-00014.

Massidda O, Novakova L & Vollmer W (2013) From models to pathogens: how much have we learned about Streptococcus pneumoniae cell division? *Environ Microbiol* **15**: 3133-3157.

Mateos-Gil P, Marquez I, Lopez-Navajas P, *et al*. (2012) FtsZ polymers bound to lipid bilayers through ZipA form dynamic two dimensional networks. *Biochim Biophys Acta* **1818**: 806-813.

McCoy AJ & Maurelli AT (2006) Building the invisible wall: updating the chlamydial peptidoglycan anomaly. *Trends Microbiol* **14**: 70-77.

Mendieta J, Rico AI, Lopez-Vinas E, Vicente M, Mingorance J & Gomez-Puertas P (2009) Structural and functional model for ionic (K(+)/Na(+)) and pH dependence of GTPase activity and polymerization of FtsZ, the prokaryotic ortholog of tubulin. *J Mol Biol* **390**: 17-25.

Mingorance J, Tamames J & Vicente M (2004) Genomic channeling in bacterial cell division. *J Mol Recognit* **17**: 481-487.

Mingorance J, Rueda S, Gomez-Puertas P, Valencia A & Vicente M (2001) Escherichia coli FtsZ polymers contain mostly GTP and have a high nucleotide turnover. *Mol Microbiol* **41**: 83-91.

Mingorance J, Rivas G, Vélez M, Gomez-Puertas P & Vicente M (2010) Strong FtsZ is with the force: mechanisms to constrict bacteria. *Trends Microbiol* **18**: 348-356.

Mizusawa S & Gottesman S (1983) Protein degradation in Escherichia coli: the lon gene controls the stability of sulA protein. *Proc Natl Acad Sci U S A* **80**: 358-362.

Mohammadi T, Ploeger GE, Verheul J, *et al*. (2009) The GTPase activity of Escherichia coli FtsZ determines the magnitude of the FtsZ polymer bundling by ZapA in vitro. *Biochemistry* **48**: 11056-11066.

Mosyak L, Zhang Y, Glasfeld E, Haney S, Stahl M, Seehra J & Somers WS (2000) The bacterial cell-division protein ZipA and its interaction with an FtsZ fragment revealed by X-ray crystallography. *Embo J*. **19**: 3179-3191.

Moy FJ, Glasfeld E, Mosyak L & Powers R (2000) Solution structure of ZipA, a crucial component of Escherichia coli cell division. *Biochemistry* **39**: 9146-9156.

Mukherjee A & Lutkenhaus J (1994) Guanine nucleotide-dependent assembly of FtsZ into filaments. *J Bacteriol* **176**: 2754-2758.

Mukherjee A & Lutkenhaus J (1998) Purification, assembly, and localization of FtsZ. *Methods Enzymol* **298**: 296-305.

Mukherjee A & Lutkenhaus J (1999) Analysis of FtsZ assembly by light scattering and determination of the role of divalent metal cations. *J Bacteriol* **181**: 823-832.

Natale P, Pazos M & Vicente M (2013) The Escherichia coli divisome: born to divide. *Environ Microbiol* **15**: 3169-3182.

Ohashi T, Hale CA, de Boer PA & Erickson HP (2002) Structural evidence that the P/Q domain of ZipA is an unstructured, flexible tether between the membrane and the C-terminal FtsZ-binding domain. *J Bacteriol* **184**: 4313-4315.

Oliva MA, Trambaiolo D & Lowe J (2007) Structural insights into the conformational variability of FtsZ. *J Mol Biol* **373**: 1229-1242.

Ortiz C, Natale P, Cueto L & Vicente M (2015) The keepers of the ring: regulators of FtsZ assembly. *FEMS Microbiol Rev*.

Park KT, Wu W, Battaile KP, Lovell S, Holyoak T & Lutkenhaus J (2011) The Min oscillator uses MinD-dependent conformational changes in MinE to spatially regulate cytokinesis. *Cell* **146**: 396-407.

Pazos M, Natale P & Vicente M (2013) A specific role for the ZipA protein in cell division: stabilization of the FtsZ protein. *J Biol Chem* **288**: 3219-3226.

Pazos M, Natale P, Margolin W & Vicente M (2013) Interactions among the early Escherichia coli divisome proteins revealed by bimolecular fluorescence complementation. *Environ Microbiol* **15**: 3282-3291.

Pazos M, Casanova M, Palacios P, Margolin W, Natale P & Vicente M (2014) FtsZ placement in nucleoid-free bacteria. *PLoS One* **9**: e91984.

References

Pichoff S & Lutkenhaus J (2005) Tethering the Z ring to the membrane through a conserved membrane targeting sequence in FtsA. *Mol Microbiol* **55**: 1722-1734.

Pilhofer M, Aistleitner K, Biboy J, *et al*. (2013) Discovery of chlamydial peptidoglycan reveals bacteria with murein sacculi but without FtsZ. *Nat Commun* **4**: 2856.

Pla J, Sanchez M, Palacios P, Vicente M & Aldea M (1991) Preferential cytoplasmic location of FtsZ, a protein essential for *Escherichia coli* septation. *Mol. Microbiol.* **5**: 1681-1686.

Popp D, Iwasa M, Narita A, Erickson HP & Maeda Y (2009) FtsZ condensates: an in vitro electron microscopy study. *Biopolymers* **91**: 340-350.

Potluri LP, Kannan S & Young KD (2012) ZipA is required for FtsZ-dependent preseptal peptidoglycan synthesis prior to invagination during cell division. *J Bacteriol* **194**: 5334-5342.

Raskin DM & de Boer PA (1999) Rapid pole-to-pole oscillation of a protein required for directing division to the middle of *Escherichia coli*. *Proc Natl Acad Sci U S A* **96**: 4971-4976.

RayChaudhuri D (1999) ZipA is a MAP-Tau homolog and is essential for structural integrity of the cytokinetic FtsZ ring during bacterial cell division. *Embo J*. **18**: 2372-2383.

RayChaudhuri D & Park JT (1994) A point mutation converts Escherichia coli FtsZ septation GTPase to an ATPase. *J Biol Chem* **269**: 22941-22944.

Rico AI, Krupka M & Vicente M (2013) In the beginning Escherichia coli assembled a proto-ring: the initial phases of bacterial division. *J Biol Chem* Doi: 10.1074/jbc.R1113.479519.

Rico AI, Garcia-Ovalle M, Mingorance J & Vicente M (2004) Role of two essential domains of Escherichia coli FtsA in localization and progression of the division ring. *Mol Microbiol* **53**: 1359-1371.

Rothfield L, Justice S & Garcia-Lara J (1999) Bacterial cell division. *Annu Rev Genet* **33**: 423-448.

Rueda S, Vicente M & Mingorance J (2003) Concentration and assembly of the division ring proteins FtsZ, FtsA, and ZipA during the *Escherichia coli* cell cycle. *J. Bacteriol.* **185**: 3344-3351.

Sanchez M, Dopazo A, Pla J, Robinson AC & Vicente M (1994) Characterisation of mutant alleles of the cell division protein FtsA, a regulator and structural component of the Escherichia coli septator. *Biochimie* **76**: 1071-1074.

Sanchez M, Valencia A, Ferrandiz MJ, Sander C & Vicente M (1994) Correlation between the structure and biochemical activities of FtsA, an essential cell division protein of the actin family. *EMBO J* **13**: 4919-4925.

Sauer RT, Bolon DN, Burton BM, *et al*. (2004) Sculpting the proteome with AAA(+) proteases and disassembly machines. *Cell* **119**: 9-18.

Scheffers DJ & Driessen AJ (2002) Immediate GTP hydrolysis upon FtsZ polymerization. *Mol Microbiol* **43**: 1517-1521.

Scheffers DJ, de Wit JG, den Blaauwen T & Driessen AJ (2002) GTP hydrolysis of cell division protein FtsZ: evidence that the active site is formed by the association of monomers. *Biochemistry* **41**: 521-529.

Schuck P (2000) Size-distribution analysis of macromolecules by sedimentation velocity ultracentrifugation and lamm equation modeling. *Biophys J* **78**: 1606-1619.

Shen B & Lutkenhaus J (2009) The conserved C-terminal tail of FtsZ is required for the septal localization and division inhibitory activity of MinC(C)/MinD. *Mol Microbiol* **72**: 410-424.

Shen B & Lutkenhaus J (2010) Examination of the interaction between FtsZ and MinCN in E. coli suggests how MinC disrupts Z rings. *Mol Microbiol* **75**: 1285-1298.

Singh JK, Makde RD, Kumar V & Panda D (2007) A membrane protein, EzrA, regulates assembly dynamics of FtsZ by interacting with the C-terminal tail of FtsZ. *Biochemistry* **46**: 11013-11022.
Singh JK, Makde RD, Kumar V & Panda D (2008) SepF increases the assembly and bundling of FtsZ polymers and stabilizes FtsZ protofilaments by binding along its length. *J Biol Chem* **283**: 31116-31124.

Small E, Marrington R, Rodger A, *et al*. (2007) FtsZ polymer-bundling by the *Escherichia coli* ZapA orthologue, YgfE, involves a conformational change in bound GTP. *J Mol Biol* **369**: 210-221.

Soderstrom B, Skoog K, Blom H, Weiss DS, von Heijne G & Daley DO (2014) Disassembly of the divisome in Escherichia coli: evidence that FtsZ dissociates before compartmentalization. *Mol Microbiol* **92**: 1-9.

Stock D, Perisic O & Lowe J (2005) Robotic nanolitre protein crystallisation at the MRC Laboratory of Molecular Biology. *Prog Biophys Mol Biol* **88**: 311-327.

Stricker J, Maddox P, Salmon ED & Erickson HP (2002) Rapid assembly dynamics of the Escherichia coli FtsZ-ring demonstrated by fluorescence recovery after photobleaching. *Proc Natl Acad Sci U S A* **99**: 3171-3175.

References

Sundararajan K, Miguel A, Desmarais SM, Meier EL, Casey Huang K & Goley ED (2015) The bacterial tubulin FtsZ requires its intrinsically disordered linker to direct robust cell wall construction. *Nat Commun* **6**: 7281.

Szeto TH, Rowland SL, Habrukowich CL & King GF (2003) The MinD membrane targeting sequence is a transplantable lipid-binding helix. *J Biol Chem* **278**: 40050-40056.

Szwedziak P, Wang Q, Freund SM & Lowe J (2012) FtsA forms actin-like protofilaments. *EMBO J* **31**: 2249-2260.

Szwedziak P, Wang Q, Bharat TA, Tsim M & Lowe J (2014) Architecture of the ring formed by the tubulin homologue FtsZ in bacterial cell division. *Elife* **3**: e04601.

Tonthat NK, Milam SL, Chinnam N, Whitfill T, Margolin W & Schumacher MA (2013) SlmA forms a higher-order structure on DNA that inhibits cytokinetic Z-ring formation over the nucleoid. *Proc Natl Acad Sci U S A* **110**: 10586-10591.

Towbin H, Staehelin T & Gordon J (1979) Electrophoretic transfer of proteins from polyacrylamide gels to nitrocellulose sheets: procedure and some applications. *Proc Natl Acad Sci U S A* **76**: 4350-4354.

Treuner-Lange A, Aguiluz K, van der Does C*, et al*. (2013) PomZ, a ParA-like protein, regulates Z-ring formation and cell division in Myxococcus xanthus. *Mol Microbiol* **87**: 235-253.

Trusca D, Scott S, Thompson C & Bramhill D (1998) Bacterial SOS checkpoint protein SulA inhibits polymerization of purified FtsZ cell division protein. *J Bacteriol* **180**: 3946-3953.

van den Ent F & Löwe J (2000) Crystal structure of the cell division protein FtsA from *Thermotoga maritima*. *Embo J* **19**: 5300-5307.

Vaughan S, Wickstead B, Gull K & Addinall SG (2004) Molecular evolution of FtsZ protein sequences encoded within the genomes of archaea, bacteria, and eukaryota. *J Mol Evol* **58**: 19-29.

Vicente M & Rico AI (2006) The order of the ring: assembly of Escherichia coli cell division components. *Mol Microbiol* **61**: 5-8.

Vicente M, Gomez MJ & Ayala JA (1998) Regulation of transcription of cell division genes in the Escherichia coli dcw cluster. *Cell Mol Life Sci* **54**: 317-324.

Vicente M, Álvarez J & Martínez-Arteaga R (2004) How similar cell division genes are located and behave in different bacteria. *Molecules in Time and Space*,ed.^eds.), p.^pp. Springer US.

Walker GC (1995) SOS-regulated proteins in translesion DNA synthesis and mutagenesis. *Trends Biochem Sci* **20**: 416-420.

Wang S, Arends SJ, Weiss DS & Newman EB (2005) A deficiency in S-adenosylmethionine synthetase interrupts assembly of the septal ring in Escherichia coli K-12. *Mol Microbiol* **58**: 791-799.

Weart RB, Nakano S, Lane BE, Zuber P & Levin PA (2005) The ClpX chaperone modulates assembly of the tubulin-like protein FtsZ. *Mol Microbiol* **57**: 238-249.

White EL, Ross LJ, Reynolds RC, Seitz LE, Moore GD & Borhani DW (2000) Slow polymerization of Mycobacterium tuberculosis FtsZ. *J Bacteriol* **182**: 4028-4034.

Whittaker MM, Lerch TF, Kirillova O, Chapman MS & Whittaker JW (2011) Subunit dissociation and metal binding by Escherichia coli apo-manganese superoxide dismutase. *Arch Biochem Biophys* **505**: 213-225.

Willemse J, Borst JW, de Waal E, Bisseling T & van Wezel GP (2011) Positive control of cell division: FtsZ is recruited by SsgB during sporulation of Streptomyces. *Genes Dev* **25**: 89-99.

Woldringh CL, Mulder E, Huls PG & Vischer N (1991) Toporegulation of bacterial division according to the nucleoid occlusion model. *Res Microbiol* **142**: 309-320.

Wu LJ & Errington J (2004) Coordination of cell division and chromosome segregation by a nucleoid occlusion protein in Bacillus subtilis. *Cell* **117**: 915-925.
Wu LJ, Ishikawa S, Kawai Y, Oshima T, Ogasawara N & Errington J (2009) Noc protein binds to specific DNA sequences to coordinate cell division with chromosome segregation. *EMBO J* **28**: 1940-1952.

Yu XC & Margolin W (1997) Ca2+-mediated GTP-dependent dynamic assembly of bacterial cell division protein FtsZ into asters and polymer networks in vitro. *EMBO J* **16**: 5455-5463.

Zhou H & Lutkenhaus J (2005) MinC mutants deficient in MinD- and DicB-mediated cell division inhibition due to loss of interaction with MinD, DicB, or a septal component. *J Bacteriol* **187**: 2846-2857.